REPUBLIQUE ALGERIENNE DEMOCRATIQUE ET POPULAIRE

MINISTERE DE L'ENSEIGNEMENT SUPERIEUR

ET DE LA RECHERCHE SCIENTIFIQUE

UNIVERSITE –EL HADJ LAKHDER- BATNA

FACULTE DES SCIENCES

DEPARTEMENT DES SCIENCES DE LA MATIERE

MEMOIRE

PRESENTE POUR L'OBTENTION DE DIPLOME

DE MAGISTER EN ASTROPHYSIQUE

PAR

Amelal Abderahim

THEME

Les étoiles à neutrons: Étude des propriétés cinétiques

Soutenu le . . / . . / 2011 , devant le jury :

Président	D. BAHLOUL	Professeur	U Batna
Rapporteur	A. BOULDJEDRI	Professeur	U Batna
Examinateur	A. SID	M-C	U Batna
Examinateur	J. MIMOUNI	Professeur	U Constantine

PEOPLE'S DEMOCRATIC AND POPULAR REPUBLIC OF ALGERIA

MINISTRY OF HIGHER EDUCATION AND SCIENTIFIC RESEARCH

EL-HADJ LAKHDAR UNIVERSITY OF BATNA

FACULTY OF SCIENCES

DEPARTMENT OF MATTER SCIENCES

DISSERTATION

SUBMITTED FOR A PARTIAL FULFILLMENT OF THE REQUIREMENT OF A MAGISTER DEGREE IN PHYSICS

OPTION : ASTROPHYSICS

PRESENTED BY

Amelal Abderahim

THEME

Neutron stars : Study of kinetic properties

Defended in . . / . . / 2011 , Jury members:

Chairman	D. BAHLOUL	Professor	U Batna
Reporter	A. BOULDJEDRI	Professor	U Batna
Examiner	A. SID	M-C	U Batna
Examiner	J. MIMOUNI	Professor	U Constantine

Acknowledgements :

I thank Pr. Abdelhamid Bouldjedri my advisor for assisting this work .

And I like to thank my teachers Pr. Derrai Bahloul, Pr Jamel Mimouni, Dr Abdelaziz Sid for being jury members and accepting the discussion of my thesis.

I heartily thank all the people who have generously assisted me in the construction of this humble work. Without their support, this project would not have been possible in its current form.

Dr. Alexander Potekhin for his comments and criticisms have greatly improved my understanding of research and consequently, the content of this investigation. And all members of the Neutron stars group in the Ioffe Physico-Technical Institute at St. Petersburg Russia.

I would like to thank Mr. Abdelghani Chadda, (British academy of sciences) for helping me with the obstacles I have had with Scientific Programming and for advising me.

I would also to thank Mr. Abderrahmen Zoghbi (Cambridge University) for offering all useful Scientific papers.

Thanks to my teachers, classmates and friends from the Physics Departments at Batna and Constantine Universities.

My heartfelt thanks go to my father, for being one of the few to understand what a work like this would mean… to my mother, for believing in me, for arranging all my life accommodations and for all the efforts she has made…, to my family.

……Thanks

To the memory of my grandfather

Table of Contenent

INTRODUCTION

An exceptional position in physics and astrophysics is taken by neutron stars. On the one hand, they have matter under extreme physical conditions, so their theories are constructed on risky extrapolations of what we now consider as reliable physical theories of the structure of matter which are experienced in the laboratory. On the other hand, the unique opportunity their observations offer to test these theories. Moreover, neutron stars are important *impressive personae* on the stage of modern astrophysics; they participate in many astronomical phenomena.

Neutron stars have the matter of density varies from some $\mathrm{g\,cm^{-3}}$ in the surface, where the pressure is small, to more than $10^{15}\,\mathrm{g\,cm^{-3}}$ at the center, where the pressure exceeds$10^{36}\,\mathrm{dyn\,cm^{-2}}$.

Many branches of physics are used in thermodynamics and kinetics studies of neutron star matter owing to the enormous ranges of temperatures and densities in neutron stars interior.

The kinetic theory (or kinetics) deals with transport coefficients, the thermal and electrical conductivities (κ andσ) as well as the shear and bulk viscosities (η and ζ) are most useful ones. Many physicists had studied kinetic theory of the matter inside the neutron stars crust , The electrons are the major contributors to the conductivities κ and σ and the viscosity η , Coulomb scattering by ions in the liquid case or scattering by phonons, which quantify vibrations of ions in solid state matter are the main scattering mechanism for the electrons. At sufficient low temperatures the electron-ion scattering is strongly suppressed and in this case the electron scattering by charged impurities which are a small fraction of ions have different charges from charges of most abundant ions and the scattering of electron by electron can be more significant.

We performs the first chapter to play a preparatory role for the future and provides a summary of key information on the envelopes of neutron stars, which we guided in the performance of work “specially the crusts”, as well as a brief overview of previous studies on this subject.

In the second chapter we examined the equilibrium properties of the plasma in the shells of neutron stars, excluding the effect of the magnetic field, but taking into account the no ideal Coulomb plasma. The main attention is paid to the Coulomb interaction in the outer shells of neutron stars. And because the physical conditions in the outer shells of neutron stars are similar to conditions in the interior of white dwarfs and in the cores of red giants, the results are useful also for these objects.

The third chapter is devoted to the calculation of thermal conductivity, electrical conductivity and thermoelectric coefficient of a fully ionized plasma physical conditions encountered in the ocean and the crust of neutron stars without a strong magnetic field, introducing what we so called “The Ioffe model”.

The fourth and fifth chapters are central to this work. They are dedicated to those effects, and we include other effects and study others situations:

- In the fourth chapter, the effect of the nuclear form factor on the electrical and thermal conductivities and we study also the multi components plasma systems.

- In the fifth chapter, based on chapters 2-4 we study the influence of a strong magnetic field on the properties of transport in the shells of neutron stars, and also the case of thermal effects. Furthermore we apply the Ioffe model to compute the shear viscosity.

Chapter I

Neutron stars, an overview

I.1. Introduction

Stellar evolution is the process by which a star experiences a succession of drastic transformations for the period of its lifetime. Depending on the mass of the star, this lifetime varies from only a few million years (case of the most massive stars) to trillions of years (for the least massive ones , which is much more than the age of the universe).

As most changes take place in stars happen too slowly to be directly perceived , so we can not study stellar evolution by observing the life of a star, , even if the observation are made over several centuries. Instead, to realize how stars evolve we must observe several stars at the diverse stages in their life, and also by using simulation and models of stellar structure.

A supernova is a kind of stellar explosion in which more energy is exploded than a nova. Supernovae are very luminous and cause a burst of radiation that often briefly outshines an entire galaxy, before deappearing from view over a several of weeks. Supernova is able to radiate as much energy as the Sun is expected to emit over its whole life during this small interval of time. The explosion expels much of a star's matter at a very high velocity of up to 30,000 km/s, causing a shock wave into the neighboring interstellar medium. This shock wave brushs up an expanding shell of dust and gas what we so called a supernova remnant.

It exist a several types of supernovae. Types I and II can be caused in one of two ways, both turning off or suddenly turning on the production of energy through the nuclear fusion. After the core of an aging massive star ceases generating energy from nuclear fusion, it may experience sudden

gravitational collapse into a neutron star or black hole, releasing gravitational energy that warms and ejects the outer layers of the star.

A neutron star is a type of remnant that can result from the gravitational collapse of a massive star during a Type II, Type Ib or Type Ic supernova event. Such stars are have a great portion of neutrons. Neutron stars are very hot and the Pauli exclusion principle supporte them against further collapse because.

The typical typical masses of neutron stars $M \sim 1.4M_{\odot}$ and their typical radii $R \sim 10\,\text{km}$. hence, their masses are close to the solar mass $M_{\odot} = 1.989 \times 10^{33}\,\text{g}$, however their radii are $\sim 10^5$ times smaller than the solar radius $R_{\odot} = 6.96 \times 10^5\,\text{km}$, thus typical masses, thus Neutron stars are compact stars which have matter of super nuclear density in their interiors with a huge portion of free neutrons.

as a result, neutron stars hold an huge gravitational energy E_{grav} and surface gravity g:

$$\boldsymbol{E_{grav} \sim \frac{GM}{R} \sim 5 \times 10^{53} erg \sim 0.2 Mc^2} \qquad (\mathbf{1.1}\boldsymbol{a}).$$

$$\boldsymbol{g \sim \frac{GM}{R} \sim 2 \times \frac{10^{14} cm}{s^2}} \qquad (\mathbf{1.1}\boldsymbol{b}).$$

Where c is the speed of light and G is the gravitational constant.
obviously, neutron stars are extremely dense. The mean mass density is :

$$\boldsymbol{\bar{\rho} \approx \frac{3M}{(4\pi R^3)} \approx \times 10^{14} g cm^{-3} \sim (2-3)\rho_0} \qquad (\mathbf{1.2}).$$

Where $\rho_0 = 2.8 \times 10^{14}\,\text{gcm}^{-3}$ is what we so called the normal nuclear density. The central density of neutron stars is bigger, attaining $(10 - 20\rho 0$. By the way, neutron stars are the most compact stars that we recognized in the Universe.

I.2. History of neutron star physics

Prediction:

- L.D.Landau (1931) – *expectation* [L.D.Landau, "On the theory of stars," *Physikalische Zs. Sowjetunion* 1 (1932) 285]: for stars with $M > 1.5M_{\odot}$ "density of matter becomes so great that atomic nuclei come in close contact, foming *one gigantic nucleus''*.

- J.Chadwick – *the neutron's discovery* [*Nature*, Feb.27, 1932].

- T***he supposition of the existence of neutron stars by*** W.Baade & F.Zwicky (1933) ["Supernovae and cosmic rays," *Phys. Rev.* 45 (1934) 138; "On super-novae," *Proc. Nat. Acad. Sci.* 20 (1934) 254]: "…supernovae represent the transitions from ordinary stars to *neutron stars*, which in their final stages consist of extremely closely packed neutrons"; "…possess a very small radius and an extremely high density.".
- ***Crab nebula*** –This is in reality a remnant of the supernova, exploded on July 4, 1054.

K.Lundmark invented the connection between the nebula and the archival Chinese **"Guest star"** in 1921.and it was confirmed as the supernova type I remnant in 1942 (Dyuvendak; Mayall & Oort; Baade; Minkowski).

In 1968, the **Crab pulsar** has been discovered in the vicinity of the center of the nebula (in radio and X-rays).

Theory before the discovery:

- T.E.Sterne (1933) – proposed the first model of the EOS (equation of state) of the nuclear matter; he predict the *neutronization* with increasing density.

- F.Zwicky ["On collapsed neutron stars," *Astrophys. J.* 88 (1938) 522].

  - ✓ Made an estimation of the maximum *binding energy* of a neutron star;
  - ✓ illustrate the difference between the Baryonic M_b and gravitational M masses;
  - ✓ show the "*huge gravitational red shifts*"

- R.C.Tolman; J.R.Oppenheimer and G.M.Volkoff (*Phys. Rev.*, 3.01. – 15.02.1939) they :

  - ✓ *Computed the "TOV equation"* (thehydrostatic equilibrium of a spherically symmetric star).

    O.&V.: founded the *maximum mass* of a neutron star using the non-interacting neutrons model as:

$$\boldsymbol{M_{max} = 0.71\, M_{\odot} < M_{max}(WD) = 1.44\, M_{\odot}).}$$

- ***EOS for dense matter.***

  - ✓ J.A.Wheeler, B.K.Harrison, *et al.* (1950s).
  - ✓ A.G.W.Cameron (1959) – nuclear forces ($M_{max} \sim 2\, M_{\odot}$); hyperons.
  - ✓ Ya.B.Zeldovich (1961) – maximally stiff EOS model.

- ***Superfluidity.***

  - ✓ BCS: J.Bardeen, L.N.Cooper, & J.R.Schrieffer (1957).

- ✓ A.Bohr, B.R.Mottelson, and D.Pines, "Possible analog between the excitation spectra of nuclei and those of superconducting metal state," [*Phys. Rev.* **110** (1958) 936].

- ✓ A.B.Migdal (1959), V.L.Ginzburg and D.A.Kirzhnits (1964):

$$(Tc \sim 10^{10}\ K, \rho \sim 10^{13} - 10^{15}\ \frac{g}{cm^3})$$

- ➢ ***Neutrino emission.***

- ✓ H.-Y.Chiu and E.E.Salpeter (1964); J.N.Bahcall & R.A.Wolf (1965).

- ➢ ***Cooling.***

- ✓ R.Stabler (1960, PhD); Chiu (1964); Chiu & Salpeter (1964);
- ✓ D.C.Morton (1964), Bahcall & Wolf; S.Tsuruta & A.G.W.Cameron (1966).

Search and discovery:

- ➢ ***Search in X-rays.*** $T \sim 10^6\ K \rightarrow$ X-rays → space observations.

- ✓ R.Giacconi et al. (1962): discovery of Sco $X-1$ (Nobel Prize of 2002 to Giacconi for outstanding contribution to X-ray astronomy).

- ✓ I.S.Shklovsky (1967): Sco $X-1$ "a neutron star in a state of accretion" (correct, *but* unnoticed).

- ➢ ***Plerion pulsar nebulae.***

- ✓ S.Bowyer et al. (1964): discovred an X-ray source in the Crab nebula ~ 10^{13} km ($\rightarrow$ *not* a neutron star).

- ✓ N.S.Kardashev (1964), F.Pacini (1967): constructed models of a nebula around a rapidly rotating strongly magnetized neutron star. Pacini – ***pulsar model***.

➢ ***Radio observations.***

- ✓ 1962, 1965 (A.Hewish) –the discovery of a pulsar in the Crab nebula, *but* unexplained and unnoticed

➢ **6.08 – 28.11.1967**:

- ✓ Jocelyn Bell, Anthony Hewish – discovery of pulsars (Nobel prize of 1974 to Hewish).

- ✓ in 1969 it become clear that pulsars are rapidly rotating neutron stars with strong magnetic fields (Thomas Gold, 1968).

Neutron stars from a hypothesis turned into reality.

Figue1.1*: Jocelyn Bell and the telescope in Cambridge, England, used to discover pulsars in 1967–68. Image Credit: Jocelyn Bell Burnell.*

I.3. Basic parameters of neutron star

For neutron stars, unlike all others, play important role effects of general relativity (GR). Therefore, the model of neutron stars should be calculated only in the framework of general relativity. The structure of the non-rotating star is determined by the relativistic equation of hydrostatic equilibrium - the equation of the Tolman - Oppenheimer - Volkov (TOV). It gives a very good approximation for spinning neutron stars, except those with millisecond rotation periods. The smallest possible rotation period is 0.7 ms, but the smallest of the observed to date period is 1.396 ms [Hes 06], which corresponds to a "regime of slow rotation, in which the effects of rotation can be accounted for by perturbation theory (see, for example., [Hae 2006], Ch. 6). Amendments by the magnetic field is negligibly small for large-scale structure of neutron stars, except for fields in the $\sim 10^{16}$ G, which has not yet been observed. Effects caused by the well-known today, the magnetic fields $B \sim 10^{14}$ G, may be important in the envelops . Solution of the equation TOV for a given equation of state of matter of the neutron star gives a

family of models of the star, a parameter which is the density of ρ_c in the center of the star. Stability condition, requiring that $M(\rho_c)$ was an increasing function is performed within a certain range of stellar masses and radii, depending on the equation of state theory, the greatest mass M_{max} can range from 1,4 to 2,5 $M_\odot$ and the smallest - $M_{min} \sim 0{,}1\, M_\odot$ (for example [Hae 2006]). For each star, the significance of the effects of general relativity is determined by the compactness parameter $x_g = r_g / R$, where:

$$\boldsymbol{r_g = \frac{2GM}{c^2} \approx \frac{2.95M}{M_\odot}} \qquad (\mathbf{1.3}).$$

- The Schwarzschild radius or gravitational radius. Acceleration due to gravity at the stellar surface is defined by :

$$\boldsymbol{g = GMR^{-2}\left(1 - x_g\right)^{-\frac{1}{2}} \approx 1.328 \times \frac{10^{14}\left(1 - x_g\right)^{-\frac{1}{2}}\left(\frac{M}{M_\odot}\right)R_6^{-2}cm}{c^2}} \qquad (\mathbf{1.4}).$$

Where $R_6 = R / (10^6\, km)$. The frequency of the photons at the surface in a locally inertial reference system (we denote this frequency ω_0) away from the star undergoes a gravitational redshift to a value ω_∞ in accordance with the formula:

$$\boldsymbol{z_g = \frac{\omega_0}{\omega_\infty} - 1 = \left(1 - x_g\right)^{-1/2} - 1} \qquad (\mathbf{1.5}).$$

Along with a radius R, determined by the length of the equator $2\pi R$ in a locally inertial reference system, often introducing the "apparent radius" for a distant observer:

$$\boldsymbol{R_\infty = R\left(1 + z_g\right)} \qquad (\mathbf{1.6}).$$

Models of the neutron star is traditionally considered a star with $M = 1.4\, M_\odot$ and $R = 10$ km ($R_\infty = 13$ km, $g = 2.425 \times 10^{14}$ cm^{-2}). Note that currently the most detailed model equations of state, is considered the

best, predicting a slightly lower compactness: R ≈ 12 km for M = 1.4 $M_{\odot}$ (see, for example. [Hae 06], Ch. 6).

I.4. Structure of neutron star envelopes

The atmosphere

Is a thin layer of plasma which establishs the spectrum of thermal electromagnetic radiation of the star. By the way, this radiation tell us about important information on many stellar parameters (eg temperature, chemical composition of the surface and gravitational acceleration, on magnetic field, etc.,) and, as a consequence, on the internal structure. The geometrical depth of the atmosphere changes from some ten centimeters in a hot neutron star down to some millimeters in a cold one. Very cold neutron stars may have no atmosphere at all but a solid surface.

Many physisicts make theoretical studies to the neutron star's atmospheres (e.g., Pavlov et al [Pav 95]; Pavlov and Zavlin [Pav 98]). The creation of the atmosphere models, in particular for the cold neutron stars (in which the surface temperature $Ts \lesssim 10^6\,K$) in the presence of strong magnetic fields 10^{11}– $10^{14}\,G$, is far from being complete due to the complication of the calculations of the equation of state and spectral opacity of the plasma atmospher.

Ocean

The bottom of the ocean of the neutron star is situated at the melting point with the mass density ρ_m, and its outer frontier is quite arbitrary, since in a usual neutron star ocean goes into the atmosphere continuously, without the interface. The exclusion, as in the case of the

solid crust, are neutron stars with sufficiently strong magnetic field, which can guide to the absence of an optically thick atmosphere and its replacement of the liquid frontier. In most parts of the ocean substance consists of "naked" nuclei surrounded by degenerate electrons. In the surface layers of the ocean, however, a nucleus with a sufficiently large charge can polarise the electrons (this happens when $\rho \ll \rho_{rigid} \approx 22Z^2 A$). Therefore, in general, one speak of ions surrounded by electrons, implying ions, both fully and partially ionize atoms.

The substance of the ocean represents a Coulomb liquid. In large parts of the ocean Coulomb liquid is strongly coupled, that is the characteristic potential energy of the Coulomb interaction of nuclei greater than their kinetic energy. As a result, one of the most significant problems in the theoretical investigation of this matter is adequately account for the influence of microscopic correlations in the positions of the ions studied the macroscopic physical properties of matter.

Outer crust

The outer crust of neutron stars have a thickness of several hundred meters and consist of electron-ion plasma, and almost everywhere (except, perhaps, the outer layer thickness of several meters, where the density does not exceed $10^6\ g\ cm^{-3}$), the ionization is complete, that is, the ions are atomic nuclei and free electrons are strongly degenerate. In this case, the total pressure is determined mainly by the pressure of degenerate electrons. At $\rho \gtrsim 10^6\ g\ cm^{-3}$ electrons become relativistic (ie, their Fermi momentum p_F is comparable to $m_e c$) and at $\rho \gg 10^6\ g\ cm^{-3}$-ultrarelativistic ($p_F \gg m_e c$). At such densities, the ions form a tightly-coupled Coulomb liquid (ie liquid, whose properties are governed mainly by the Coulomb interaction between ions) or Coulomb crystals.

In the deep layers of the outer shells of the electron Fermi energy increases so that the cores are enriched by neutrons due to beta-grabs, and finally, at $\rho = \rho_{drip}$, where free neutrons appear, the border between the outer and inner crust of neutron stars.

The inner crust (the inner envelope)

The inner crust can be about one kilometer to several kilometers thick. The density ρ in the inner crust varies from $\rho_{drip} \approx 4.3 \times 10^{11}\ g\ cm^{-3}$ at the upper boundary in which neutrons start to drip from nuclei producing a free–neutron gas to $\sim 0{,}5\ \rho_0$ at the base. Here, ρ_0 is the saturation nuclear matter density the matter of the inner crust consists of electrons, free neutrons, and neutron-rich atomic nuclei The fraction of free neutrons increases with growing ρ. The neutronization at $\rho \approx \rho_{drip}$ greatly softens the EOS, but at the crust bottom the repulsive short-range component of the neutron-neutron interaction comes into play and introduces a considerable stiffness.

The pressure in the inner crust of a neutron star is created mainly degenerate neutrons. At the same time, superfluidity can lead to suppression of heat, and as a result - to the fact that the contribution of atomic nuclei in the heat capacity of the inner crust becomes crucial. Nucleus form a crystal lattice, supported mainly by the Coulomb interaction - the Coulomb (or Wigner) crystal. Therefore, an adequate description of their contribution can be obtained by considering the gas collective vibrational excitations of phonons. Electrons, being a relativistic and highly degenerate, do not give a significant contribution to the heat inside the crust is not too low temperatures. However, their contribution can be decisive when the temperature of the Coulomb crystal falls far below the Debye temperature, which leads to "freezing out" of the phonon excitations.

Electrical conductivity principally is supplied by electrons in the inner crust of a neutron star. In this case, it is essentially due to the scattering of electrons by phonons of ionic crystal lattice, the dominant at relatively high temperatures, and their scattering by lattice defects and impurities, giving a residual resistance at low temperatures. Ions (atomic nuclei) do not provide a tangible contribution to the conductivity, being mounted in the Coulomb crystal lattice. At the same time as the thermal conductivity is provided by electrons (the main scattering mechanisms are the same as that for electrical conductivity, but in addition thereto may be significant and electron-electron collision), and phonons and neutrons. In the presence of lattice defects and impurities that impede electronic heat transfer, phonons can be major agents of heat transfer [Chu 07]. Significant heat carriers in the inner crust and neutrons can be, especially the superfluid [Agu 09].

Mantle

The mantle situate between the bottom of the outer crust and the core of a neutron star may be a layer, in the density range from $\approx \frac{1}{3}\rho_0$ *to* $\approx \frac{1}{2}\rho_0$ called in [Pet 98], mantle, where the equilibrium atomic nuclei take exotic forms. Mantle, if it exists, consists of several layers containing such phases of matter, in which atomic nuclei become essentially nonspherical**.** Whereas the spherical nucleus form a three-dimensional crystal lattice, the phases of matter containing a “pasta” phases such as slabs or cylinders, have similar properties to liquid crystals.

The presence of the mantle is predicted not all modern equations of state of nuclear matter: for some models of such a state of matter is energetically unfavorable. As shown in [Gus 04], in the mantle may be allowed direct Urca process of neutrino emission, impossible in the other shells of neutron stars and have a high intensity. Therefore, the presence

of the mantle can accelerate the cooling of neutron stars and thus appear in the observations.

The outer core

The outer core of a neutron star typically has a thickness of several kilometers and the density of matter in the range $0.5\rho_0 \lesssim \rho \lesssim 2\rho_0$. Its matter consists of neutrons with several per cent admixture of protons p, electrons, and possibly muons μ (the so called $npe\mu$ composition). The conditions of electric neutrality and beta equilibrium establish the state of his matter, by using a microscopic model of many-body nucleon interaction. The beta equilibrium implies the equilibrium with respect to the beta (muon) decay of neutrons and inverse processes. All $npe\mu$-plasma components are strongly degenerate. An ideal Fermi gases is made by electrons and muons. The neutrons and protons interact by strong nuclear forces, which make a strongly interacting Fermi liquid and it may be in superfluid state.

The inner core

It can be more than a few kilometers in radius and contain a central density as high $0.5\rho_0 \lesssim \rho \lesssim 2\rho_0$. We don't know a lot about the composition and neither the equation of state of the inner core. Only we have several hypotheses thet have been talked about in the literature and it is impossible to refuse any of them at present:

(1) Large proton portion ($> 11\%$) and/or hyperonization of matter - the emergence of various hyperons like Σ^- and Λ and other hyperons.

(2) The second hypothesis supposes the appearance of pion condensation.

(3) The third hypothesis tell us about a phase transition to the strange quark matter composed of almost free u, d and s quarks with small portion of electrons .

(4) This hypothesis considers the emerges of kaon condensation.

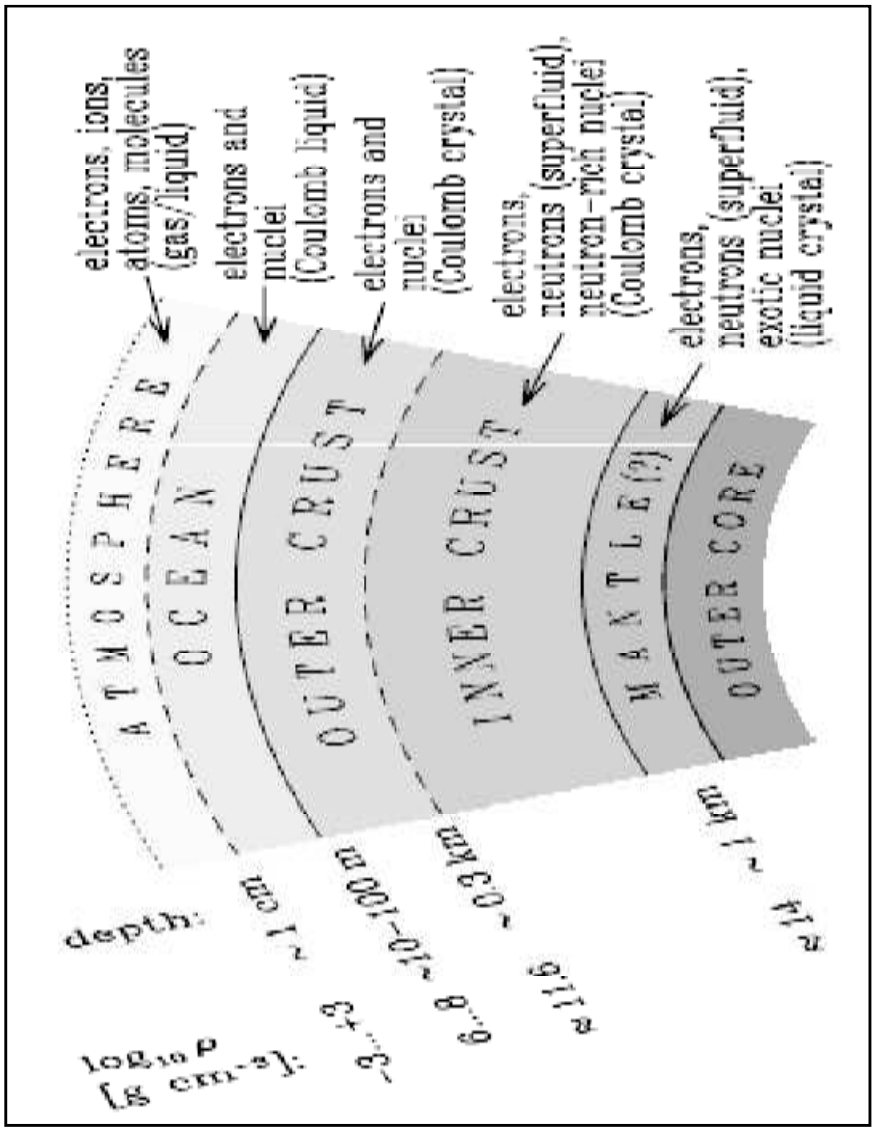

Figure 1.2:
Schematic structure of an envelope of a neutron star with the internal temperature $\sim 10^8\,K$ (From [Hae 07]).

I.5. Magnetic field and its evolution

Most known neutron stars today have magnetic fields attainable in the laboratory, with typical values on the surface in the $\sim 10^8 - 10^9\,\mathrm{G}$ for

millisecond pulsars, $B \sim 10^{10} - 10^{13}$ G for the "ordinary" radio pulsars $\sim 10^{14}$ G for the anomalous X-ray pulsars (AXP) and, according to the most widely accepted models of m today, in $\sim 10^{14} - 10^{15}$ G for the source of soft gamma repeaters (SGR). The field strength inside the star may be even higher. So, to explain the energy and AXP and SGR involved magnetic fields that reach the core of a neutron star at its birth in the values of $\sim 10^{16} - 10^{17}$ G. The theoretical limit, obtained numerically, is $B_{max} \sim 10^{18} - 10^{19}$ G, which agrees with the estimate based on the virial theorem . What creates these fields are still not reliably known. Magnitude of the magnetic field of a neutron star in $\sim 10^{12}$ G was predicted W. L. Ginsburg in 1964 (even before the discovery of pulsars), based on the assumption of conservation of magnetic flux of the supernova progenitor star during its collapse. Subsequently proposed various theoretical models of field generation with differential rotation, convection, magneto-rotational instability and thermomagnetic effects either in the explosion and collapse of a supernova, or in young neutron stars . In particular, According to the P- dynamo model, the core of a neutron star, born with a fairly short (millisecond) rotation period, acquires through its differential rotation of the toroidal magnetic field to $B \sim 10^{16}$ gauss, and for the initial rotation period ~ 30 ms pulsar magnetic field is created by convection. However, each of the proposed models is facing some difficulties when compared with the totality of data on neutron stars.

During the evolution of the neutron star, its magnetic field changes. These changes depend on many parameters and related physical processes. Occurs ohmic decay of the field, changing its configuration as a result of the Hall drift, possible reconnection of magnetic field lines at *quark* star.

Thermoelectric effects, as well as the significant dependence of the components of thermal conductivity, electrical conductivity and thermoelectric coefficients of the plasma temperature and magnetic field leads to the interdependence of the magnetic and thermal evolution. Accretion can also strongly influence the magnetic field near the surface.

If the magnetic field has its source Abrikosov vortices in the core of a neutron star, its evolution is largely determined by their interaction with other components of the nucleus, in particular - with the Feynman-Onsager vortices in a neutron superfluid, as well as conditions on core boundary, ie, the interaction of these vortices with the substance of the envelope.

Chapter II

General properties of neutron star's Coulomb plasma

II.1. The method of minimizing the free energy

When we consider the equilibrium properties of plasma in the envelopes of neutron stars in this work, we rely on a method of minimizing the Helmholtz free energy, the introduction of the model calculations, the equations of state of the plasma in [Har 60].Here and henceforth one mean by an equation of state significance of the term in a broad sense, ie not only the dependence of pressure on the density of matter, but also the values of other thermodynamic functions which are needed for modeling stellar structure and evolution. Unlike some other approaches, the method of minimizing the free energy ensures the consistency of calculations of various thermodynamic functions - in particular, the implementation of the Maxwell relations. The method consists in constructing the free energy $F(V,T,\{N_j\})$, where $\{N_j\}$ - a set of numbers of different particles that make up the plasma in the volume V, and finding the minimum of F for fixed V, taking into account the stoichiometric relationships: for example, if the system can proceed the reaction type $A \leftrightarrow B + C$, then the equilibrium must be satisfied the relation:

$$\frac{\partial F}{\partial N_A} = \frac{\partial F}{\partial N_B} + \frac{\partial F}{\partial N_C} \qquad (\mathbf{2.1}).$$

As is well known [LL5], if the free energy is given as a function of V and T, then all other thermodynamic functions can be obtained by

differentiating it. The pressure P, internal energy U and the entropy S are given by the first derivatives:

$$\boldsymbol{P} = -\left(\frac{\partial \boldsymbol{F}}{\partial \boldsymbol{V}}\right)_{T,\{N_j\}}, \boldsymbol{U} = -\left(\frac{\partial\left(\frac{\boldsymbol{F}}{\boldsymbol{T}}\right)}{\partial\left(\frac{\boldsymbol{1}}{\boldsymbol{T}}\right)}\right)_{\boldsymbol{V},\{N_j\}}, \boldsymbol{S} = -\left(\frac{\partial \boldsymbol{F}}{\partial \boldsymbol{T}}\right)_{\boldsymbol{V},\{N_j\}} \quad (\mathbf{2.2}).$$

Functions of the second order are obtained by differentiating the functions (2.2). In particular, astrophysical simulations play an important role logarithmic derivative of pressure on density and temperature.

$$\boldsymbol{\chi_T} = \left(\frac{\partial \ln \boldsymbol{P}}{\partial \ln \boldsymbol{T}}\right)_{\boldsymbol{V}}, \boldsymbol{\chi_\rho} = \left(\frac{\partial \ln \boldsymbol{P}}{\partial \ln \boldsymbol{V}}\right)_{\boldsymbol{T}} \quad (\mathbf{2.3}).$$

Specific heat at fixed volume and fixed pressure:

$$\boldsymbol{C_V} = \left(\frac{\partial \boldsymbol{S}}{\partial \ln \boldsymbol{T}}\right)_{\boldsymbol{V}}, \boldsymbol{C_p} = \left(\frac{\partial \boldsymbol{S}}{\partial \ln \boldsymbol{T}}\right)_{\boldsymbol{P}} \quad (\mathbf{2.4}).$$

As well as the adiabatic temperature gradient:

$$\boldsymbol{\nabla_{ad}} = \left(\frac{\partial \log \boldsymbol{T}}{\partial \log \boldsymbol{P}}\right)_{\boldsymbol{S}} \quad (\mathbf{2.5}).$$

In principle, all thermodynamic functions of the second order can be obtained from χ_T, χ_ρ and C_V on the basis of Maxwell's relations. In particular:

$$\boldsymbol{C_P} = \boldsymbol{C_V} + \frac{\boldsymbol{PV}}{\boldsymbol{T}}\frac{\boldsymbol{\chi_T^2}}{\boldsymbol{\chi_\rho}}, \boldsymbol{\nabla_{ad}} = \frac{\boldsymbol{\chi_T}}{\boldsymbol{\chi_T^2} + \boldsymbol{\chi_\rho}\, \boldsymbol{C_V T/(PV)}} \quad (\mathbf{2.6}).$$

The fundamental difficulty is that in many important cases F is not known explicitly, but it requires either the finding of constructing approximate models or complex numerical calculations. The technical and astrophysical applications, especially where we need to know the equation of state in a wide range of plasma parameters is practically impossible to carry out such numerical calculations required in each

point. In this chapter one developed approximate methods for calculating free energy and, through them, all the necessary thermodynamic functions of plasma, the most consistent with the current state of theory and, in particular, with the available literature results of numerical simulation from first principles. In the next section we introduce the basic parameters of plasma, and continue to consistently examine its thermodynamic functions in various approximations are valid for different ratios between these parameters that are running in various envelopes of neutron stars.

II.2. Parameters of the plasma

II.2.1. General settings

Let n_e - electron number density, and n_j - ion number density sorts $j = 1,2,\ldots$ with charges $Z_j e$ and masses $m_{ion}^{(j)} = A_j m_u$ where $m_u = 1.6605 \times 10^{-24}\, g$ - atomic mass unit, e - elementary charge. The index j enumerates how different chemical elements present in the mixture and ions of different ionization stages of one and the same element. Total number density of atomic nuclei (ions) is equal to the $n_{ion} = \sum_j n_j$. Electroneutrality requires:

$$\boldsymbol{n_e = \langle Z \rangle n_{ion}} \qquad (\mathbf{2.7}).$$

Here and below angular brackets without subscripts $\langle \ldots \rangle$ Denote an average over the ion species j:

$$\boldsymbol{\langle f \rangle = \frac{1}{n_{ion}} \sum_j n_j f_j} \qquad (\mathbf{2.8}).$$

When examined only one species of ions, we shall omit brackets and either omit the index j, or replace it on the index «ion» or «i», denoting the ions.

Total concentration of baryons in the envelopes of neutron stars, n_b, is approximately equal to $A' n_{ion}$ where $A' = \langle A \rangle + A''$ and A''- the number

of free neutrons attributable to a single atomic nucleus: $A''n_{ion} = n_n(1 - w)$ where n_n - the local number density of free neutrons (obviously, in the outer envelopes of $A'' = 0$ and $A' = \langle A \rangle$, but in the inner envelopes $A' > \langle A \rangle$.

Generally speaking, the mass density of relativistic objects is defined as $\rho = \mathcal{E}/c^2$, where $\mathcal{E}$ - the total energy density. However, in the shells of neutron stars is sufficiently accurate approximation$\rho = m_u n_b$.

At sufficiently low density or high temperature equilibrium composition of matter includes positrons and photons in quantities that may affect the thermodynamic properties. For simplicity, we neglect their contribution, because it is negligible for most considered in this thesis's applications. If necessary, the contribution of positrons can easily be taken into account by the following formula for electrons by replacing them in the chemical potential of the electron μ_e the chemical potential of positrons in equilibrium equal$-m_e c^2 - \mu_e$, a contribution of the photon gas is given to its free energy:

$$\boldsymbol{F_{rad} = -\left(\frac{4\sigma_{SB}}{3c}\right) VT^4} \qquad (\mathbf{2.9}).$$

II.2.2. Electrons

The state of the electron gas in thermodynamic equilibrium is determined by the electron number density n_e, and temperature T. In plasma physics, instead of n_e, and often introduce the dimensionless density parameter $r_s = a_e/a_B$, where a_B - the Bohr radius, and $a_e = \left(\frac{4}{3}\pi n_e\right)^{-1/3}$. The r_s is easy to assess the to relation $r_s = 1.1723\, n_{24}^{-1/3}$, where the $n_{24} = n/10^{24}\ \mathrm{cm}^{-3}$, or $r_s = (\rho_{0s}/\rho)^{1/3}$, where $\rho_{0s} = 2{,}6752\,(A'/\langle Z \rangle)\ g\ cm^{-3}$. In astrophysics, instead of T it is convenient to introduce the parameter of relativity:

$$\boldsymbol{x_r = \frac{p_F}{m_e c} = 1.00884\left(\frac{\rho_6\langle Z\rangle}{A'}\right)^{1/3} = 0.014005 r_s^{-1}} \qquad (\mathbf{2.10}).$$

Where $p_F = \hbar k_F = \hbar\,(3\pi n_e)^{1/3}$ - is the Fermi momentum, and $\rho_6 = \rho/10^6\ \mathrm{g\,cm^{-3}}$ - mass density in grams per cubic centimeters. The momentum of p_F corresponds to the kinetic Fermi energy $\epsilon_F = \sqrt{m_e^2c^2 + p_F^2}$ equal chemical potential μ_e at $T \to 0$, and the Fermi temperature $T_F = \epsilon_F/k_B = T_r(\gamma_r - 1)$,where $T_r = m_e c^2/k_B = 5.93 \times 10^9\ K$ - the relativistic temperature unit, and ($\gamma_r = \sqrt{1 + x_r^2}$ the Lorentz factor of electrons at the Fermi surface. If $x_r \ll 1$, then $T_F \approx 1{,}163 \times 10^6\ r_S^{-2}\ K$. Effects special theory of relativity controlled parameter x_r, in a degenerate plasma (for $T \ll T_F$) and the parameter: $t_r \equiv T/T_r$; in a nondegenerate plasma (for $T \gg T_F$).

The degeneracy parameter is defined as:

$$\boldsymbol{\theta = \frac{T}{T_F}} \qquad (\mathbf{2.11}).$$

In the no relativistic case ($x_r \ll 1$) it is equal to $\theta = \frac{0.543 r_s}{\Gamma_e} = 3.411837\left(\frac{a_e}{\lambda_e}\right)^2$ here we have introduced two more parameters:

$$\boldsymbol{\Gamma_e = \frac{e^2}{a_e k_B T} \approx \frac{22.75}{T_6}\left(\rho_6 \frac{\langle Z\rangle}{A'}\right)^{1/3}} \qquad \mathbf{2.12}).$$

Where $T_6 = T/\,10^6\ K$, characterizes the Coulomb interaction between the nondegenerate electrons, and:

$$\boldsymbol{\lambda_e = \left(\frac{2\pi\hbar^2}{m_e\, k_B T}\right)^{1/3}} \qquad (\mathbf{2.13}).$$

Is the thermal de Broglie wavelength. In contrast, the ultra relativistic, if ($x_r \gg 1$) we have $\theta = (263\Gamma_e)^{-1}$.

Another convenient parameter characterizing chemical degeneration is the ratio:

$$\boldsymbol{\chi_e = \frac{\mu_e}{k_B T}} \qquad (\mathbf{2.14}).$$

There are also useful to introduce the electron plasma temperature T_{pe}, relevant energy $\hbar\omega_{pe}$:

$$\boldsymbol{T_{pe} = \frac{\hbar\omega_{pe}}{k_B} \approx 3.3 \times 10^8 x_r\sqrt{x_r/\gamma_r}\, K} \qquad (\mathbf{2.15}).$$

Where

$$\boldsymbol{\omega_{pe} = \left(\frac{4\pi e^{2n_e}}{m_e^*}\right)^{\frac{1}{2}}} \qquad (\mathbf{2.16}).$$

Is the plasma 'frequency of electrons, typical for their collective oscillations, and $m_e^* = m_e\gamma_r$- effective dynamic mass of the electron at the Fermi surface. Electromagnetic oscillations with angular frequency $\omega < \omega_{pe}$ can not be distributed freely in non-magnetic plasma, and hence the thermal spectrum of the star is formed mainly in the region where $\gtrsim T_{pe}$.

Later, we need the values that characterize the response of the electron gas at the Coulomb effects. The relevant parameters - the radius of the electronic screening r_e and its inverse wave vector of Thomas-Fermi k_{TF}:

$$\boldsymbol{k_{TF} = r_e^{-1} = \left(4\pi e^2 \frac{\partial n_e}{\partial \mu_e}\right)^{1/2}} \qquad (\mathbf{2.17}).$$

In a no degenerate gas ($T \gg T_F$) $\partial n_e/\partial\mu_e = n_e/(k_BT)$, so those $r_e \approx a_e/\sqrt{\Gamma_e}$. In the opposite limiting case of strongly degenerate gas ($T \ll T_F$) we have:

$$\boldsymbol{k_{TF} = 2\sqrt{\frac{\alpha_f\gamma_r}{(\pi x_r)}}k_F = 0.185\, a_e^{-1}\sqrt{\frac{\gamma_r}{x_r}}} \qquad (\mathbf{2.18}).$$

Where $\alpha_f = e^2/c = 1/136.037$ – is the fine structure constant.

II.2.3. Ions

In the envelopes of neutron stars, the ions are always no relativistic, so only this case we will consider. Coulomb interaction of ions of species j characterized by the parameter:

$$\boldsymbol{\Gamma_j = \Gamma_e Z_j^{5/3} = \frac{(Z_j e)^2}{a_{ion}^{(j)} k_B T}} \qquad (\mathbf{2.19}).$$

Where

$$\boldsymbol{a_{ion}^{(j)} = a_e Z_j^{1/3}} \qquad (\mathbf{2.20}).$$

Called the radius of the ion sphere. The other characteristic length parameter – the thermal De Broglie wavelength of ions of species j,

$$\boldsymbol{\lambda_j = \left(\frac{2\pi\hbar^2}{m_j k_B T}\right)^{1/3}} \qquad (\mathbf{2.21}).$$

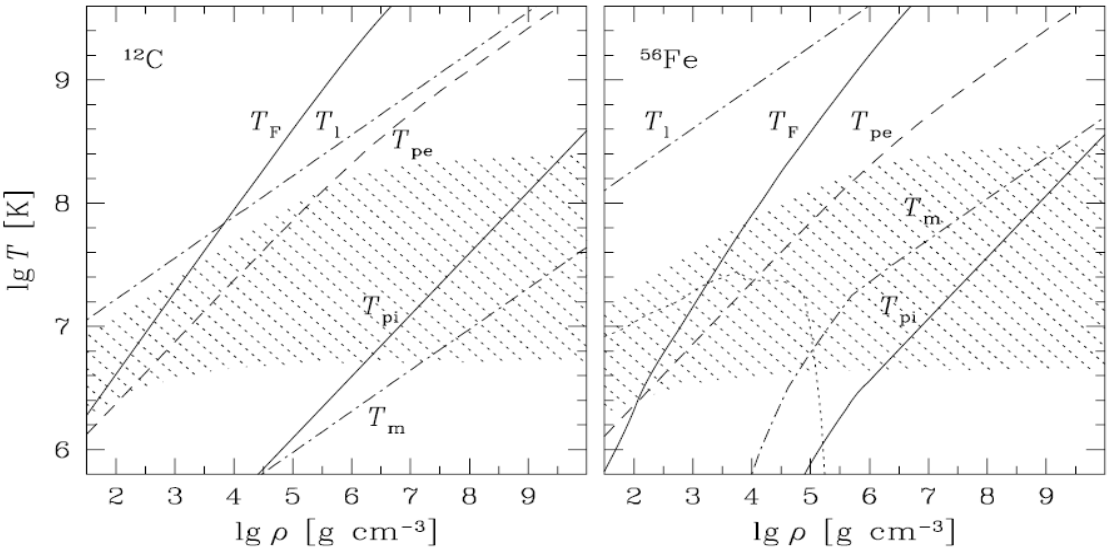

Figure 2.1. *Density-temperature diagram for the outer envelope composed of carbon (left) or iron (right). We show the electron Fermi temperature (T_F), the electron and ion plasma temperatures (T_{pe} and T_{pi}), the temperature of the gradual gas-liquid transition (T_l), and the temperature of the sharp liquid-solid phase transition (T_m). Shaded are the regions of typical temperatures in the outer envelopes of middle-aged cooling neutron stars (which are $\sim 10^4 - 10^6$ years old). The lower left domain on the right panel, separated by the dotted line, is characterized by strong electron response or bound-state formation. From [Hae 07].*

Similar to Γ_e , in a multicomponent plasma, the Coulomb coupling strength is characterized by the average parameter:

$$\boldsymbol{\Gamma = \Gamma_e \langle Z_j^{5/3} \rangle} \qquad (\mathbf{2.22}).$$

This parameter specifies, in particular, states of matter: if $\Gamma \ll 1$ ions form a classical Boltzmann gas, with increasing Γ with increasing density or decreasing temperature to $T \approx T_1$, where T_1 corresponds to the value $\Gamma = 1$, the gas gradually acquires the properties of liquid : with further increase of Γ phase transition of a Coulomb fluid in a Coulomb crystal (temperature $T = T_m$, "where T_m corresponds to $\Gamma = \Gamma_m$,).

In the gas phase the characteristic length of the Coulomb screening by ions is the Debye length r_D or his inverse the Debye wave number q_D:

$$r_D = q_D^{-1} = \left[\frac{4\pi}{k_B T} \sum_j n_j \left(Z_j e \right)^2 \right]^{-1/2} \qquad (2.23).$$

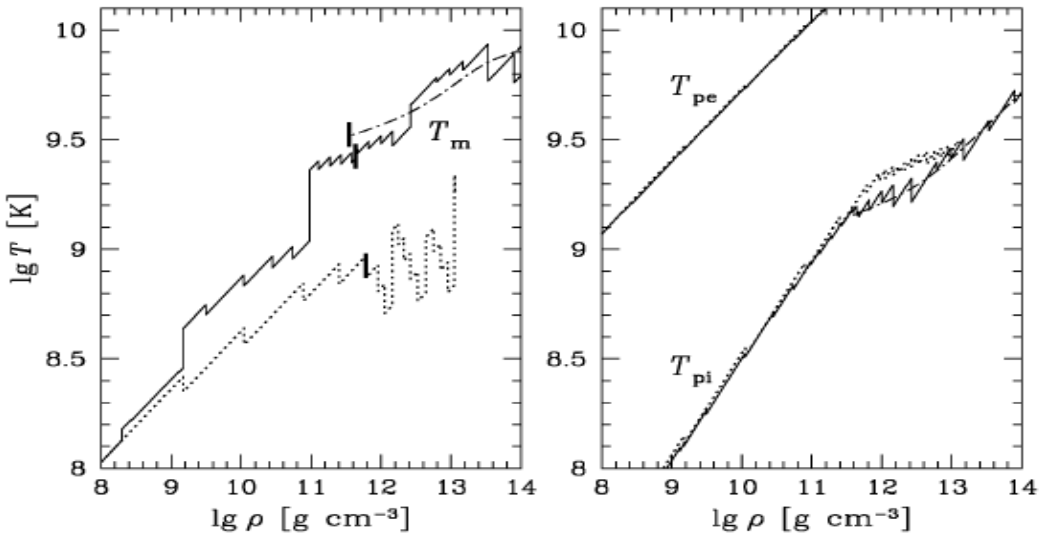

Figure 2.2: *Left panel: melting temperature versus density. Right panel: electron and ion plasma temperature versus density. Solid lines: the ground-state composition of the crust is assumed: Haensel and Pichon [Hae 94] for the outer crust, and Negele and* Vautherin [Neg 73] for the inner crust. Dot lines: accreted *crust, as calculated by Haensel and Zdunik [Hae 08]. Jumps result from discontinuous changes of Z and A.Dot-dash line: results obtained for the compressible liquid drop model of Douchin and Haensel [Dou 01] for the ground state of the inner crust; a smooth behavior (absence of jumps) results from the approximation inherent in the compressible liquid drop model. Thick vertical dashes: neutron drip point for a given crust model. Figure made by A.Y. Potekhin (eg [Hae 07])*

- and the total plasma screening - wave number :

$$\boldsymbol{k_s = \left(q_D^2 + k_{TF}^2\right)^{1/2}} \quad (\mathbf{2.24}).$$

Influence of quantum effects on the dynamics and thermodynamics of the ion becomes important when $T \ll T_{pi}$ where:

$$\boldsymbol{T_{pi} = \frac{\hbar \omega_{pi}}{k_B} \approx 7.832 \times 10^6 \left(\frac{\rho_6}{A'} \langle \frac{Z^2}{A} \rangle\right)^{\frac{1}{2}} K} \quad (\mathbf{2.25}).$$

- is the ion plasma temperature, and :

$$\boldsymbol{\omega_{pi} = \left(4\pi e^2 n_{ion} \langle \frac{Z^2}{m_{ion}} \rangle\right)^{1/2}} \quad (\mathbf{2.26}).$$

- is the ion plasma frequency. Quantum ion parameter is $\eta = T/T_{pi}$.

In one-component plasma of ions (OCP- one-component plasma) can be written:

$$\boldsymbol{\eta = \Gamma \sqrt{3/R_S}} \quad (\mathbf{2.27}).$$

Where $R_S = a_{ion} m_{ion} (Ze)^2 / \hbar^2 = r_s (m_{ion} / m_e) Z^{7/3}$ – The ion density parameter.

The course introduced in this section, the characteristic temperature depending on the density for carbon and iron plasma in the outer shells of neutron stars is shown in Fig. 1, and for the substance of external and internal envelopes of stars in the ground state (the composition is taken according to the classical model than – [Neg 73]).

II.3. Fully ionized Coulomb plasma

The majority of the envelopes of neutron stars are fully ionized. The case of complete ionization is determined by the requirement that the characteristic distance between the ions a_{ion} was small compared with the Thomas-Fermi radius of the atomic core, $r_a \sim a_B/Z^{1/3}$ that is equivalent to $\rho \gg \rho_{eip} = (m_u/a_B^3)AZ \approx 11AZ\ g/cm^3$ =. In $\rho \gg \rho_{eip}$ in the outer envelopes of the neutron star model can be applied electron-ion plasma,

which addresses the point ions in an electron liquid. In general, the electron fluid is compressible, the ions and electrons interact via Coulomb forces and are therefore correlated. Coulomb correlations between ions and the ions with electrons and electrons with each other, tend to be much different in strength, so it makes sense to study them in sequence on the basis of expansion of the free energy of the form:

$$\boldsymbol{F = F_{id}^{(i)} + F_{id}^{(e)} + F_{ii} + F_{ie} + F_{ee}} \qquad (\mathbf{2.28}).$$

Here $F_{id}^{(i)}$ and $F_{id}^{(e)}$ – are the free energy of an ideal Boltzmann gas of ions and the Fermi gas of electrons, respectively, without taking into account the correlations, in F_{ii} included the Coulomb interaction between the ions without regard to their correlations with the electrons, but with the Coulomb energy of their interaction with "incompressible" electronic background providing electrical neutrality of the plasma; F_{ie} includes interactions between the ions and polarizable electron background related to deviations from the approximation of an incompressible background and, finally, F_{ee} a member of the deviations takes into account the interaction of the electronic subsystem. The last three terms in the sum contribute to the free energy due to interactions.

$$\boldsymbol{F_{ex} = F_{ii} + F_{ie} + F_{ee}} \qquad (\mathbf{2.29}).$$

The expansion (2.28) induces the corresponding expansion of other thermodynamic functions. In particular, the pressure appears in the form.

Table 2.1. *Order-of-magnitude of the pressure components in Eq. (2.30) for the matter containing strongly degenerate electrons and fully ionized, strongly coupled ions (after Yakovlev & Shalybkov 1989). The parameter $a_B = \alpha_f/\beta_r$ is small at $\rho \ll 1\ g\ cm^{-3}$. [Hae 07]*

$P_{\rm part}$	$\lvert P_{\rm part}\rvert/P_{\rm id}^{(e)}$	Comment
$P_{\rm id}^{(e)}$	1	Ideal degenerate electron gas, leading term
$P_{\rm xc}$	$\lesssim \alpha_{\rm B}$	Exchange-correlation corrections in electron gas
$P_{\rm id}^{(\rm i)}$	$\sim T/(ZT_{\rm F}) \sim \alpha_{\rm B} Z^{2/3}/\Gamma$	Ideal ion gas contribution
$P_{\rm ii}$	$\sim \alpha_{\rm B} Z^{2/3}$	Coulomb corrections in the rigid electron background
$P_{\rm ie}$	$\sim \alpha_{\rm B}^2 Z^{4/3}$	Coulomb corrections owing to electron polarization

$$\boldsymbol{P = P_{id}^{(i)} + P_{id}^{(e)} + P_{ii} + P_{ie} + P_{ee}} \qquad (\mathbf{2.30}).$$

Table 1 gives an idea of the characteristic ratios on the order of magnitude between the different components in a strongly degenerate plasma. The corresponding contributions to the internal energy have the same order of magnitude as the contributions to the pressure, but the contribution of second-order functions can be ranked differently (for example, as will be shown below, the heat of the Coulomb crystal can be determined not by electrons and ions).

In a weakly degenerate plasma hierarchy of contributions shown in Table 1, collapsing: different terms may become comparable in magnitude.

II.3.1. Ideal electron gas

The free energy of an ideal electron gas can be obtained from the general formula:

$$\boldsymbol{F_{id}^{(e)} = \mu_e N_e - P_{id}^{(e)} V} \qquad (\mathbf{2.31}).$$

and the pressure $P_{id}^{(e)}$ and electron density n_e, in turn, expressed in terms of μ_e and T as:

$$\boldsymbol{P_{id}^{(e)} = 2k_BT \int \ln\left[1 + \exp\left(\frac{\mu_e - \epsilon_e}{k_BT}\right)\right] \frac{d^3p}{(2\pi\hbar)^3} =}$$

(2.32).

$$\boldsymbol{= \frac{8}{3\sqrt{\pi}} \frac{k_BT}{\lambda_e^3} \left[I_{3/2}(\chi_e, t_r) + \frac{t_r}{2} I_{5/2}(\chi_e, t_r)\right]}$$

$$\boldsymbol{n_e = \int \frac{1}{\left[1 + \exp\left(\frac{\epsilon_e - \mu_e}{k_BT}\right)\right]} \frac{d^3p}{(2\pi\hbar)^3} =}$$

(2.33).

$$\boldsymbol{= \frac{4}{\sqrt{\pi}\lambda_e^3} \left[I_{1/2}(\chi_e, t_r) + t_r I_{3/2}(\chi_e, t_r)\right]}$$

where $\epsilon_e = c\sqrt{(m_ec)^2 + p^2} - m_ec^2$ - kinetic energy of the electron with momentum p, and:

$$\boldsymbol{I_\nu(\chi_e, \tau) = \int_0^\infty \frac{x^\nu (1 + \tau x/2)^{1/2}}{\exp(x - \chi) + 1} dx} \qquad \textbf{(2.34)}.$$

- is the Fermi-Dirac integrals. The internal energy equals to:

$$\boldsymbol{U_{id}^{(e)} = \frac{4k_BT}{\sqrt{\pi}} \frac{V}{\lambda_e^3} \left[I_{3/2}(\chi_e, t_r) + t_r I_{5/2}(\chi_e, t_r)\right]} \qquad \textbf{(2.35)}.$$

II.3.2. Coulomb crystal (harmonic approximation)

Below the melting temperature $T < T_m$ an infinite ion motion is replaced by oscillations near equilibrium positions, which means that a crystal is formed. The ground state of the OCP of ions corresponds to the body-centered cubic (bcc) lattice. In a real crystal, this happens at high

densities (at $r_s \ll 1$), whereas other types of lattices (face-centered cubic, fcc; hexagonal close-packed, hcp) may form the ground state at $r_s \gtrsim 1$ [Koh 96]). Note that the simple cubic Coulomb lattice is unstable (as any simple cubic lattice of particles interacting via central forces; M. Born in 1940).

We recall some standard definitions [Kit 86], which will be useful later. The primitive cell of the crystal lattice, whose center coincides with the equilibrium position of the ion, called the Wigner-Seitz cell. In the study of strongly coupled Coulomb systems, it is often very useful to deal with the model of the ion sphere in which the real cell is approximately replaced by a sphere of the same volume, the radius of the Wigner-Seitz cell for the case considered here of ions of one species is a_{ion}. The reciprocal lattice is determined by the primitive translation vector $\vec{b}_l$, defined by the equalities $\vec{b}_l \cdot \vec{a}_m = 2\pi\delta_{lm}$, where $\vec{a}_m$ – is the primitive translation vectors of the crystal lattice. Wigner-Seitz cell has an reciprocal lattice called the Brillouin zone, and its volume is equal :

$$\boldsymbol{V_{BZ} = \frac{4\pi}{3} q_{BZ}^3 = (2\pi)^3 n_{ion}} \qquad (\mathbf{2.36}).$$

To study the Coulomb (Wigner) crystals has been used successfully (see, for example. [Bai 01][Pol 73]) the harmonic approximation in which the potential energy of each ion in the crystal is described by the harmonic oscillator potential (eg, [LL5]). In this approximation the free energy of the lattice is:

$$\boldsymbol{F_{lat} = U_0 + U_{quant} + 3N_{ion} k_B T \langle \ln\left[1 - \exp(-z_{\vec{ks}})\right] \rangle_{ph}} \qquad (\mathbf{2.37}).$$

where $U_0 = N_{ion} C_0 (Ze)^2 / a_{ion}$-is the classical static-lattice energy, $C_0 \approx -0{,}9$ is the Madelung constant, $U_{quant} = \frac{3}{2} N_{ion} \hbar \omega_{pi} u_1$ – is the zero-point energy of quantum vibrations, u_1 – belongs to the family of average phonon frequency moments:

$$u_p \equiv \frac{\langle \omega^p_{\vec{k}s} \rangle_{ph}}{\omega^p_{pi}} \quad (2.38).$$

$\omega_{\vec{k}s}$ – the eigenfrequencies:

$$z_{\vec{k}s} \equiv \frac{\hbar \omega_{\vec{k}s}}{k_B T} \quad (2.39).$$

the $\langle \dots \rangle_{ph}$ denotes the average over the phonon wave vectors $\vec{k}$ in the first Brillouin zone and the branches of crystal oscillation modes s:

$$\langle f_s(\vec{k}) \rangle_{ph} = \frac{1}{3V_{BZ}} \sum_s \int_{V_{BZ}} f_s(\vec{k}) d\vec{k} \quad (2.40).$$

the values of C_0 and u_p are given in Table 2.1. In the crystal, we can not distinguish the energy of an ideal gas, so F_{lat} replaces $F_{id}^{(i)} + F_{ii}$ in equation (2.28).

In the general case that goes beyond the harmonic approximation, we have:

$$f_{lat} \equiv \frac{F_{lat}}{N_{ion} k_B T} = C_0 \Gamma + \frac{3}{2} u_1 \eta + f_{lat} + f_{ah} \quad (2.41).$$

Where the first three terms on the right side correspond to the three terms in the right side of equation (2.37), and f_{ah} - is a correction for anharmonicity.

II.3.3. Ionic Coulomb liquid (theory)

Taken to separate the free energy of the Coulomb fluid component that describes the Boltzmann gas of ions, and the term describing the Coulomb interaction, as in equation (2.28). In this section we consider a single-component ion plasma in an incompressible background - OCP. In this case,

$$F_{id}^{(i)} = N_{ion} k_B T \left[\ln \left(n_{ion} \frac{\lambda_{ion}^3}{g_{spin}^{(i)}} \right) - 1 \right] \quad (2.42).$$

where $g_{spin}^{(i)}$ is the spin degeneracy of the ion.

Equation (2.60) for the OCP can be expressed in terms of dimensionless parameters:

$$\frac{\boldsymbol{F_{id}^{(i)}}}{\boldsymbol{N_{ion}\ k_BT}} = \mathbf{3}\ln\boldsymbol{\eta} - \frac{\mathbf{3}}{\mathbf{2}}\ln\boldsymbol{\Gamma}\ - \frac{\mathbf{1}}{\mathbf{2}}\ln\frac{\mathbf{6}}{\boldsymbol{\pi}} - \ln\boldsymbol{g_{spin}^{(i)}} - \mathbf{1} \qquad (\mathbf{2.43}).$$

the subscript *"ii."* distinct the *excess* terms their study is little bit more complex (we talk about terms that occur from the Coulomb interactions in the case of rigid electron background) in a classical OCP the quantity The function $F_{ii}/N_{ion}k_BT$ depend on a single argument Γ. It determines all other excess (e.g., [Yak 89]).

the theory of Debye & Huckel (1923) is appropriate in the case ($\Gamma \ll 1$),. And it gives a formula for the free energy of a mixture of non-relativistic weakly coupled ions with charges Z_je and number densities n_j [LL5] :

$$\frac{\boldsymbol{F_{ex}(\Gamma \to 0)}}{\boldsymbol{V}} = -\frac{\mathbf{2}\boldsymbol{e^3}}{\mathbf{3}}\left(\frac{\boldsymbol{\pi}}{\boldsymbol{k_BT}}\right)^{\mathbf{1/2}}\left(\sum_j \boldsymbol{n_jZ_j^2}\right)^{\mathbf{3/2}} \qquad (\mathbf{2.44}).$$

It becomes for the OCP:

$$\boldsymbol{U_{ii,DH}} = -\left(\frac{\sqrt{\mathbf{3}}}{\mathbf{2}}\right)\boldsymbol{N_{ion}k_BT\ \Gamma^{3/2}}\ ,\boldsymbol{F_{ii,DH}} = -\left(\frac{\mathbf{1}}{\sqrt{\mathbf{3}}}\right)\boldsymbol{N_{ion}k_BT\ \Gamma^{3/2}}, \quad (\mathbf{2.45}).$$

The perturbation theory gives corrections of the order Γ^3 to Eq. (2.45) [Abe 59] . Cohen and Murphy [Coh 69] computed the correction up to the order $\Gamma^{9/2}$. The low-Γ expansion of the internal energy is given by:

$$\frac{\boldsymbol{U_{ii}}}{\boldsymbol{N_{ion}k_BT}} = -\frac{\sqrt{\mathbf{3}}}{\mathbf{2}}\boldsymbol{\Gamma^{\frac{3}{2}}} - \mathbf{3}\boldsymbol{\Gamma^3}\left[\frac{\mathbf{3}}{\mathbf{8}}\ln(\mathbf{3}\boldsymbol{\Gamma}) + \frac{\boldsymbol{C_E}}{\mathbf{2}} - \frac{\mathbf{1}}{\mathbf{3}}\right] - \qquad (\mathbf{2.46}).$$

$$-\boldsymbol{\Gamma^{9/2}}\left(\mathbf{1.6875}\sqrt{\mathbf{3}}\ln\boldsymbol{\Gamma} - \mathbf{0.23511}\right) + \cdots$$

where $C_E = 0.57721\ldots$ is the Euler constant. So, one have:

$$\frac{F_{ii}}{N_{ion}k_BT} = -\frac{\Gamma^{\frac{3}{2}}}{\sqrt{3}} - \Gamma^3\left(\frac{3}{8}\ln(\Gamma) + 0.24225\right) - \quad (2.47).$$

$$-\Gamma^{9/2}\,(0.64952\,\ln\Gamma - 0.19658) + \cdots$$

To study liquid and solid phases of the OCP of ions at large value of the coulomb coupling parameter Γ authors used numerical methods (typical examples, one would see Baus and Hansen [Bau 80] ; Ichimaru *et al.*[Ich 87]). the Monte Carlo method (Brush *et al.*,.[Bru 1966]) and the hypernetted chain (HNC) method (e.g., Hansen and McDonald.[Han 76]) The most powerful of them.

The Monte Carlo methods begin with an initial configuration that contains N_{ion} ions and one allow make succeeding ion displacements. The potential energy $\mathcal{U}(\vec{r}_1\ldots,\vec{r}_{N_{ion}})$ reside from ions-ions Coulomb interaction and between ions and the uniform electron background is computed in each step and one sums those contributions with a suitable weight to have the excess internal energy :

$$U_{ii} = \frac{1}{V^N\mathcal{Z}_{conf}}\int \mathcal{U}\exp\left(-\frac{\mathcal{U}}{k_BT}\right)\prod_{q=1}^{N_{ion}} d\vec{r}_q \quad (2.48).$$

where:

$$\mathcal{Z}_{conf} = \frac{1}{V^N}\int \exp\left(-\frac{\mathcal{U}}{k_BT}\right)\prod_{q=1}^{N_{ion}} d\vec{r}_q \quad (2.49).$$

is the so-called the configurationally part of the partition function.

The hypernetted chain method –on the contrary- is based on integrating equation for the radial pair distribution Function :

$$g(|\vec{r}_1 - \vec{r}_2|) = \frac{1}{N^2\,\mathcal{Z}_{conf}\,V^{N-2}}\int \exp\left(-\frac{\mathcal{U}}{k_BT}\right)\prod_{q=3}^{N_{ion}} d\vec{r}_q \quad (2.50).$$

It can be obtained in different approximations.

II.3.4. Structural factor: Multiphonon processes

We need the characteristics of pair correlations of ions, called the dynamic structure factor. Ion structure factor describes the correlation of their position in space and time. The ion correlations in momentum space are described by the dynamical ion structure factor:

$$\boldsymbol{S(\vec{q},\omega) = \frac{1}{2\pi N}\int_{-\infty}^{+\infty} dt \int d\vec{x}\, d\vec{x}' e^{i\vec{q}\cdot(\vec{x}-\vec{x}')-i\omega t}\langle \tilde{n}(\vec{x},t)\tilde{n}(\vec{x}',0)\rangle_{th}} \qquad (2.51).$$

where i – The imaginary unit number, $\tilde{n}(\vec{x},t) = \sum_{\vec{r}_q}\delta(\vec{x}-\vec{r}_q) - n_{ion}$ - Is the instantaneous charge density distribution in units of Ze, and $\langle \dots \rangle_{th}$ denotes the Gibbs average over the ensemble of particles (thermal average should be distinguished from averaging over the phonon spectrum, a certain equation (2.40)).

The static structure factor which describes the instantaneous spatial correlation of the charges is:

$$\boldsymbol{S(\vec{q}) = \int_{-\infty}^{+\infty} S(\vec{q},\omega) d\omega} \qquad (2.52).$$

II.3.4.a The structure factor of the classical isotropic plasma

For isotropic plasma the static structure factor (2.52) is:

$$\boldsymbol{S(q) = 1 + \frac{3\Gamma}{a_{ion}^3}\int_0^{\infty} \frac{\sin(qr)}{qr}[g(r)-1]r^2 dr} \qquad (2.53).$$

where g(r) – is the pair correlation function.

In the limit $q \to 0$ have $S(q) = (qa_{ion})^2/(3\Gamma)$ (eg, [Han 73]). The approximation of the Debye-Hückel corresponds to the formula:

$$\boldsymbol{S(q) = \frac{q^2}{\left(q^2 + 3\Gamma a_{ion}^{-2}\right)}} \qquad (\mathbf{2.54}).$$

In general, $S(q)$ are found numerically from Eq (2.51) (see, eg., A review [Bau 80]). Contribution of ion-ion interaction in the internal energy is expressed through $g(r)$ or $S(q)$ as:

$$\boldsymbol{U_{ii} = \frac{N^2}{2V}\int \frac{(Ze)^2}{r}[g(r) - 1]d^3r = Nk_BT\frac{\Gamma a_{ion}}{\pi}\int_0^\infty [S(q) - 1]dq} \qquad (\mathbf{2.55}).$$

II.3.4.b Structure factor of the Coulomb crystal and Debye-Waller factor

As is well known (eg, [Kit 63], [Kit 86],), in the general case, taking into account the quantization of the ions motion, their local density $n(\vec{x},t) = \sum_j \delta\left(\vec{x} - \vec{R}_j - \vec{u}_j(t)\right)$ is replaced by the density operator $\hat{\rho}\,(\vec{x},t)$, which operates in the space of quantum states characterized by phonon's number, and the displacement vector $\vec{u}_j$ is replaced by the displacement operator $\hat{u}_j$. More precisely, $\hat{\rho}\,(\vec{x},t)$ is defined as the operator of the charge density in units of Ze.The equation (2.51) for the dynamic structure factor is generalized as follows:

$$\boldsymbol{S(\vec{q},\omega) = \frac{1}{2\pi N_{ion}}\int_{-\infty}^{+\infty} dt \int d\vec{x}\, d\vec{x}' e^{i\vec{q}\cdot(\vec{x}-\vec{x}') - i\omega t}\langle\hat{\rho}^+(\vec{x},t)\hat{\rho}(\vec{x}',0)\rangle_{th}} \qquad (\mathbf{2.56}).$$

using just the described quantized density from equation (2.56) is easily obtained the structure factor of the ion density fluctuations in the solid phase:

$$\boldsymbol{S(\vec{q},\omega) = \frac{1}{2\pi N_{ion}}\int_{-\infty}^{+\infty} e^{-i\omega t}\langle\sum_{i,j} e^{i\vec{q}\cdot(\vec{R}_i - \vec{R}_i)}\left[e^{i\vec{q}\cdot\hat{u}_i(t)} - 1\right]\left[e^{i\vec{q}\cdot\hat{u}_j(0)} - 1\right]\rangle_{th} dt} \qquad (\mathbf{2.57}).$$

expanding the ion displacement operator $\hat{u}_j$ in term of the phonon creation-annihilation operators and using the Weyl operator identity $e^A e^B = e^{A+B}e^{(AB-BA)/2}$ (see [Kit 86]), can be divided into structural factors on two terms:

$$\boldsymbol{S(\vec{q},\omega) = S'(\vec{q})\delta(\omega) + S''(\vec{q},\omega)} \qquad (\mathbf{2.58}).$$

where the term $S^{'}(\vec{q})$ is associated with an ordered lattice (so-called Bragg term), while the "inelastic" term $S^{''}(\vec{q},\omega)$ due to ionic fluctuations around the equilibrium positions. In the harmonic approximation we have (eg, [Kit 63]):

$$\boldsymbol{S'(\vec{q}) = (2\pi)^3 n_{ion} e^{-2W(\vec{q})} \sum_{\vec{G}\neq 0} \delta(\vec{q} - \vec{G})} \qquad (\mathbf{2.59}).$$

where:

$$\boldsymbol{\exp\left(-2W(\vec{q})\right) = \langle e^{i\vec{q}\cdot\hat{u}_j}\rangle_{th}^2} \qquad (\mathbf{2.60}).$$

is the Debye-Waller factor. In equation (2.59) $\sum_{\vec{G}\neq 0}$ denotes summation over all reciprocal lattice vectors $\vec{G}$ with the exception of $\vec{G} = 0$.

In isotropic (eg, cubic) crystals we have (eg [Kit 86]):

$$\boldsymbol{W(\vec{q}) = \frac{r_T^2 \vec{q}^2}{6}} \qquad (\mathbf{2.61}).$$

where $r_T^2 = \langle \hat{u}^2 \rangle_{th}$ is the mean-squared ion displacement from equilibrium. In the harmonic approximation:

$$\boldsymbol{r_T^2 = \frac{3\hbar}{2m_{ion}} \left\langle \frac{1}{\omega_{\vec{k}s} \tanh(z_{\vec{k}s}/2)} \right\rangle_{ph}} \qquad (\mathbf{2.62}).$$

where $z_{\vec{k}s}$ defined by equation (2.39). In classical crystal (at $T \gtrsim T_{pi}$) typical values $z_{\vec{k}s}$ are small, and equation (2.62) make simpler to:

$$\boldsymbol{r_T^2(\eta \lesssim 1) = \frac{3k_B T u_{-2}}{4\pi Z^2 e^2 n_{ion}} = \frac{u_{-2}}{\Gamma} a_{ion}^2} \qquad (\mathbf{2.63}).$$

Formally, in this case we can write $r_T^2 = 3u_{-2}r_D^2$, where r_D-is the Debye length (2.23). In the opposite case, when $T \ll T_{pi}$,

$$\boldsymbol{r_T^2(\eta \gg 1) \approx \frac{3\hbar u_{-1}}{2m_{ion}\omega_{pi}} = \frac{u_{-1} a_{ion}^2 \eta}{\Gamma}} \qquad (\mathbf{2.64}).$$

For an arbitrary value of η, r_T^2 can be estimated by the following formula :

$$r_T^2 = \frac{a_{ion}^2 \eta}{\Gamma}\left[\frac{u_{-1}}{2} + \frac{\eta}{3\alpha_l(e^{\alpha_l \eta} - 1)} + \frac{2}{\alpha_l^2} D_1(\alpha_t \eta)\right] \quad (2.65).$$

here, $\alpha_t = 0{,}426548$ and $\alpha_l = 0{,}88412$ for the bcc, $\alpha_t = 0{,}436671$ and $\alpha_l = 0{,}87817$ for the fcc, $\alpha_t = 0{,}436671$ and $\alpha_l = 0\,,87817$ for the hcp lattice, and $D_1(x)$- is the Debye function, for which in [Pot 2000], A.Y. Potekhin et al constructed the approximation:

$$D_1(x) \approx \frac{1 + \frac{R_1(x)}{x}}{1 + \frac{1}{4}x + \frac{5}{144}x^2 + 0.00139x^4 + \left(\frac{6}{\pi^2}\right) R_1(x)},$$

(2.66).

$$R_1(x) = (440x + 9e^x)(0.1x)^6$$

The relative error of this approximation is hundredths of a percent.

II.3.4.c Multiphonon processes

D.A. Baiko et al [Bai 98] have shown that the inelastic part of the structure factor can be written:

$$S''(\vec{q}, \omega) = \frac{1}{2\pi N_{ion}} \int_{-\infty}^{+\infty} dt e^{-i\omega t - 2W(\vec{q})} \sum_{i,j} e^{i\vec{q}\cdot(\vec{R}_i - \vec{R}_j)} \sum_{n=1}^{\infty} \frac{1}{n!} \times \quad (2.67).$$

$$\times \left\{ \frac{\hbar}{2m_{ion}N_{ion}} \sum_{\vec{k}s} \frac{\left(\vec{q}\cdot\vec{e}_{\vec{k}s}\right)^2}{\omega_{\vec{k}s}} \left[\alpha_{ij\vec{k}s}\left(\bar{n}_{\vec{k}s} + 1\right) + \alpha^*_{ij\vec{k}s}\bar{n}_{\vec{k}s}\right] \right\}^n$$

where $\alpha_{ij\vec{k}s} = exp\left[m_{ion}\vec{k}\cdot\left(\vec{R}_i - \vec{R}_j\right) - m_{ion}\omega_{\vec{k}s}t\right]$ and

$$\bar{n}_{\vec{k}s} = \frac{1}{e^{z_{\vec{k}s}} - 1} \quad (2.68).$$

is the mean occupation number of the phonon mode $(\vec{k}, s)$. Expression (2.67) takes into account the contribution of phonon correlations in the structural factor of the crystal. Each n-th term in the sum according to claim corresponds to the contribution of n-phonon processes in the scattering sample particle in the crystal. Summing over i, j gives the delta function that eliminates one of the summation over $\vec{k}$. Thus, we have n sums over s and $n-1$ sums over $\vec{k}$ in each of the n-th term of the formula (2.67).

The expression for the static structure factor (2.52) becomes:

$$\boldsymbol{S(\vec{q}) = \frac{1}{N_{ion}} \sum_{ij} e^{i\vec{q}\cdot(\vec{R}_i - \vec{R}_j)} \langle e^{i\vec{q}\cdot\hat{u}_i} e^{-i\vec{q}\cdot\hat{u}_j} \rangle_{th}} \qquad \textbf{(2.69)}.$$

It just may be divided into "elastic" (the Bragg) and inelastic components:

$$\boldsymbol{S(\vec{q}) = S'(\vec{q}) + S''(\vec{q})},$$

where:

$$\boldsymbol{S''(\vec{q}) = e^{-2W(\vec{q})} \sum_{\vec{R}_j} e^{i\vec{q}\cdot\vec{R}_j} \left[e^{v(\vec{q},\vec{R}_j)q^2} - 1 \right]} \qquad \textbf{(2.70)}.$$

and

$$\boldsymbol{v(\vec{q}, \vec{R}) = \frac{3\hbar}{2m_{ion}} \left\langle \frac{(\vec{q}\cdot\vec{e}_{\vec{k}s})^2}{q^2} \frac{\cos(\vec{k}\cdot\vec{R})}{\omega_{\vec{k}s} \tanh\left(\frac{z_{\vec{k}s}}{2}\right)} \right\rangle_{ph}} \qquad \textbf{(2.71)}.$$

Generally speaking, a function in $S''(\vec{q})$ has sharp peaks, whose calculation is difficult (eg, [Bai 00]). But in the integrals over $\vec{q}$ when $q \gg q_{BZ}$ these peaks can often be smeared out, and thus the a method introduced by M.E. Raikh and D.G. Yakovlev [Rai 82] is applicable, which uses the fact that these integrals of the vector $\vec{q}$ runs on many Brillouin's zones,of which has its own principal vectors of polarization $\vec{e}_{\vec{k}s}$ Therefore, the polarization is changing rapidly on the scale $q \sim q_{BZ}$, and for $q \gg q_{BZ}$ one can use the approximate substitution :

$$\sum_{s}(\vec{q}\cdot\vec{e}_{\vec{k}s})^2 f(\omega_{\vec{k}s}) \to q^2\langle f(\omega_{\vec{k}s})\rangle_{ph} \qquad (2.72).$$

provided that the $f(\omega)$ - sufficiently smooth function. Then from (2.69) after averaging over orientations of the vectors $\vec{q}$, one obtain [Bai 98] [Bai 00] [Rai 82] [Kam 99]:

$$S''(q,\omega) = \exp\left[-2W(q) - \frac{\hbar\omega}{2k_BT}\right]\int_{-\infty}^{+\infty} e^{-i\omega t}K(q,T,t)\frac{dt}{2\pi} \qquad (2.73).$$

$$K(q,T,t) = \exp\left[\frac{\hbar q^2}{2m_{ion}}\left\langle\frac{\cos(\omega_{\vec{k}s}t)}{\omega_{\vec{k}s}\sinh\left(\frac{z_{\vec{k}s}}{2}\right)}\right\rangle_{ph}\right] - 1 \qquad (2.74).$$

Equation (2.73) takes into account the correlation of ions caused by the absorption and emission of any number of phonons. In the literature, quantum-mechanical amplitude interactions of interactions are often linearized with respect to $\hat{u}$ with, thus neglecting multiphonon processes. In this one-phonon approximation (eg, [Flo 76]) the structure factor reduces to (2.74).

$$S''_{1ph}(q,\omega) = e^{-2W(\vec{q})}\frac{\hbar q^2}{2m_{ion}}\left\langle\frac{\delta(\omega-\omega_{\vec{k}s})+\delta(\omega+\omega_{\vec{k}s})}{\omega_{\vec{k}s}\left|\exp\left(\frac{\hbar\omega}{k_BT}\right)-1\right|}\right\rangle_{ph} \qquad (2.75).$$

which is equivalent to replacing $\{exp[\ldots]-1\} \to [\ldots]$ in the equation (2.74). This approximation is justified only when $T \ll T_{pi}$. In a dense astrophysical plasmas multiphonon processes are important near the boundary of the melting of the Coulomb crystal [Bai 98].

In [Bai 98], D.A. Baiko et al derived an approximate expression for the inelastic part of the static structure factor, corresponding to equation (2.73):

$$S''_0(q) = 1 - e^{-2W(\vec{q})} \qquad (2.76).$$

this approach, as tested in [Bai 00], is very accurate when $q \lesssim 3/a_{ion}$.

In [Kam 99] the dynamic structure factor (2.73) was applied to the calculation of the contribution of electron scattering in the crust of a neutron star the neutrino luminosity of the crust. It was shown that the inclusion of multiphonon processes significantly (by tens of percent) increases the total neutrino luminosity in the outer region of the crust, near its border with the ocean. As we shall see, even more strongly influenced by multiphonons processes on the conductivity and thermal conductivity of this part of the crust.

II.3.5. Melting

The phase transition between the Coulomb and Coulomb liquid crystal occurs at $\Gamma = \Gamma_m$ where the free energy $F(\Gamma)$ of liquid and solid phases intersect. This point is difficult to determine with great accuracy, because the intersection of the free energy curves is strongly affected by the thermal corrections which are small at $\Gamma \sim \Gamma_m$ (the free energy curves are nearly parallel). And therefore the position of point of intersection of Γ_m depends strongly on the small corrections. For example, changing F_{ii} by 0,1% shifts the Γ_m on, $\Delta\Gamma \approx 15$, ie ~ 9% [Pol 73] .

A good first approximation to determine the Γ_m can be considered as approximation of an incompressible background. The first is a realistic assessment of $\Gamma_m = 170 \pm 10$, was Van Horn [Hor 69] based on the Lindemann criterion according to which the crystal melts when the r_T the root-mean-square ion vibrations in a lattice site (2.63) becomes a sizable fraction of inter-ion distance. Specifically, Van Horn equated the ratio r_T / a_{ion} to the experimental value $r_T / a_{ion} = 0.070 \pm 0.004$ for alkali metals This value of Γ_m was considerably larger than numerical estimates available at that time, but it proved to be remarkably close to the value obtained twenty years later from sophisticated theoretical studies. Those studies included numerical evaluation of the internal energy of the classical liquid and solid OCP and used quantum

expansions of thermodynamic functions of OCP, as well as Monte Carlo simulations.

II.3.6. Polarization of the electrons in the Coulomb liquid

In electron-ion plasma, the interaction of ions partly shielded by the polarization of the electronic background. Effect of polarization on the thermodynamic functions of a Coulomb fluid is calculated by using perturbation theory [Yak 89] [Gal 76] and by using HNC method [Cha 09] [Pot 00] [Cha 90a]. At the same time in [Yak 89] and [Pot 00] into account relativistic effects. When the electron-ion interaction is small compared with the kinetic energy of electrons (for example, $Ze^2/a_e \ll \epsilon_F$ for degenerate electrons), this interaction can be taken into account by the linear response theory. In this case the exact Hamiltonian of the electron-ion plasma can be divided into two parts, the first of which describes the ions screened by electrons, and the second - the Hamiltonian of the rigid electron background, the so-called "Jelly" [Gal 76].

The polarization properties of the electron gas described by the dynamic dielectric tensor, as in the case of an isotropic gas (in particular, in the absence of a magnetic field) - the dielectric function $\varepsilon(k,\omega)$, where k - is the wave vector, and ω - frequency. For processes with a characteristic length $\gg \omega_{pe}^{-1}$, we can replace $\varepsilon(k,\omega)$ on the static dielectric function $\varepsilon(k) \equiv \varepsilon(k,0)$. For her, in the degenerate relativistic gas is the most widely used analytical expression [Jan 62], resulting in the random-phase approximation (RPA - random-phase approximation), which is valid for $r_s \ll 1$ and $T \ll T_F$:

$$\boldsymbol{\varepsilon(k)} = \mathbf{1} + \frac{\boldsymbol{k_{TF}^2}}{\boldsymbol{k^2}}\left\{\frac{\mathbf{2}}{\mathbf{3}} - \frac{\mathbf{2}}{\mathbf{3}}\frac{\boldsymbol{y^{2x_r}}}{\boldsymbol{\gamma_r}}\ln(\boldsymbol{x_r}+\boldsymbol{\gamma_r}) + \right.$$

$$\left. + \frac{\boldsymbol{x_r^2}+\mathbf{1}-\mathbf{3}\boldsymbol{x_r^2}\boldsymbol{y^2}}{\mathbf{6}\boldsymbol{y}\boldsymbol{x_r^2}}\ln\left|\frac{\mathbf{1}+\boldsymbol{y}}{\mathbf{1}-\boldsymbol{y}}\right| + \right.$$

(2.77).

$$+\frac{2y^2x_r^2-1}{6yx_r^2}\frac{\sqrt{1+x_r^2y^2}}{\gamma_r}\ln\left|\frac{y\gamma_r+\sqrt{1+x_r^2y^2}}{y\gamma_r-\sqrt{1+x_r^2y^2}}\right|\Bigg\}$$

where $y=(k/2k_F)$

Static dielectric function satisfies the important relation

$$\boldsymbol{\varepsilon(k)=1+\frac{k_{TF}^2}{k^2}\ at\ \ k\ll k_{TF}} \qquad (\mathbf{2.78}).$$

If the $r_s \gtrsim 1$ and $T \gtrsim T_F$, we should take into account the finite temperature and non-linear effects, which are in the no relativistic case can be included in the dielectric function according to [Cha 90b]:

$$\boldsymbol{\varepsilon(k)=1+\frac{\varepsilon_{RPA}(k)-1}{1-[\varepsilon_{RPA}(k)-1]G(k)}} \qquad (\mathbf{2.79}).$$

where $\varepsilon_{RPA}(k)$ - is the dielectric function obtained in the random phase approximation, and $G(k)$ – the local field correction (LFC - local field correction), which is estimated numerically.

Screening can also be estimated by the method of effective potential (eg, [Ich 1987]). In this method, the Coulomb potential in the expression for the electrostatic energy is replaced by an effective potential, in which the Fourier transform is equal to $V_{eff}(k)=4\pi(Ze)^2/\left(k^2\varepsilon(k)\right)$, where $\varepsilon(k)$ - is the static dielectric function of the electron gas (2.77) or liquid (2.79).

II.3.7. Polarization of the electrons in the Coulomb crystal

Correlations between the ions - and, consequently, the crystallization - affect the electronic screening. Calculation of thermodynamic functions for the Coulomb crystal, taking into account electronic polarization is a task not yet completely solved. For classical ions simplest model screening is to replace the Coulomb potential on the Yukawa potential. Simulation of the system by the method of molecular dynamics were

carried out in [Ham 97], where it was found that Γ_m increases with decreasing screening radius. Moreover, there may be a transition from bcc to fcc structure. Subsequently, the same model system was studied using the method of integration over trajectories [Mil 06].

However, the Yukawa potential is not an exact model for the screening, since its use is tantamount to limiting the long-wavelength asymptotic behavior of the dielectric function However, the Yukawa potential is not an exact model for the screening, since its use is tantamount to limiting the long-wavelength asymptotic behavior of the dielectric function (2.78). The exact solution requires the calculation of the dynamic matrix of the crystal with electron-ion interaction and the solution of the dispersion relation for the phonon spectrum.

In the first order perturbation theory the dynamic matrix of the classical Coulomb crystal was obtained in [Pol 73] and the phonon spectrum of the quantum Coulomb crystal with polarization was calculated in the harmonic approximation in [Bai 02]. Note that the harmonic approximation only has limited applicability to the problem of screening in a Coulomb crystal: for example, in the classical limit ($T \gg T_{pi}$), it certainly gives a zero contribution to the electron-ion interaction in the heat capacity.

Chapter III

Electronic transport coefficients without magnetic field

A- Basic relations for the electronic transport coefficients

This section has an introductory character. Original results are presented in later sections, but here we summarize the basic approaches and formulas for calculating the kinetic coefficients in the plasma to be used later.

III.1. Boltzmann equation: General relationships

To be specific, as carriers of heat and charge we shall consider the electrons as their contribution to the thermal and electrical conductivity of the plasma, usually dominates. The basis of consideration of the well-known (eg, [LL10]), Boltzmann kinetic equation for the distribution function $f = f(\vec{r}, \vec{p}, s, t)$.

$$\frac{df}{dt} \equiv \frac{\partial f}{\partial t} + \vec{v} \cdot \vec{\nabla}_{\mathrm{r}} f + \vec{F} \cdot \vec{\nabla}_{\mathrm{p}} f = I_e, \quad I_e = \sum_j I_{ej}\,[f], \qquad (3.1).$$

Where $\vec{p}, \vec{r}, \vec{v}$ and s - are the momentum, the radius vector, velocity, and electron spin index, respectively; t - the time; $\vec{F}$ denotes the external force acting on the electrons; I_{ej} - Collision integral of electrons with

particles of species j (electrons, ions and etc). The collision integrals are functionals of f.

Suppose that in the plasma there small stationary perturbations characterized by a temperature gradient $\vec{\nabla}$T and a gradient in chemical potential $\vec{\nabla}\mu_e$ and the electric field $\vec{E}$ (then $\vec{F} = -e\vec{E}$), and that these gradients and the field is so weak that the characteristic scale of the resultant non-uniformity of the plasma is much higher than the average characteristic length of electron free path . This volume element of matter is close to the thermodynamic equilibrium, and deviations from the strict equilibrium associated with the currents of heat and charge. Solution of equation (3.1) has the in the form:

$$\boldsymbol{f = f^{(0)} + \delta f}, \qquad (\mathbf{3.2}).$$

$$\boldsymbol{f^{(0)}(\epsilon - \mu_e, T) \equiv \frac{1}{\exp\left(\frac{\epsilon - \mu_e}{k_B T}\right) + 1}} \qquad (\mathbf{3.3}).$$

- is the local function of Fermi-Dirac distribution, and δf –is a correction due to disequilibrium in the first approximation linear in $\vec{\nabla}T$, $\vec{\nabla}\mu_e$and $\vec{E}$. In view of the smallness of the gradients on the left side of the equation (3.1) in a first approximation we can neglect δf on compared with $f^{(0)}$:

$$\boldsymbol{\frac{df}{dt} \approx \frac{df^{(0)}}{dt} = -\left(\frac{\epsilon - h}{T}\vec{\nabla}T + e\vec{E}^*\right)\cdot\vec{v}\frac{\partial f^{(0)}}{\partial \epsilon}} \qquad (\mathbf{3.4}).$$

here $h = \mu_e + (S_e/N_e)T$ - enthalpy for electron:

$$\boldsymbol{\vec{E}^* \equiv \vec{E} + \frac{\vec{\nabla}\mu_e}{e} + \frac{S_e}{N_e}\frac{\vec{\nabla}T}{e}} \qquad (\mathbf{3.5}).$$

and

$$\boldsymbol{S_e = -\frac{2k_e V}{(2\pi\hbar)^3}\int [f \ln f + (1-f)\ln(1-f)]\, d^3p} \qquad (\mathbf{3.6}).$$

-is the electronic entropy. The collision integral vanishes at $f = f^{(0)}$ so the first nontrivial approximation for it gives terms linear in δf. Restricting the expansion from δf only by those members, from (3.1) we obtain linearized -Boltzmann equation, corresponding to the first approximation in the method of Chapman-Enskog expansion of the distribution function of the small parameter. In the case when the medium is isotropic, we can write (eg, [Zim 1960]).

$$\boldsymbol{\delta f = \Phi \frac{\partial f^{(0)}}{\partial \epsilon} = \frac{\Phi}{k_B T} f^{(0)} \left(1 - f^{(0)}\right)},$$

$$\boldsymbol{\Phi = \frac{\epsilon - h}{T} A_e(\epsilon)\vec{v} \cdot \vec{\nabla} T + e\, A_e(\epsilon)\vec{v} \cdot \vec{E}^*} \qquad (\mathbf{3.7}).$$

Where $A_e(\epsilon)$ and $A_e(\epsilon)$ - some functions of electron energy to be determined.

Using equations (3.2) and (3.7), we can derive some general relations connecting the $\vec{\nabla} T$, $\vec{\nabla}\mu_e$ and $\vec{E}$ with the density of electric current:

$$\boldsymbol{\vec{j}_e = -\frac{2e}{(2\pi\hbar)^3} \int \vec{v} f\, d^3p} \qquad (\mathbf{3.8}).$$

And the heat flux density:

$$\boldsymbol{\vec{j}_T = -\frac{2e}{(2\pi\hbar)^3} \int \vec{v}(\epsilon - h)\, d^3p} \qquad (\mathbf{3.9}).$$

And energy flux density $\vec{j}_E = \vec{j}_T - (h/e)\vec{j}_e$, from (3.8) and (3.9), we obtain:

$$\boldsymbol{\vec{j}_e = \sigma \vec{E}^* - \alpha_T \vec{\nabla} T \;, \quad \vec{j}_T = \alpha_T T \vec{E}^* - \tilde{\kappa} \vec{\nabla} T} \qquad (\mathbf{3.10}).$$

Where :

$$\begin{Bmatrix} \boldsymbol{\sigma} \\ \boldsymbol{\alpha_T} \\ \boldsymbol{\tilde{\kappa}} \end{Bmatrix} = \frac{\mathbf{1}}{\mathbf{12\pi^3\hbar^3}} \int (-\frac{\boldsymbol{\partial f^{(0)}}}{\boldsymbol{\partial \epsilon}})\ \boldsymbol{v^2} \begin{Bmatrix} \boldsymbol{e^2 A_e(\epsilon)} \\ \boldsymbol{eA_{e,T}(\epsilon)} \\ \boldsymbol{A_T(\epsilon)(\epsilon - h)^2/T} \end{Bmatrix} \begin{matrix} \\ (\boldsymbol{h-\epsilon})/\boldsymbol{T} \\ \\ \end{matrix} \boldsymbol{d^3p} \qquad (\mathbf{3.11}).$$

Here σ –is the electrical conductivity, α_T and $\tilde{\kappa}$ - auxiliary transport coefficients (the same ratio α_T is included in both equations (3.10) due to the Onsager symmetry principle - eg. [LL5], § 120, [Zim 60]).

It is convenient to rewrite relation (3.10) in the form:

$$\vec{\boldsymbol{E}}^* = \frac{\vec{\boldsymbol{j}}_e}{\boldsymbol{\sigma}} - \boldsymbol{Q_T}\,\vec{\boldsymbol{\nabla}}\boldsymbol{T}\,, \qquad \vec{\boldsymbol{j}}_T = -\boldsymbol{Q_T}\,\boldsymbol{T}\,\vec{\boldsymbol{j}}_e - \boldsymbol{\kappa}\,\vec{\boldsymbol{\nabla}}\boldsymbol{T} \quad (\mathbf{3.12}).$$

$$\boldsymbol{Q_T} = -\frac{\boldsymbol{\alpha_T}}{\boldsymbol{\sigma}}\,, \quad \boldsymbol{\kappa} = \tilde{\boldsymbol{\kappa}} - \frac{\boldsymbol{T\alpha_T^2}}{\boldsymbol{\sigma}} \qquad (\mathbf{3.13}).$$

- Respectively, the thermoelectric coefficient and heat conductivity. Each set of transfer coefficients - $(\sigma, \alpha_T, \tilde{\kappa})$ or $(\sigma, \mathrm{Q_T}, \kappa)$ - completely determines the transport of heat and charge in an isotropic medium.

Substituting relation (3.4) in equation (3.1), multiplying both sides by $2\,(2\pi\hbar)^{-3}\Phi$ and integrating over $\vec{\mathrm{p}}$, we obtain the useful relation.

$$\frac{\dot{\boldsymbol{Q}}}{\boldsymbol{V}} = \frac{(\boldsymbol{\nabla T})^2}{\boldsymbol{T}} - \dot{\boldsymbol{\kappa}} - \mathbf{2}\boldsymbol{\alpha_T}\,\vec{\boldsymbol{E}}^* \cdot \vec{\boldsymbol{\nabla}}\boldsymbol{T} + (\vec{\boldsymbol{E}}^*)^2\,\boldsymbol{\sigma} = \vec{\boldsymbol{E}}^* \cdot \vec{\boldsymbol{j}}_e - \frac{\vec{\boldsymbol{j}}_T \cdot \vec{\boldsymbol{\nabla}}\boldsymbol{T}}{\boldsymbol{T}} \qquad (\mathbf{3.14}).$$

Where:

$$\dot{\boldsymbol{Q}} = \frac{\mathbf{2}\boldsymbol{V}}{(\mathbf{2\pi\hbar})^3} \int \boldsymbol{d^3p} \left[(\boldsymbol{\epsilon - h}) \boldsymbol{A_T(\epsilon)} \frac{\vec{\boldsymbol{\nabla}}\boldsymbol{T}}{\boldsymbol{T}} + \boldsymbol{e}\vec{\boldsymbol{E}}^* \boldsymbol{A_e(\epsilon)} \right] \cdot \vec{\boldsymbol{v}}\,\boldsymbol{I_e} \qquad (\mathbf{3.15}).$$

Using Equations (3.1) - (3.7) and taking into account the conservation of the number of electrons and their total energy in elastic collisions, we can show (for example, [LL10]) that $\dot{Q} = T\dot{S}_{coll}$ where $\dot{S}_{coll}$ – is the rate of entropy production by collisions. This allows us to consider the ratio (3.14) and (3.15) as a variation, in which $\mathrm{A_e}(\epsilon)$ and $\mathrm{A_T}(\epsilon)$ are test functions (eg, [Zim 1960]). Putting them in $\vec{\nabla}T = 0$ or $\vec{\mathrm{E}}^* = 0$, we obtain, respectively:

$$\frac{\mathbf{1}}{\boldsymbol{\sigma}} = \frac{\dot{\boldsymbol{Q}}}{\boldsymbol{j_e^2}} = \frac{(\vec{\boldsymbol{E}}^*)^2}{\dot{\boldsymbol{Q}}}\,, \qquad \frac{\mathbf{1}}{\tilde{\boldsymbol{\kappa}}} = \frac{\dot{\boldsymbol{Q}}\boldsymbol{T}}{\boldsymbol{j_e^2}} = \frac{(\vec{\boldsymbol{\nabla}}\boldsymbol{T})^2}{\boldsymbol{T}\dot{\boldsymbol{Q}}} \qquad (\mathbf{3.16}).$$

III.2. Electron-electron scattering

The exact form of the collision integral I_{ee}, depends on the scattering mechanism. We first consider the collision of electrons with each other - its scattering, which can be schematically represented as $(\vec{p}_1 s_1, \vec{p}_2 s_2 \rightarrow \vec{p}_1' s_1', \vec{p}_2' s_2')$, where the non primed momentum p and spin indices s determine the state of the electrons 1 and 2 before the collision, and the primed - after the collision. Denote a quantum mechanical transition matrix element in the collision through $M_{1,2\rightarrow 1',2'}$ The transition probability per unit time is (eg, [LL3]).

$$\boldsymbol{W(12;1'2') = \frac{2\pi}{\hbar}\ \left|M_{1,2\rightarrow 1',2'}\right|^2\ \delta\left(\epsilon_1' + \epsilon_2' - \epsilon_1 - \epsilon_2\right)} \qquad \textbf{(3.17)}.$$

According to the principle of microscopic reversibility, $\left|\mathrm{M}_{1,2\rightarrow 1',2'}\right|^2 = \left|\mathrm{M}_{1',2'\rightarrow 1,2}\right|^2$, so according to the principle of detailed balance the identity:

$$\boldsymbol{f_1^{(0)'} f_2^{(0)'} \left(1 - f_1^{(0)}\right)\left(1 - f_2^{(0)}\right) = f_1^{(0)} f_2^{(0)} \left(1 - f_1^{(0)'}\right)\left(1 - f_2^{(0)'}\right)} \qquad \textbf{(3.18)}.$$

For the collision integral we have:

$$\boldsymbol{I_{ee}[f_1] = \sum_{s_2, s_1' s_2'} \int \frac{d^3 p_1'\, d^3 p_2\, d^3 p_2'}{2(2\pi\hbar)^9} W(12;1'2') \times}$$

$$\boldsymbol{\times [f_1 f_2 (1 - f_1)(1 - f_2) - f_1 f_2 (1 - f_1)(1 - f_2)]} \qquad \textbf{(3.19)}.$$

Where the additional factor 2 in the denominator ensures the exclusion of double counting the same index, differing by permutation of indices 1 and 2.

Linearization $\mathrm{I_{ee}}$ in accordance with (3.2) and (3.7) leads to the expression:

$$\boldsymbol{I_{ee}[f_1] = \frac{1}{k_B T} \sum_{\sigma_2,\sigma_1'\sigma_2'} \int \frac{d^3p_1' \, d^3p_2 \, d^3p_2'}{2(2\pi\hbar)^9} W(12;1'2') \times}$$

(3.20).

$$\boldsymbol{\times f_1^{(0)'} f_2^{(0)'} \left(1 - f_1^{(0)}\right)\left(1 - f_2^{(0)}\right) \times \left(\Phi_1 + \Phi_2 - \Phi_1' - \Phi_2'\right)}$$

III.3. Electron-ion scattering. Approximation of the relaxation time

As another important example, consider the scattering of electrons by ions in the case when the characteristic energy transfer $\delta\epsilon$ in a single collision is small: $\delta\epsilon \ll k_B T$. Then [Zim 60]:

$$\boldsymbol{I_{ei} = -\frac{\delta f}{\tau_0(\epsilon)}} \qquad (3.21).$$

Where $\tau_0(\epsilon)$ - the effective relaxation time for the electronic distribution function. This approximation is called the relaxation time approximation; If this type of collision dominated, the solution of the linearized Boltzmann equation is simply:

$$\boldsymbol{A_e(\epsilon) = A_T(\epsilon) = \tau_0(\epsilon)} \qquad (3.22).$$

If the provisions of the ions are uncorrelated, then the relaxation time is estimated as:

$$\boldsymbol{\tau_0(\epsilon) = n_{ion} v \frac{1}{\sigma_{tr}(\epsilon)}} \qquad (3.23).$$

Where:

$$\boldsymbol{\sigma_{tr}(\epsilon) = \int \sigma(\vartheta, \phi)\,(1 - cos\vartheta) d\Omega} \qquad (3.24).$$

- is the transport scattering cross section, ϑ - scattering angle, and $\sigma(\vartheta,\phi)d\Omega$ –is the cross section of an electron in an element of solid angle $d\Omega = 2\pi\sin\vartheta d\vartheta$

Differential scattering cross section is equals to:

$$\boldsymbol{\sigma(\vartheta,\phi) = \frac{|U_q|^2 m_e^2}{4\pi^2\hbar^4}} \quad (\mathbf{3.25}).$$

Where U_q - the Fourier transform of the screened Coulomb potential, depending on $\hbar q = 2p\sin(\vartheta/2)$ – is the momentum transferred in the collision. Define the screening function ϕ_q by equality:

$$\boldsymbol{|U_q|^2 = -4\pi Ze^2\phi_q} \quad (\mathbf{3.26}).$$

Then the transport cross section (3.24) is:

$$\boldsymbol{\sigma_{tr} = 4\pi\left(\frac{Ze^2}{pv}\right)^2 \Lambda_{ei}(p)} \quad (\mathbf{3.27}).$$

Where:

$$\boldsymbol{\Lambda_{ei}(p) = \int_0^{2p/\hbar} q^3|\phi_q|^2 dq} \quad (\mathbf{3.28}).$$

- Coulomb logarithm, which depends on the electron momentum p. For the unscreened Coulomb potential $|\phi_q| = 1/q^2$, so integral in (3.28) diverges logarithmically at small q. Plasma shielding eliminates this divergence. Energy-dependent relaxation time in (3.23) becomes:

$$\boldsymbol{\tau_{ei}(\epsilon) = \frac{p^2 v}{4\,\pi\, Z^2 e^4\, n_{ion}\, \Lambda_{ei}(p)}} \quad (\mathbf{3.29}).$$

III.4. General expressions for the nondegenerate plasma

Kinetic coefficients of degenerate ($T \gg T_F$) nonrelativistic ($x_r \ll 1$), electron-ion plasma, taking into account both the electron-ion (ei), and electron-electron (ee) collisions were discussed in detail by Spitzer [Spi 62] using the expansion of the functions $A_e(\epsilon)$ and $A_T(\epsilon)$ on the attached Sonin- Laguerre polynomials, traditionally used in the kinetics of rarefied gases (eg, [Hir 54]). In the nondegenerate plasma, The effective energy-averaged collision time for ei-scattering is given by:

$$\boldsymbol{\tau_{ei} = \frac{1}{\nu_0 \Lambda_{ei}}} \qquad (\mathbf{3.30}).$$

where:

$$\boldsymbol{\nu_0 = \frac{4}{3}\sqrt{\frac{2\pi}{m_e}}\frac{Z^2 e^4}{(k_B T)^{3/2}} n_{ion}} \qquad (\mathbf{3.31}).$$

And Λ_{ei} -the so-called Coulomb logarithm, has an order of magnitude:

$$\boldsymbol{\Lambda_{ei} \approx \ln\left(\frac{r_{max}}{r_{min}}\right)} \qquad (\mathbf{3.32}).$$

Where r_{max} and r_{min} -, respectively, maximum and minimum impact parameter. The maximum impact parameter can be set equal to the Debye screening length $r_{scr} = 1/k_s$, where k_s is defined by equation (3.24). Minimum impact parameter can be estimated as $r_{min} = \max(\lambda_e, Ze^2/k_B T)$. Where λ_e the thermal de Broglie wavelength of the electron limits r_{min} at high temperatures, and $Ze^2/k_B T$ - is the classical closest approach distance of a thermal electron, which limits r_{min} in the low-temperature, quasiclassical regime.

Coulomb logarithm depends only weakly on the plasma parameters and usually ranges from several to ~ 20. The effective relaxation time τ_{ei}

characterizes the efficiency of electron-ion collisions. A similar effective relaxation time for ee collisions:

$$\boldsymbol{\tau_{ee} = \frac{3\sqrt{m_e}(k_B T)^{3/2}}{8\sqrt{\pi} e^4 n_e \Lambda_{ee}}} \qquad (\mathbf{3.33}).$$

Characterizes the efficiency of collisions. If $\Lambda_{ee} \sim \Lambda_{ei}$, the $\frac{\tau_{ee}}{\tau_{ee}} \sim Z$, ie, ei-collision at about Z times more effective than ee- collisions .

Consider a plasma of heavy ions, in which ee collisions can be neglected, and for ei-collision is a fairly accurate approximation of (3.23). Moreover, if in (3.29) one neglect the dependence of Λ on p (eg, [ref]) and use the relaxation time approximation (3.22) , one can make explicit integration in (3.11), which leads to the equalities:

$$\boldsymbol{\sigma = \frac{32 n_e e^2 \tau_{ei}}{3\pi m_e}}, \boldsymbol{\alpha_T = -\frac{16 n_e e \tau_{ei}}{\pi m_e}}, \boldsymbol{\tilde{\kappa} = \frac{200 k_B^2 T n_e \tau_{ei}}{3\pi m_e}} \qquad (\mathbf{3.34}).$$

Hence, using (3.13):

$$\boldsymbol{\sigma = \frac{32}{3\pi}\frac{n_e e^2 \tau_{ei}}{m_e}}, \boldsymbol{Q_T = \frac{3}{2}\frac{k_B}{e}}, \boldsymbol{\kappa = \frac{128\, k_B^2 T n_e \tau_{ei}}{3\pi m_e}} \qquad (\mathbf{3.35}).$$

III.5. Strongly degenerate electron gas

We now consider the opposite limiting case, when electrons are strongly degenerate. An analysis of electron transfer in this simplified by the fact that the main contribution is only the electron, whose energies lie in a narrow range near the Fermi level. The enthalpy h (and chemical potential μ_e different from the Fermi energy ϵ_F small terms $\mu_e (T / T_F)^2$. Therefore, it suffices to put in (3.11) $h = \mu_e$. In addition, the second ratio (3.13) $\alpha_T^2/\sigma \sim (T / T_F)^2$, so $\kappa \approx \tilde{\kappa}$. It is convenient to write the transport coefficients in the form:

$$\boldsymbol{\sigma = \frac{n_e e^2 \tau_\sigma}{m_e^*}}\ , \boldsymbol{\kappa = \frac{\pi^2 k_B^2 T n_e \tau_\kappa}{3 m_e^*}}\ , \boldsymbol{Q_T = \frac{\pi^2 k_B^2 T}{3 e p_F v_F}(3+\xi)} \qquad (3.36).$$

Where $m_e^* = \frac{\epsilon_F}{c^2} = m_e \gamma_r$ - dynamic electron mass, $v_F = \frac{p_F}{\gamma_r}$ - the speed on the Fermi surface, and those τ_σ , $\tau_\kappa$and ξ - values to be determined on the basis of the Boltzmann equation (3.1). The values of τ_σ and τ_κ called the effective electron relaxation time in relation to the charge transfer and heat transfer, respectively; $\xi \sim 1$ - dimensionless factor, which depends on the mechanism of electron scattering.

For numerical estimates there is convenient ratios:

$$\boldsymbol{\sigma = 1.485 \times 10^{22} \frac{x_r^3}{\gamma_r}\left(\frac{\tau_\sigma}{10^{-16}}\right)}\ , \boldsymbol{\kappa = 4.038 \times 10^{15} T_6 \frac{x_r^3}{\gamma_r}\left(\frac{\tau_\kappa}{10^{-16}}\right)} \qquad (3.37).$$

When considered the scattering of electrons by heavy particles, the approximation of relaxation time (3.22). In this case, from (3.11) and (3.22) easily obtain expressions:

$$\boldsymbol{\tau_\sigma = \tau_\kappa = \tau_{ei}(\mu_e)} \qquad (3.38).$$

$$\boldsymbol{\xi = \frac{p_F}{v_F}\frac{\partial[\ln \sigma(\mu_e)]}{\partial \mu_e} - 3 = p_F v_F \frac{\partial\left[\ln \frac{\tau_{ei}}{\mu_e}(\mu_e)\right]}{\partial \mu_e}} \qquad (3.39).$$

As well as Wiedemann – Franz law:

$$\boldsymbol{\kappa = \frac{\pi^2 k_B^2 T}{3e^2}\sigma} \qquad (3.40).$$

That Function $\tau_{ei}(\mu_e)$ The right side of (3.38), as previously determined by formulas (3.23) and (3.24), in which section of the scattering electron with a given total energy at a given potential, and does not depend on the statistical distribution of electrons. Therefore, the function $\tau_{ei}(\epsilon)$ is given by (3.29), regardless of the degree electronic degeneracy.

III.6. Matthiessen's rule

If there are several scattering mechanisms, the solution is complicated. But with strong electron degeneracy we can independently calculate the effective frequencies ν_j for different scattering mechanisms and to obtain the effective relaxation time $\tau = 1/\upsilon$ based on the Mattissena's rule (eg, [Zim 60]): $\nu_{tot} = \nu_1 + \nu_2 + \cdots$ In practice, this rule provides a good approximation in the absence of strong degeneracy. In particular, if there are two scattering mechanisms with effective frequencies υ_1 and υ_2, then using the variational principle (3.16) can be shown that the resulting effective frequency and satisfies $\nu_1 + \nu_2 \leq \nu \leq \nu_1 + \nu_2 + \delta\nu$ and, where $\delta\nu \ll min\,(\nu_1, \nu_2)$ [Zim 60]. In this case the ionic liquid and the crystal are different.

In a liquid or gas (at $T > T_m$) is the main Coulomb scattering of electrons by ions. Electron-electron collisions are virtually absent in charge transfer due to conservation of momentum, and hence the average current in the pair collisions, so they usually can be neglected when calculating the conductance (see, for example., [ref]). However, they may be important for the thermal conductivity. Consequently, the Mattissena's rule :

$$\frac{\mathbf{1}}{\boldsymbol{\tau_\sigma}} = \frac{\mathbf{1}}{\boldsymbol{\tau_{ei}^{\sigma}}}, \frac{\mathbf{1}}{\boldsymbol{\tau_\kappa}} = \frac{\mathbf{1}}{\boldsymbol{\tau_{ei}^{\kappa}}} + \frac{\mathbf{1}}{\boldsymbol{\tau_{ee}}} \qquad (\mathbf{3.41a}).$$

We can rewrite the second equation (3.41a) in the form:

$$\boldsymbol{\kappa} = \left(\boldsymbol{\kappa_{ei}^{-1}} + \boldsymbol{\kappa_{ee}^{-1}}\right) \qquad (\mathbf{3.41b}).$$

The crystal (at $T < T_m$) of the main scattering mechanism - a scattering electrons on phonons (it is preferable for the scattering by ions in the liquid, use the notation «ei») and charged inhomogeneities (the index «imp»). Electron-phonon scattering usually dominates at temperatures not too small compared to the T_m If $T \gg T_m$, then the determinant can become the scattering of electrons by impurities or

lattice defects." Scattering by inhomogeneities can be described by an effective relaxation time τ_{imp} . Thus, the combined effect of scattering of electrons by phonons, electrons and impurities can be represented as:

$$\frac{\mathbf{1}}{\boldsymbol{\tau_\sigma}} = \frac{\mathbf{1}}{\boldsymbol{\tau_{ei}^\sigma}} + \frac{\mathbf{1}}{\boldsymbol{\tau_{imp}}} , \frac{\mathbf{1}}{\boldsymbol{\tau_\kappa}} = \frac{\mathbf{1}}{\boldsymbol{\tau_{ei}^\kappa}} + \frac{\mathbf{1}}{\boldsymbol{\tau_{imp}}} + \frac{\mathbf{1}}{\boldsymbol{\tau_{ee}}} \qquad (\mathbf{3.42}).$$

B- Outline OCP calculations (IOFFE model)

III.7. Scattering of electrons on ions

III.7.1. Ion gas

In the case where ions are virtually uncorrelated, the effective relaxation time τ_{ei} for electrical and thermal conductivity, resulting ei-collisions, may be obtained by using the equations (3.23) and (3.24) differential scattering cross section for relativistic electron Mott, was amended to second-order Born approximation (eg, [Akh 65]):

$$\boldsymbol{\sigma(\epsilon,\vartheta) = \frac{4Z^2e^4\epsilon^2}{(\hbar c)^4}\left|\phi_q\right|^2\left[\left(1-\frac{v^2}{c^2}\sin\frac{\vartheta}{2}\right)+\pi Z\alpha_f\frac{v}{c}\sin\frac{\vartheta}{2}\left(1-\sin\frac{\vartheta}{2}\right)\right]} \qquad (3.43).$$

Where ϕ_q – is screening function, introduced in (3.26). Thus we arrive at formula (3.29) with the refined expression for the Coulomb logarithm $\Lambda_{ei}(p)$: instead of (3.28) we now have:

$$\boldsymbol{\Lambda_{ei}(p) = \int_0^{\frac{2p}{\hbar}} q^3\left|\phi_q\right|^2\left[\left(1-\frac{v^2}{c^2}sin\frac{\vartheta}{2}\right)+\pi Z\alpha_f\frac{v}{c}sin\frac{\vartheta}{2}\left(1-sin\frac{\vartheta}{2}\right)\right]dq} \quad (3.44).$$

That reflects the account of relativistic and non- Born corrections. Neglecting these amendments of plasma shielding, one can perform analytical integration of the last two terms in (3.44), which arrive at the explicit expression for them, just a weak screening (ie $2pr_D \gg 1$) [Yak 87] [Pot 97]:

$$\boldsymbol{\Lambda_{ei}(p) = \Lambda_{ei}^{(0)}(p) - \frac{1}{2}\left(\frac{v}{c}\right)^2\frac{\pi Z\alpha_f}{2}\frac{v}{c}} \qquad (3.45).$$

Where the first term, $\Lambda_{ei}^{(0)}(p)$ - Coulomb logarithm beyond the relativistic Born approximation, which is calculated taking into account the dynamic screening on the basis of the formalism of Williams and DeWitt [Wil 69] and is:

$$\boldsymbol{\Lambda_{ei}(p) = \ln\left(\frac{2pr_D}{\hbar}\right) - \left(\frac{r_D}{r_e}\right)^2 \ln\left(\frac{r_e}{r_D}\right) - \frac{1}{2}\left[1 + \left(\frac{r_D}{r_e}\right)^2\right] \ln\left[1 + \left(\frac{r_D}{r_e}\right)^2\right]} \qquad (3.46).$$

Where r_D and r_e those defined by (2.23) and (2.17), respectively.

According to (3.38) and (3.29), for strongly degenerate electrons effective relaxation time can be estimated as:

$$\boldsymbol{\tau_{ei} = \tau_{ei}(\mu_e) = \frac{3\pi\hbar}{4Zm_e^*\alpha_f^2\Lambda_{ei}(\mu_e)c^2} = \frac{5.7 \times 10^{-17}}{Z\Lambda_{ei}(\mu_e)\gamma_r}c} \qquad (3.47).$$

If $\Lambda_{ei} = const$, the τ_{ei} will be independent of temperature, while in the non-relativistic electrons also on the density.

III.7.2. Ionic liquids (degenerate electrons)

Let us now consider most important case in neutron stars, the case of strongly Coulomb plasma, $\Gamma \sim 1$ In this case, the ionic screening is strong: the formal expression for the Debye screening length (2.23) gives the results $r_D < a_{ion}$. Assuming that the successive acts of scattering incoherent with each other, the total number of transitions per unit time "the differential scattering rate" between states with given initial (p) and final (p') momenta are obtained by summing over final (σ)and averaging over initial (σ') spin states (cf. [Hub 66]):

$$\boldsymbol{W(\vec{p} \to \vec{p}') = \frac{2\pi N_i}{\hbar^2}\frac{1}{2}\sum_{\sigma\sigma'}\left|U_{\vec{q},\sigma\sigma'}\right|^2 S(\vec{q},\omega)} \qquad (3.47).$$

Where $\hbar\vec{q} = \vec{p} - \vec{p}'$ is the momentum transfer, $\hbar\omega$ is the transmitted energy, $U_{\vec{q},\sigma\sigma'}$ is the matrix element of the operator of elementary ei interaction, and $S(q,\omega)$ is the dynamic structure factor (2.51). Screening of the Coulomb potential are taken into account with dielectric function (2.77), and the finite size of ions - using the form factor (Fourier transform of the

charge density) F_q As a result of the formula (3.44) for the Coulomb logarithm has an extra integral factors that take into account the correlation of the ions and their finite size, and thus refined the formula in the Born approximation (ie without the last term in brackets) can be written as:

$$\boldsymbol{\Lambda_{ei}(p) = \Lambda_{ei}(p) = \int_0^{2k_F} q^3 \left|\phi_q\right|^2 S_{eff}(q) \left[1 - \frac{v_F^2}{c^2}\left(\frac{q}{2k_F}\right)^2\right] dq} \qquad (\mathbf{3.49}).$$

$$\boldsymbol{\phi_q = \frac{F_q}{q^2 \varepsilon_e(q)}} \qquad (\mathbf{3.50}).$$

And $S_{eff}(q)$ – is the effective static structure factor, is expressed through the dynamic structure factor $S(\vec{q}, \omega)$ by the integral over ω with weighting factors that allows for the dependence of the distribution of ion plasma oscillations in frequency.

These factors are different for different transport coefficients, which serves as the cause of differences in the effective relaxation time τ_σ and τ_κ in (3.36), which manifests itself in at $T \lesssim T_{pi}$ The explicit form of the Coulomb crystal will be presented later. These weight tend to unity at $\hbar\omega \ll k_B T$, so in the classical region ($T \gg T_{pi}$), to which we confine ourselves to the case of ionic liquid as an effective structure factor $S_{eff}(q)$ is often used static structure factor $S(q)$. But in the article [Bai 98] D.A. Baiko et al gave arguments in favor of certain modifications $S_{eff}(q)$, which becomes important at$\Gamma \sim 100$. Considering these modifications.

III.7.2.a Effective structure factor of strongly coulomb liquid

Formally, the liquid is no long-range order. However, it is known that strongly coupled Coulomb liquid has much in common with a Coulomb crystal. Thus, modeling the molecular dynamics method along

with the familiar longitudinal ion Plasmon [Sch 97] demonstrated the emergence of collective shear vibration modes (typical for crystals) in a Coulomb liquid at $\Gamma \gtrsim 120$. This means that in the ionic liquid appear a quasi-ordered structure, D.A. Baiko et al [Bai 98] had verified that the spectrum of these modes can be described by the phonon spectrum averaged over orientations of a crystal. Although the long-range order does not persist forever, it may be well preserved during typical electron scattering time. Thus a temporary electron band structure emerges, and an associated elastic scattering does not contribute. to the conduction (as in solid). This means that one should deal with a local disorder "observed" by an electron along its mean free path, rather than with the global disorder [Edw 62]. Allowance for the influence of quasi-ordering of ions on the electronic transport coefficients of the Coulomb liquid was first implemented in [Bai 98], in which they deal with $S_{eff}(q)$ instead of the full structure factor S(q) including its inelastic component Therefore it suggests to subtract the elastic contribution from the total static structure factor in the liquid phase (e.g., [Edw 62][Han 73]).

$$\boldsymbol{S''(q) = S(q) - S'(q)} \qquad (\mathbf{3.51}).$$

Where $S'(q)$ is the elastic (Bragg) component, which by analogy with (2.59) is calculated by the formula:

$$\boldsymbol{S'(q) = e^{-2W(q)}(2\pi)^3 n_{ion} \sum_{\vec{G}} \overline{\delta(\vec{q} - \vec{G})}} \qquad (\mathbf{3.52}).$$

Where $e^{-2W(q)}$ is the Debye-Waller factor, determined by formulas (2.61) and (2.64), and the bar over the delta function represents an average over orientations of wave vector $\vec{q}$ in the bcc structure "There may be various types of periodic structures in this regime, but they are very similar and one can use the bcc lattice.

D.A. Baiko et al [4-5] had checked that the result is almost the same for face-centered cubic (fcc) and hexagonal close-packed (hcp)

lattices ».which it means that the Selection of the type of crystal lattice for such averaging is ambiguous, but the result is insensitive to this choice.

III.7.2.b Nuclear form factor

In the inner crust of a neutron star the size of the nuclei are no longer negligible compared with the distances between them. In this case, we should take into account the distribution of electric charge on the volume of the nucleus. It must take into account the nuclear form factor F_q in the expression for the screening function (3.50).

For spherical nuclei the assumption that the nuclear charge is distributed uniformly inside a sphere of radius r_{nuc} , the nuclear form factor is given by:

$$\boldsymbol{F_q = \frac{3}{(qr_{nuc})^3}[\sin(qr_{nuc}) - qr_{nuc}\cos(qr_{nuc})]} \qquad (\mathbf{3.53}).$$

The dimensionless parameter characterizing the ratio of core size to the distance between the nuclei is determined the charge radius of the atomic nucleus r_{nuc} to the radius of the ion sphere: $x_{nuc} = r_{nuc}/a_{ion}$ 'This parameter can be approximately expressed in terms of x_r (see [Hae 06], Appendix B):

$$\boldsymbol{x_{nuc} = \begin{cases} 0.00155(A/Z)^{1/3}x_r & if\ \rho \le \rho_{drip} \\ 0.00247x_r & if\ \rho > \rho_{drip} \end{cases}} \qquad (\mathbf{3.54}).$$

In fact, the proton charge in the atomic nucleus is not quite uniformly distributed: the density falls off smoothly from a maximum to zero near the nucleus surface, which becomes especially noticeable at high density near the bottom of inner crust of neutron stars.

III.7.2.c Going beyond the Born approximation

NonBornian corrections are taken into account by multiplying the integral (3.49) on $\sigma(\epsilon,q)/\sigma_{Born}(\epsilon,q)$ where $\sigma(\epsilon,q)$ is the exact nonBornian differential cross section of electron scattering by the Coulomb potential [Dog 56] at the energy ϵ and the transmitted momentum $\hbar q$ and $\sigma_{Born}(\epsilon,q)$ is the scattering cross section in the Born approximation, i.e. the expression (3.43) without the last term.

III.7.2.d Accounting the polarizability of electronic background

Electronic screening not only leads to $\varepsilon_e(q)$ in the denominator of (3.49) but also affects the structure factor $S(q)$ in (3.50). The latter effect is usually ignored in the calculation of transport coefficients in the Coulomb liquid, that is, the model of the OCP. In order to assess the acceptability of this approximation, in [Pot 97] in the calculation of $S(q)$ was taken into account the polarizability of the electronic background as amended LFC, according to [Cha 90b]. Such an accounting background polarizability leads to an increase Λ_{ei} for hydrogen about $\lesssim$15% at $\rho = 100 g/cm^3$ and $\Gamma = 10$ and 40% for largeΓ. For the helium effect is several times weaker, while for heavy elements it is negligible.

III.7.3. Ionic Crystal (multiphonon processes)

In the crystal, ei-scattering can be described in terms of absorption and emission of phonons. It can happen through normal processes, and through Umklapp processes (eg, [Kit 1986]): In the first case, the momentum transfer $\hbar\vec{q} = \vec{p}' - \vec{p}$ lies in the first Brillouin zone and the second over and through the zone. The wave vectors $\vec{k}$ absorbed and emitted phonons, by definition, lie in the first Brillouin zone. Therefore,

for normal processes, $\vec{k} = \vec{q}$, and for the umklapp processes $\vec{k} = \vec{q} - \vec{q}_0$, where $\vec{q}_0$ –is the equivalent radius of the Brillouin zone, which reaches the vector $\vec{q}$. If the electron momentum $\vec{p}$ on the Fermi surface is free to disperse to any other point of the Fermi sphere ($q \leq 2\,k_F$), then according to the equation $q_{BZ} = (6\pi n_{ion})^{1/3}$ (2.36), the ratio of the normal process to the umklapp scattering $is\,(2\,k_F / q_{BZ})^2 \sim (4Z)^{2/3}$. In the laboratory, the number of conduction electrons per ion Z is small, so it is usually the most important are the normal processes, but in dense astrophysical plasmas of heavy elements, on the contrary, $Z \gg 1$, and therefore dominated by the Umklapp processes (if not too low temperatures, as explained below).

As noted above, the Bragg scattering does not contribute to the electronic relaxation, so in the collision one consider only the inelastic component of the structural factor. Inelastic dynamic structure factor is calculated by formula (2.67). If in this formula, if one shaves off the amount of n. $n = 1$, he arrives at the one-phonon approximation (2.75) which is used in earlier studies [Flo 76] [Ito 83] [Ito 93] [Bai 95]. However, as it was noted in the paper [Bai 98], that one-phonon approximation breaks down when T approaches to T_m - Contribution of the n-phonon processes (n-th term) for T above the Debye temperature can be estimated as $(qr_T)^{2n}/\,n! \sim (k_F r_T)^{2n}/\,n!$, where $r_T^2 \approx \frac{u_{-2}a^2}{\Gamma}$ can be estimated by the formula (2.63). For example, for iron at $\Gamma \sim \Gamma_m$ obtained subsection $(k_F r_T)^2 \sim 3$ - no small number.

Given the dominance of Umklapp processes for calculating the Coulomb logarithm can use the approximation (2.73).

As noted above, in the general case to distinguish between the effective relaxation time to calculate the conductivity τ_σ and τ_κ in the heat equation (3.36). Therefore, in equation (3.29) and (3.49) will, generally speaking, different Coulomb logarithms Λ_{ei}^{σ} and Λ_{ei}^{κ} (the difference between them can be neglected when scattering quasielastic,

ie at $T \sim T_{pi}$). Accordingly, in (3.49) as $S_{eff}(q)$ using different effective static structure factors $S_\sigma(q)$ and $S_\kappa(q)$ [Bai 98]:

$$\Lambda_{ei}^{\sigma,\kappa} = \int_0^{2k_F} q^3 \left|\phi_q\right|^2 S_{\sigma,\kappa}(q) \left[1 - \frac{v_F^2}{c^2}\left(\frac{q}{2k_F}\right)^2\right] dq \qquad (3.55).$$

$$\tau_{ei}^{\sigma} = \frac{p_F^2 v_F}{4\pi Z^2 e^4 n_{ion}\, \Lambda_{ei}^{\sigma}}\,, \tau_{ei}^{\kappa} = \frac{p_F^2 v_F}{4\pi Z^2 e^4 n_{ion} \Lambda_{ei}^{\kappa}} \qquad (3.56).$$

Factors and $S_\sigma(q)$ and $S_\kappa(q)$ to be expressed through $S''(q,\omega)$ by the equalities:

$$S_\sigma(q) = \int_{-\infty}^{+\infty} \frac{z}{1 - e^{-z}} S''(q,\omega) d\omega \qquad (3.57).$$

$$S_\kappa(q) = S_\sigma(q) + \left(\frac{3k_F^2}{q^2} - \frac{1}{2}\right) \delta S_\kappa(q) \qquad (3.58).$$

$$\delta S_\kappa(q) = \int_{-\infty}^{+\infty} \frac{z^3}{1 - e^{-z}} S''(q,\omega)\, d\omega \qquad (3.59).$$

Where $z = \hbar\omega / k_B T$.

Using (2.74), one can rewrite (3.57) and (3.59) as:

$$S_\sigma(q) = \frac{1}{2} e^{-2W(q)} \int_{-\infty}^{+\infty} K(q,T,t) \frac{dx}{\cosh^2 x} \qquad (3.60).$$

$$\delta S_\kappa(q) = e^{-2W(q)} \int_{-\infty}^{+\infty} K(q,T,t) \frac{1 - 2\sinh^2 x}{\cosh^4 x} dx \qquad (3.61).$$

Where x = πtT/ n, and the function K (q, T, t) defined in (2.75). Calculations [Bai 98] [Pot 99a] show that these functions are almost independent of the type of crystal lattice.

Consider the classic crystal: $T \gtrsim T_{pi}$. Then the characteristic phonon energy is much smaller than $k_B T$. Consequently, only the values of $z \ll 1$ give a contribution to the integrals (3.57) and (3.58), and it can be a good approximation to put:

$$\boldsymbol{S_\sigma(q) = S_\kappa(q) = \int_{-\infty}^{+\infty} S''(q,\omega)\, d\omega} \qquad (\mathbf{3.62}).$$

Finding $\Lambda_{ei}^{\sigma} = \Lambda_{ei}^{\kappa}$ from (3.49) (with the substitution of $S''(q,\omega)$ instead of $S(q)$), and $\tau_{ei}^{\sigma} = \tau_{ei}^{\kappa}$. This approximation is equivalent to the relaxation time approximation used before . In this case, $\Lambda_{ei}^{\sigma,\kappa}$ (in the formula (3.56) usually takes values ~ 1.

In the opposite limiting case of low temperature ($T \ll T_{pi}$) correlation ions - essentially dynamic. In this case $\Lambda_{ei}^{\sigma} \neq \Lambda_{ei}^{\kappa}$ and $\Lambda_{ei}^{\sigma,\kappa} \ll 1$.

Effective structural factors: First of all, using the fact that in high temperature Coulomb crystal ($T_{pi} \lesssim T < T_m$), one can use the equation (3.62) with $S''(q)$, defined by equation (2.76). Debye-Waller factor$e^{-2W(q)}$, the incoming In this equation, and it can be estimated by formulas (2.61) and (2.63).

In general, the effective structure factors in (3.55) can be described by the approximation formulas [Pot 99a]:

$$\boldsymbol{S_\sigma(q) = e^{-2W(q)}\left(e^{-2W_1(q)} - 1\right)} \qquad (\mathbf{3.63}).$$

$$\boldsymbol{\delta S_\kappa(q) = \alpha_1 \left[\frac{91\eta^2 e^{-2W(q)}}{(1+111.4\eta^2)^2} + \frac{0.101\eta^4}{(0.06408+\eta^2)(0.001377+\eta^2)^{3/2}}\right]} \qquad (\mathbf{3.64}).$$

$$\boldsymbol{W_1(q) = \frac{\alpha_1 u_{-2}\eta^2}{2\sqrt{\eta^2 + (\frac{u_{-2}}{117})^2}}}$$

Where:

$$\boldsymbol{\alpha_1 = \alpha_0 \frac{q^2}{2k_F^2} = \frac{(qr_D)^2}{\eta}}\ , \boldsymbol{\alpha_0 = \frac{4k_F^2 a_i^2}{3\Gamma\eta} = 1.683\sqrt{\frac{x_r}{AZ}}} \qquad (\mathbf{3.65}).$$

These formulas cover a fairly wide range of parameters $0{,}001 \leq \eta \leq 10$, and $0 \leq \alpha_1 \leq 0.3$. Equations (3.63) and (3.64) also reproduce the asymptotics of effective structural factors at large and small η, which can be obtained from formulas (3.60) and (3.61). The maximum approximation error of 4%, achieved with $\alpha_1 = 0{,}001$ and $\eta = 0{,}04$.

III.7.3.a Low temperature: the case of normal processes

Near the boundaries of Brillouin zones, dispersion relation for electrons of $\epsilon(\vec{p})$ differs from the free-electron case, and at the boundaries the electron energy spectrum contains gaps. The gaps $\Delta\epsilon$ can be estimated in the weak coupling approximation (eg, [Kit 86]) as $\Delta\epsilon \sim \phi(k_F) = 4\pi Ze^2 n_{ion} k_F^{-2} = 4e^2/(3\pi k_F)$. The effect of gaps is most significant if the deviation of the electron momentum from the intersection line between the Fermi surface and the Brillouin zone boundary does not exceed $\Delta k \sim \Delta\epsilon/(\hbar v_F) \sim (4/3\pi)\left(\alpha_f \gamma_r / x_r\right) k_F$. However, with decreasing temperature the strips of the Fermi surface, between which the umklapps proceed effectively, become narrower and closer to these intersection lines. When the widths of the strips $\sim q_{BZ}/\eta$ become smaller than Δk, the umklapp processes are frozen out and the normal processes prevail. The above estimates indicate that this happens when the temperature falls below:

$$\boldsymbol{T_u \sim \frac{T_{pi} Z^{\frac{1}{3}} \alpha_f \gamma_r}{(3x_r)}} \qquad (\mathbf{3.66}).$$

In this case (3.55)should be replaced by:

$$\begin{Bmatrix}\Lambda_{ei}^{\sigma}\\ \Lambda_{ei}^{\sigma}\end{Bmatrix}=\frac{2p_F^2}{m_iT}\int\frac{d\Omega}{4\pi}\int\frac{d\Omega'}{4\pi}|\phi_q|^2\left[1-\frac{v_F^2}{c^2}\left(\frac{q}{2k_F}\right)^2\right]\times$$
$$\times\sum\nolimits_s\left[\vec{q}\vec{e}_s(\vec{k})\right]^2\frac{e^{-z}}{(1-e^{-z})^2}\begin{Bmatrix}q^2\\ q^2-(qz/\pi)^2+3(k_Fz/\pi)^2\end{Bmatrix} \quad (3.67).$$

Where $d\Omega$ and $d\Omega'$ - elements of solid angle near the directions of $\vec{p}$ and $\vec{p}',p=p'=p_F$. Expression equivalent to (3.67) was obtained in [Rai 82] using the general method [Zim 61] and the spherical Wigner-Seitz cell and single-phonon scattering.

At $T\ll T_u$ from (3.67) can be possible to obtain precise asymptotics for the Coulomb logarithm [Rai 1982], which are expressed in terms of plasma parameters as follows:

$$\begin{Bmatrix}\Lambda_{ei}^{\sigma}\\ \Lambda_{ei}^{\sigma}\end{Bmatrix}=\frac{a_\zeta x_r^{1/2}}{A^{1/2}Z^{1/2}}\begin{Bmatrix}(4\pi/3)(\alpha_f\gamma_r/x_r)\eta^{-5}\\ \eta^{-3}\end{Bmatrix} \quad (3.68).$$

Where: $a_\zeta=\frac{180}{\pi}\left(\frac{3}{\pi\alpha_f}\frac{m_e}{m_u}\right)^{1/2}\zeta(5)\approx 15.9$ and $\zeta(5)=1.0369$ here $\zeta(x)$ - Riemann zeta function).

III.8. Overall approximation for the outer shells

In this section we present unified analytical approximations to calculate the electronic thermal conductivity, conductivity and thermoelectric coefficient caused by electron scattering on ions.

Let us start treat the case when $T\ll T_F$. the Strongly degenerate case, the classical Coulomb liquid of strongly bound and the classical ionic crystal have similar physical properties. Calculations [Gne 01] [Bai 1998] [ref214] show that due to this similarity jump kinetic coefficients at the phase boundary between Coulomb and liquid crystal is very small, provided that of strongly degenerate Coulomb fluid used inelastic structure factor (3.51), and in the crystal are taken into account multiphonon processes according to (3.62) and (2.73). Carrying out the calculations for $\Gamma\geq 1$ facilitated by the approximate formulas (3.63)

(3.64). On the other hand, when $\Gamma \ll 1$, one can use the formula (3.45). The Coulomb logarithms, calculated by this formula for $\Gamma < 1$, sufficiently smoothly matched with the Coulomb logarithms, calculated at $\Gamma > 1$. This allowed one to construct a unified approximate formula for calculating the electronic conductivity due to ei-scattering, applicable in all phases [Pot 99a]. It is based on the expression (3.49), in which a $\left|\phi_q\right|^2 S\,(q)$ is replaced by effective screening function:

$$\left|\boldsymbol{\phi_q^{eff}}\right|^2 = \frac{\mathbf{1}}{(\boldsymbol{q^2 + q_s^2})^2}\left[\mathbf{1} - \boldsymbol{e^{-s_0 q^2}}\right]\boldsymbol{e^{-s_1 q^2}}\boldsymbol{G_{\sigma,\kappa}}\boldsymbol{D(\eta)} \qquad (\mathbf{3.69}).$$

Here the first factor has the form of the Debye screening function with the effective inverse screening length:

$$\boldsymbol{q_s} = \sqrt{(\boldsymbol{q_i^2 + k_{TF}^2})\boldsymbol{e^{-\beta}}} \qquad (\mathbf{3.70}).$$

Where the parameter $\beta = \frac{\pi \alpha_f Z x_r}{\gamma_r}$ associated with the second Born correction in (3.45), and:

$$\boldsymbol{q_i^2} = \boldsymbol{q_D^2}(\mathbf{1 + 0.06\Gamma})\boldsymbol{e^{-\sqrt{\Gamma}}} \qquad (\mathbf{3.71}).$$

-is the effective length of the inverse ion screening. Thus, q_s becomes k_s at $\Gamma \ll 1$ and k_{TF} at $\Gamma \gg 1$. The second factor (in brackets), in form similar to (2.76), plays the role of an effective structure factor, so the s_0 on the order of magnitude close to the r_T^2 / 3, expressed by the formula (2.63), and namely :

$$\boldsymbol{s_0} = \boldsymbol{u_{-2} r_D^2}\left(\mathbf{1} + \frac{\boldsymbol{\beta}}{\mathbf{3}}\right) \qquad (\mathbf{3.72}).$$

The third factor is introduced in [Gne 01], takes into account the ionic form factor and, thus, allows expanding the range of applicability of approximation to the inner crust too. Included in this factor is a parameter:

$$\boldsymbol{s_1 = r_{nuc}^2 \left(1 + \sqrt{x_{nuc}}\frac{Z}{13}\right)\left(1 + \frac{\beta}{3}\right)} \qquad (\mathbf{3.73}).$$

Order of magnitude close to the r_{nuc}^2 where r_{nuc} - proton radius of the atomic nucleus (ie the characteristic radius of the distribution of positive charge in the nucleus). For the calculations is useful to note that $k_F r_{nuc} = (9\pi / 4)^{1/3} x_{nuc}$, but x_{nuc} is given by (3.54). Finally, the functions G and D describe the quantum effects at low temperature. the function:

$$\boldsymbol{D(\eta) = exp\left[-\alpha_0 u_{-1} e^{-9.1/\eta}/4\right]} \qquad (\mathbf{3.74}).$$

- Is associated with the quantum correction to the Debye-Waller factor . and G is a phenomenological factor that describes the reduction of ion thermal displacements in quantum solid at $T \lesssim T_{pi}$ and contains non-Born corrections expressed through the argument β:

$$\boldsymbol{G_\sigma = \frac{1 + (Z/125)^2}{\sqrt{1 + (0.19\eta)^2 Z^{-1/3}}}} \qquad (\mathbf{3.75}).$$

$$\boldsymbol{G_\kappa = G_\sigma + \delta G\,, \delta G = \frac{0.0105\eta^2}{(1 + 0.0081\eta^2)^{3/2}}[1 + (x_r/\gamma_r)^3\beta](1 - Z^{-1})} \qquad (\mathbf{3.76}).$$

G Increases with Z and decreases as η^{-1} at $\eta \gg 1$. Note that one can safely put $G = 1$ at $T \gtrsim T_{pi}$ and $Z \lesssim 30$.

Equation (3.49) with the effective screening function (3.69) can be integrated. As a result, O.Y. Gnedin et al obtain [Gne 01]:

$$\boldsymbol{\Lambda_{\sigma,\kappa}^{fit} = [\Lambda_0(s, w + w_1) - \Lambda_0(s, w_1)]G_{\sigma,\kappa}D(\eta)} \quad (\mathbf{3.77}).$$

Where: $s = \frac{q_s^2}{4k_F^2}$, $w = 4k_F^2 s_0$, $w_1 = 4k_F^2 s_1$

$$\boldsymbol{\Lambda_0(s, w) = \Lambda_1(s, w) - \frac{v^2}{c^2}\Lambda_2(s, w)} \quad (\mathbf{3.78}).$$

$$\boldsymbol{2\Lambda_1(s, w) = \ln\frac{s+1}{s} + \frac{s}{s+1}(1 - e^{-w}) - (1 + sw)e^{sw}[E_1(sw) - E_1(sw + w)]} \quad (\mathbf{3.79}).$$

$$\boldsymbol{2\Lambda_2(s, w) = \frac{e^{-w} - 1 + w}{w} - \frac{s^2}{s+1}(1 - e^{-w}) -} \quad \textit{(3.80).}$$

$$\boldsymbol{-2s\ln\frac{s+1}{s} + s(2 + sw)e^{sw}[E_1(sw) - E_1(sw + w)]}$$

Where $E_1(x) = \int_x^\infty y^{-1}e^{-y}dy$ is the exponential integral given, for example, by the rational-polynomial approximations in Abramowitz and Stegun [Abr 72].

Note that the direct use of (3.79) (3.80) can be difficult in various limiting cases when $s \ll 1$, $w \ll 1$, or $w \gg 1$. In these cases it is better to use explicit asymptotic limit [Pot 99a]:

$$\boldsymbol{\Lambda_1(s, w \ll 1) \approx w\left(\frac{2s+1}{2s+2} - s\ln\frac{s+1}{s}\right)} \quad (\mathbf{3.81}).$$

$$\boldsymbol{\Lambda_2(s, w \ll 1) \approx w\left(\frac{1 - 3s - 6s^2}{4s+4} - \frac{3}{2}\ln\frac{s+1}{s}\right)} \quad (\mathbf{3.82}).$$

$$\boldsymbol{\Lambda_1(s, w \gg 1) \approx \frac{1}{2}\left(\ln\frac{s+1}{s} - \frac{1}{s+1}\right)} \quad (\mathbf{3.83}).$$

$$\boldsymbol{\Lambda_2(s, w \gg 1) \approx \frac{2s+1}{2s+2} - s\ln\frac{s+1}{s}} \quad (\mathbf{3.84}).$$

$$\boldsymbol{\Lambda_1(s \ll 1, w \ll s^{-1}) = \frac{1}{2}[E_1(w) + \ln w + C_E]} \quad (\mathbf{3.85}).$$

$$\boldsymbol{\Lambda_2(s \ll 1, w \ll s^{-1}) = \frac{e^{-w} - 1 + w}{2w}} \qquad (\mathbf{3.86}).$$

Where $C_E = 0.5772\ldots$ – is the Euler's constant.

These formulas are obtained for not too low temperatures, when not frozen transfer processes. At low temperatures , one incorporate by interpolation:

$$\boldsymbol{\Lambda_{ei}^{\sigma,\kappa} = \Lambda_{\sigma,\kappa}^{fit} \exp(-T_u/T) + \Lambda_{ei,low}^{\sigma,\kappa}[1 - \exp(-T_u/T)]} \qquad (\mathbf{3.87}).$$

Where $\Lambda_{\sigma,\kappa}^{fit}$, defined by (3.77) and $\Lambda_{ei,low}^{\sigma,\kappa}$- low-temperature asymptotic (3.68). Note that despite the practical convenience of such interpolation the actual behavior of the Coulomb logarithm in the intermediate temperature regime requires a separate study, which is still lacking.

Thus, the kinetic coefficients in the strongly degenerate plasma, one can obtain using (3.36) (3.47) and (3.87).

Chapter IV

Electrical and thermal conductivities in dense plasma

A- Theoretical contribution

IV.1. The effect of the nuclear form factor

Basing on the Ioffe model that unifies the description of the transport phenomena in both liquid and solid states of matter inside the extremely dense matter of neutron star crusts , our first contribution is to study some aspect of nuclear physics , the main characteric parameter is the nuclear form factor that we talked about.

IV.1. 1. The Gaussian Charge distribution

The general form of the Gaussian Charge distribution is given by (eg [Pov 08]):

$$\varrho(r) = \left(\frac{a^2}{2\pi}\right)^{3/2} e^{-\frac{a^2 r^2}{2}} \qquad (4.1).$$

The Fourier transform of the relation (4.1) gives the so called the Gaussian nuclear form factor:

$$F_q^{Gauss} = \exp\left(-\frac{q^2}{2a^2\hbar^2}\right) \qquad (4.2).$$

To apply this formulate to neutron star crust, first we must replace the term $a\hbar$ by r_{nuc}^{-1} then our Gaussian nuclear form factor (4.2) become:

$$F_q^{Gauss} = exp\left(-\frac{q^2 r_{nuc}^2}{2}\right) \qquad (4.3).$$

Replacing (4.3) in (3.69) we get the effective screening potential of an exponential charge distribution of the ions :

$$\left|\boldsymbol{\phi}_{\boldsymbol{q}}^{\boldsymbol{eff}}\right|_{\boldsymbol{Gauss}}^{\boldsymbol{2}} = \frac{\exp(-\boldsymbol{q}^{\boldsymbol{2}}\boldsymbol{r}_{\boldsymbol{nuc}}^{\boldsymbol{2}})}{(\boldsymbol{q}^{\boldsymbol{2}}+\boldsymbol{q}_{\boldsymbol{s}}^{\boldsymbol{2}})^{\boldsymbol{2}}}\left[\boldsymbol{1}-\boldsymbol{e}^{-\boldsymbol{s}_{\boldsymbol{0}}\boldsymbol{q}^{\boldsymbol{2}}}\right]\boldsymbol{G}_{\boldsymbol{\sigma},\boldsymbol{\kappa}}\boldsymbol{D}(\boldsymbol{\eta}) \qquad (\boldsymbol{4.4}).$$

$$= \left|F_{q}^{Gauss}\right|^{2}\left|\boldsymbol{\phi}_{\boldsymbol{q}}^{\boldsymbol{eff}}\right|_{\boldsymbol{PL}}^{\boldsymbol{2}}$$

By combining equations (3.55) and (4.4), we:

$$\left(\boldsymbol{\Lambda}_{\boldsymbol{ei}}^{\boldsymbol{\sigma},\boldsymbol{\kappa}}\right)_{\boldsymbol{Gauss}} = \int_{\boldsymbol{0}}^{\boldsymbol{2k_F}} \boldsymbol{q}^{\boldsymbol{3}}\left|\boldsymbol{\phi}_{\boldsymbol{q}}^{\boldsymbol{eff}}\right|_{\boldsymbol{Gauss}}^{\boldsymbol{2}}\left[\boldsymbol{1}-\frac{\boldsymbol{v}_{\boldsymbol{F}}^{\boldsymbol{2}}}{\boldsymbol{c}^{\boldsymbol{2}}}\left(\frac{\boldsymbol{q}}{\boldsymbol{2k_F}}\right)^{\boldsymbol{2}}\right]\boldsymbol{dq} \qquad (\boldsymbol{4.5}).$$

$$= \int_{\boldsymbol{0}}^{\boldsymbol{2k_F}} \boldsymbol{q}^{\boldsymbol{3}}\left|F_{q}^{Gauss}\right|^{2}\left|\boldsymbol{\phi}_{\boldsymbol{q}}^{\boldsymbol{eff}}\right|_{\boldsymbol{PL}}^{\boldsymbol{2}}\left[\boldsymbol{1}-\frac{\boldsymbol{v}_{\boldsymbol{F}}^{\boldsymbol{2}}}{\boldsymbol{c}^{\boldsymbol{2}}}\left(\frac{\boldsymbol{q}}{\boldsymbol{2k_F}}\right)^{\boldsymbol{2}}\right]$$

Also:

$$\left(\boldsymbol{\Lambda}_{\boldsymbol{ei}}^{\boldsymbol{\sigma},\boldsymbol{\kappa}}\right)_{\boldsymbol{Gauss}} = \int_{\boldsymbol{0}}^{\boldsymbol{2k_F}} \boldsymbol{q}^{\boldsymbol{3}}\frac{\exp(-\boldsymbol{q}^{\boldsymbol{2}}\boldsymbol{r}_{\boldsymbol{nuc}}^{\boldsymbol{2}})}{(\boldsymbol{q}^{\boldsymbol{2}}+\boldsymbol{q}_{\boldsymbol{s}}^{\boldsymbol{2}})^{\boldsymbol{2}}}\times \qquad (\boldsymbol{4.6}).$$

$$\times\left[\boldsymbol{1}-\boldsymbol{e}^{-\boldsymbol{s}_{\boldsymbol{0}}\boldsymbol{q}^{\boldsymbol{2}}}\right]\boldsymbol{G}_{\boldsymbol{\sigma},\boldsymbol{\kappa}}\boldsymbol{D}(\boldsymbol{\eta})\left[\boldsymbol{1}-\frac{\boldsymbol{v}_{\boldsymbol{F}}^{\boldsymbol{2}}}{\boldsymbol{c}^{\boldsymbol{2}}}\left(\frac{\boldsymbol{q}}{\boldsymbol{2k_F}}\right)^{\boldsymbol{2}}\right]\boldsymbol{dq}$$

And then we get by computing analytical formulae for the Coulomb logarithm:

$$\boldsymbol{\Lambda}_{\boldsymbol{1}}^{\boldsymbol{GS}} = \frac{\boldsymbol{1}}{\boldsymbol{s}_{\boldsymbol{0}}^{\boldsymbol{2}}}\left(\frac{\boldsymbol{1}}{\boldsymbol{r}_{\boldsymbol{nuc}}^{\boldsymbol{2}}}\boldsymbol{e}^{-\frac{\boldsymbol{w}\boldsymbol{r}_{\boldsymbol{nuc}}^{\boldsymbol{2}}}{\boldsymbol{s}_{\boldsymbol{0}}}}\left(-\boldsymbol{e}^{\frac{\boldsymbol{w}\boldsymbol{r}_{\boldsymbol{nuc}}^{\boldsymbol{2}}(\boldsymbol{s}^{\boldsymbol{2}}\boldsymbol{w}+\boldsymbol{s}_{\boldsymbol{0}})}{\boldsymbol{s}_{\boldsymbol{0}}^{\boldsymbol{2}}}}\boldsymbol{s}^{\boldsymbol{2}}\boldsymbol{w}^{\boldsymbol{2}}\times\right.\right.$$

$$\times \left(\mathbf{E}_1\left[\frac{s^2w^2r_{\mathrm{nuc}}^2}{s_0^2}\right] - \mathbf{E}_1\left[\frac{wr_{\mathrm{nuc}}^2\left(s^2w+s_0\right)}{s_0^2}\right]\right)r_{\mathrm{nuc}}^2 + \left(-1+e^{\frac{wr_{\mathrm{nuc}}^2}{s_0}}\right)s_0^2\Big)$$
$$-\frac{1}{r_{\mathrm{nuc}}^2+s_0}e^{-\frac{w\left(r_{\mathrm{nuc}}^2+s_0\right)}{s_0}}\Big(-e^{\frac{w\left(s^2w+s_0\right)\left(r_{\mathrm{nuc}}^2+s_0\right)}{s_0^2}}s^2w^2\left(\mathbf{E}_1\left[\frac{s^2w^2\left(r_{\mathrm{nuc}}^2+s_0\right)}{s_0^2}\right]\right.$$
$$\left.-\mathbf{E}_1\left[\frac{w\left(s^2w+s_0\right)\left(r_{\mathrm{nuc}}^2+s_0\right)}{s_0^2}\right]\right)r_{\mathrm{nuc}}^2$$
$$-s_0\Big(e^{\frac{w\left(s^2w+s_0\right)\left(r_{\mathrm{nuc}}^2+s_0\right)}{s_0^2}}s^2w^2\left(\mathbf{E}_1\left[\frac{s^2w^2\left(r_{\mathrm{nuc}}^2+s_0\right)}{s_0^2}\right]\right.$$
$$\left.-\mathbf{E}_1\left[\frac{w\left(s^2w+s_0\right)\left(r_{\mathrm{nuc}}^2+s_0\right)}{s_0^2}\right]\right)+\left(-1+e^{w+\frac{wr_{\mathrm{nuc}}^2}{s_0}}\right)s_0\Big)\Big)\Big)$$

$$(4.7).$$

$$\Lambda_2^{\mathrm{GS}}=\frac{1}{ws_0^3}\Big(-\frac{1}{r_{\mathrm{nuc}}^4}e^{-\frac{wr_{\mathrm{nuc}}^2}{s_0}}\Big(-e^{\frac{wr_{\mathrm{nuc}}^2\left(s^2w+s_0\right)}{s_0^2}}s^4w^4\times$$
$$\times\left(\mathbf{E}_1\left[\frac{s^2w^2r_{\mathrm{nuc}}^2}{s_0^2}\right]-\mathbf{E}_1\left[\frac{wr_{\mathrm{nuc}}^2\left(s^2w+s_0\right)}{s_0^2}\right]\right)r_{\mathrm{nuc}}^4+\left(-1+e^{\frac{wr_{\mathrm{nuc}}^2}{s_0}}\right)s_0^4$$
$$-wr_{\mathrm{nuc}}^2s_0^2\left(\left(-1+e^{\frac{wr_{\mathrm{nuc}}^2}{s_0}}\right)s^2w+s_0\right)\Big)$$
$$+\frac{1}{\left(r_{\mathrm{nuc}}^2+s_0\right)^2}e^{-\frac{w\left(r_{\mathrm{nuc}}^2+s_0\right)}{s_0}}\Big(-e^{\frac{w\left(s^2w+s_0\right)\left(r_{\mathrm{nuc}}^2+s_0\right)}{s_0^2}}s^4w^4\Big(\mathbf{E}_1\Big[\frac{s^2w^2\left(r_{\mathrm{nuc}}^2+s_0\right)}{s_0^2}\Big]$$
$$-\mathbf{E}_1\Big[\frac{w\left(s^2w+s_0\right)\left(r_{\mathrm{nuc}}^2+s_0\right)}{s_0^2}\Big]\Big)r_{\mathrm{nuc}}^4$$
$$+wr_{\mathrm{nuc}}^2s_0\Big(-2e^{\frac{w\left(s^2w+s_0\right)\left(r_{\mathrm{nuc}}^2+s_0\right)}{s_0^2}}s^4w^3\Big(\mathbf{E}_1\Big[\frac{s^2w^2\left(r_{\mathrm{nuc}}^2+s_0\right)}{s_0^2}\Big]$$
$$-\mathbf{E}_1\Big[\frac{w\left(s^2w+s_0\right)\left(r_{\mathrm{nuc}}^2+s_0\right)}{s_0^2}\Big]\Big)+\left(-1+e^{w+\frac{wr_{\mathrm{nuc}}^2}{s_0}}\right)s^2ws_0+s_0^2\Big)$$
$$-s_0^2\Big(e^{\frac{w\left(s^2w+s_0\right)\left(r_{\mathrm{nuc}}^2+s_0\right)}{s_0^2}}s^4w^4\Big(\mathbf{E}_1\Big[-\frac{s^2w^2\left(r_{\mathrm{nuc}}^2+s_0\right)}{s_0^2}\Big]$$
$$-\mathbf{E}_1\Big[-\frac{w\left(s^2w+s_0\right)\left(r_{\mathrm{nuc}}^2+s_0\right)}{s_0^2}\Big]\Big)-\left(-1+e^{w+\frac{wr_{\mathrm{nuc}}^2}{s_0}}\right)s^2w^2s_0+\left(-1$$
$$+e^{w+\frac{wr_{\mathrm{nuc}}^2}{s_0}}-w\right)s_0^2\Big)\Big)\Big)$$

$$(4.8).$$

IV.1. 2. The homogeneous sphere charge distribution

The general form of the homogeneous sphere Charge distribution is given by (eg [Pov 08]):

$$\boldsymbol{\varrho(r)} = \begin{cases} \dfrac{\mathbf{1}}{\dfrac{\mathbf{4}}{\mathbf{3}}\boldsymbol{\pi R^3}} & \boldsymbol{for \;\; r \leq R} \\ \mathbf{0} \qquad \boldsymbol{for \;\; r > R} \end{cases} \qquad (\mathbf{4.9}).$$

Where:

R : Is The nuclear radius, for ordinary nuclei in neutron star crusts is usually given by $r_0 Z^{1/3}$ instead of the well known formula in nuclear physics $r_0 A^{1/3}$ (eg: [Hae 06]) where $r_0 \approx 1.2 \times 10^{15} fm$.

The Fourier transform of the relation (4.10) gives the so called the oscillating nuclear form factor;

$$\boldsymbol{F_q^{osc}} = \frac{\mathbf{3}}{\boldsymbol{\alpha^3}}[\mathbf{sin(\alpha) - \alpha\, cos(\alpha)}] \qquad (\mathbf{4.10}).$$

where: $\alpha = R.q$.

To apply this formulate to neutron star crust, first we must replacing the term R by r_{nuc} (§III.7.2.b), then our oscillating nuclear form factor (4.10) becomes:

$$\boldsymbol{F_q^{osc}} = \frac{\mathbf{3}}{\mathbf{(qr_{nuc})^3}}[\mathbf{sin(qr_{nuc}) - qr_{nuc}\, cos(qr_{nuc})}] \qquad (\mathbf{4.11}).$$

Which is the same result given in [Hae.07], and used by authors in previews work, but we shall use it in different way,

Replacing (4.11) in (3.69) we get the effective screening potential of an exponential charge distribution of the ions:

$$\left|\boldsymbol{\phi}_{q}^{eff}\right|_{osc}^{2}=\frac{\mathbf{1}}{(q^{2}+q_{s}^{2})^{2}}\left\{\frac{\mathbf{3}}{(\mathbf{qr_{nuc}})^{3}}[\mathbf{sin(qr_{nuc})-qr_{nuc}cos(qr_{nuc})}]\right\}^{2}\times$$

$$\times\left[\mathbf{1}-e^{-s_{0}q^{2}}\right]\boldsymbol{G_{\sigma,\kappa}D(\eta)}\;=\;\left|F_{q}^{osc}\right|^{2}\left|\boldsymbol{\phi}_{q}^{eff}\right|_{PL}^{2}\qquad(\mathbf{4.12}).$$

$$\left(\boldsymbol{\Lambda}_{ei}^{\sigma,\kappa}\right)_{osc}=\int_{0}^{2k_{F}}q^{3}\left|F_{q}^{osc}\right|^{2}\left|\boldsymbol{\phi}_{q}^{eff}\right|_{PL}^{2}\left[\mathbf{1}-e^{-s_{0}q^{2}}\right]\boldsymbol{G_{\sigma,\kappa}D(\eta)}\times$$

$$\times\left[\mathbf{1}-\frac{v_{F}^{2}}{c^{2}}\left(\frac{q}{2k_{F}}\right)^{2}\right]dq\qquad(\mathbf{4.13}).$$

To have an analytical formula for $\left(\Lambda_{\mathrm{ei}}^{\sigma,\kappa}\right)_{\mathrm{osc}}$ we must first take into account Gneding result [Gne. 01]:

$$\left|\boldsymbol{\phi}_{\mathbf{q}}^{\mathbf{eff}}\right|_{\mathbf{osc}}^{\mathbf{2}}=\frac{\mathbf{e}^{-\mathbf{s_{1}q^{2}}}}{(\mathbf{q^{2}+q_{s}^{2}})^{\mathbf{2}}}\qquad(\mathbf{4.14}).$$

Then our Coulomb logarithm can be written as:

$$\left(\boldsymbol{\Lambda}_{ei}^{\sigma,\kappa}\right)_{osc}=\int_{0}^{2k_{F}}q^{3}\frac{e^{-s_{1}q^{2}}}{(q^{2}+q_{s}^{2})^{2}}\times$$

$$\times\left[\mathbf{1}-e^{-s_{0}q^{2}}\right]\boldsymbol{G_{\sigma,\kappa}D(\eta)}\left[\mathbf{1}-\frac{v_{F}^{2}}{c^{2}}\left(\frac{q}{2k_{F}}\right)^{2}\right]dq\qquad(\mathbf{4.15}).$$

Thus the exact result is:

$$\Lambda_1^{osc} = \frac{1}{s_0^2}\left(\frac{1}{s_1} e^{-\frac{ws_1}{s_0}}\left(\left(-1 + e^{\frac{ws_1}{s_0}}\right)s_0^2 + e^{\frac{w(s^2w+s_0)s_1}{s_0^2}} s^2w^2 \times\right.\right.$$

$$\times \left(\mathrm{E}_1\left[-\frac{s^2w^2s_1}{s_0^2}\right] - \mathrm{E}_1\left[-\frac{w(s^2w+s_0)s_1}{s_0^2}\right]\right)s_1\Big)$$

$$-\frac{1}{s_0+s_1} e^{-\frac{w(s_0+s_1)}{s_0}}\left(e^{\frac{w(s^2w+s_0)(s_0+s_1)}{s_0^2}} s^2w^2\left(\mathrm{E}_1\left[-\frac{s^2w^2(s_0+s_1)}{s_0^2}\right]\right.\right.$$

$$\left.\left.- \mathrm{E}_1\left[-\frac{w(s^2w+s_0)(s_0+s_1)}{s_0^2}\right]\right)s_0 + \left(-1 + e^{w+\frac{ws_1}{s_0}}\right)s_0^2\right.$$

$$+ e^{\frac{w(s^2w+s_0)(s_0+s_1)}{s_0^2}} s^2w^2\left(\mathrm{E}_1\left[-\frac{s^2w^2(s_0+s_1)}{s_0^2}\right]\right.$$

$$\left.\left.- \mathrm{E}_1\left[-\frac{w(s^2w+s_0)(s_0+s_1)}{s_0^2}\right]\right)s_1\right)\Big) \tag{4.16}$$

$$\Lambda_2^{osc} = \frac{1}{ws_0^3}\left(\frac{1}{r_{nuc}^4} e^{-\frac{wr_{nuc}^2}{s_0}}\left(-e^{\frac{wr_{nuc}^2(s^2w+s_0)}{s_0^2}} s^4w^4 \times\right.\right.$$

$$\times \left(\mathrm{E}_1\left[-\frac{s^2w^2r_{nuc}^2}{s_0^2}\right] - \mathrm{E}_1\left[-\frac{wr_{nuc}^2(s^2w+s_0)}{s_0^2}\right]\right)r_{nuc}^4 + \left(-1 + e^{\frac{wr_{nuc}^2}{s_0}}\right)s_0^4 -$$

$$wr_{nuc}^2 s_0^2\left(\left(-1 + e^{\frac{wr_{nuc}^2}{s_0}}\right)s^2w + s_0\right) +$$

$$\frac{1}{(r_{nuc}^2+s_0)^2} e^{-\frac{w(r_{nuc}^2+s_0)}{s_0}}\left(e^{\frac{w(s^2w+s_0)(r_{nuc}^2+s_0)}{s_0^2}} s^4w^4\left(\mathrm{E}_1\left[-\frac{s^2w^2(r_{nuc}^2+s_0)}{s_0^2}\right] -\right.\right.$$

$$\left.\left.\mathrm{E}_1\left[-\frac{w(s^2w+s_0)(r_{nuc}^2+s_0)}{s_0^2}\right]\right)r_{nuc}^4 +\right.$$

$$wr_{nuc}^2 s_0\left(2e^{\frac{w(s^2w+s_0)(r_{nuc}^2+s_0)}{s_0^2}} s^4w^3\left(\mathrm{E}_1\left[-\frac{s^2w^2(r_{nuc}^2+s_0)}{s_0^2}\right] -\right.\right.$$

$$\left.\left.\mathrm{E}_1\left[-\frac{w(s^2w+s_0)(r_{nuc}^2+s_0)}{s_0^2}\right]\right) + \left(-1 + e^{w+\frac{wr_{nuc}^2}{s_0}}\right)s^2ws_0 + s_0^2\right) -$$

$$s_0^2\left(-e^{\frac{w(s^2w+s_0)(r_{nuc}^2+s_0)}{s_0^2}} s^4w^4\mathrm{E}_1\left[-\frac{s^2w^2(r_{nuc}^2+s_0)}{s_0^2}\right] - \mathrm{E}_1\left[-\frac{w(s^2w+s_0)(r_{nuc}^2+s_0)}{s_0^2}\right]\right) -$$

$$\left.\left.\left(-1 + e^{w+\frac{wr_{nuc}^2}{s_0}}\right)s^2w^2s_0 + \left(-1 + e^{w+\frac{wr_{nuc}^2}{s_0}} - w\right)s_0^2\right)\right)\Big) \tag{4.17}.$$

IV.1. 3. The exponential charge distribution

The general form of the exponential Charge distribution is given by (eg [Pov 08]):

$$\boldsymbol{\varrho(r) = \left(\frac{a^3}{8\pi}\right) e^{-ar}} \qquad (\mathbf{4.18})$$

The Fourier transform of the relation (4.12) gives the so called the Gaussian nuclear form factor:

$$\boldsymbol{F_q^{dip} = \frac{1}{\left(1 + \frac{q^2}{a^2\hbar^2}\right)^2}} \qquad (\mathbf{4.19}).$$

To apply this formulate to neutron star crust, first we must replacing the term $a\hbar$ by r_{nuc}^{-1} (§III.7.2.b) then our Gaussian nuclear form factor (4.19) become:

$$\boldsymbol{F_q^{dip} = \frac{1}{\left(1 + q^2 r_{nuc}^2\right)^2}} \qquad (\mathbf{4.20}).$$

Replacing (4.20) in (3.69) we get the effective screening potential of an exponential charge distribution of the ions:

$$\boldsymbol{\left|\phi_q^{eff}\right|^2_{dip} = \frac{1}{(1 + q^2 r_{nuc}^2)^4 (q^2 + q_s^2)^2}\left[1 - e^{-s_0 q^2}\right] G_{\sigma,\kappa} D(\eta)}$$

$$\boldsymbol{= \left|F_q^{dip}\right|^2 \left|\phi_q^{eff}\right|^2_{PL}} \qquad (\mathbf{4.21}).$$

And we have by substituting the equation (4.21) into equation (3.55):

$$\boldsymbol{\left(\Lambda_{ei}^{\sigma,\kappa}\right)_{dip} = \int_0^{2k_F} q^3 \left|\phi_q^{eff}\right|^2_{dip} \left[1 - \frac{v_F^2}{c^2}\left(\frac{q}{2k_F}\right)^2\right] dq}$$

$$(\mathbf{4.22}).$$

$$\boldsymbol{= \int_0^{2k_F} q^3 \left|F_q^{dip}\right|^2 \left|\phi_q^{eff}\right|^2_{PL} \left[1 - \frac{v_F^2}{c^2}\left(\frac{q}{2k_F}\right)^2\right] dq}$$

Also:

$$\left(\Lambda_{ei}^{\sigma,\kappa}\right)_{dip} = \int_0^{2k_F} q^3 \frac{1}{(1+q^2 r_{nuc}^2)^4 (q^2+q_s^2)^2}\left[1-e^{-s_0 q^2}\right] G_{\sigma,\kappa} D(\eta) \times \tag{4.23}$$

$$\times \left[1 - \frac{v_F^2}{c^2}\left(\frac{q}{2k_F}\right)^2\right] dq$$

To have an analytical formula for $(\Lambda_{ei}^{\sigma,\kappa})_{dip}$ we must first write:

$$\begin{aligned}\frac{1}{(1+q^2 r_{nuc}^2)^4 (q^2+q_s^2)^2} = {} & \frac{4r_{nuc}^2}{(q^2+q_s^2)(-1+q_s^2 r_{nuc}^2)^5} - \\ & - \frac{4r_{nuc}^4}{(1+q^2 r_{nuc}^2)(-1+q_s^2 r_{nuc}^2)^5} + \\ & \frac{1}{(q^2+q_s^2)^2(-1+q_s^2 r_{nuc}^2)^4} + \\ & + \frac{3r_{nuc}^4}{(1+q^2 r_{nuc}^2)^2(-1+q_s^2 r_{nuc}^2)^4} \\ & - \frac{2r_{nuc}^4}{(1+q^2 r_{nuc}^2)^3(-1+q_s^2 r_{nuc}^2)^3} + \\ & + \frac{r_{nuc}^4}{(1+q^2 r_{nuc}^2)^4(-1+q_s^2 r_{nuc}^2)^2}\end{aligned} \tag{4.24}$$

Then we find:

$$\left(\Lambda_{ei}^{\sigma,\kappa}\right)_{dip} = \frac{\left(\Lambda_{ei}^{\sigma,\kappa}\right)_{PL}}{\left(-1+q_s^2 r_{nuc}^2\right)^4} + \text{corrective terms} \tag{4.25}$$

Thus the dipolar Coulomb logarithm can be written as:

$$\begin{aligned}\Lambda_1^{dip} = {} & (s_0^2(s^3(1+s)w^6 r_{nuc}^{12} + 3s^2(-3-2s+s^2)w^5 r_{nuc}^{10} s_0 - \\ & 3sw^4(3+6s+5s^2-6(1+s)Log[sw]+6(1+s)Log[(1+ \\ & s)w]-6Log[1+\tfrac{wr_{nuc}^2}{s_0}]-6sLog[1+\tfrac{wr_{nuc}^2}{s_0}])r_{nuc}^8 s_0^2 +\end{aligned}$$

$$w^3(17-22s-15s^2+6(1+10s+9s^2)\text{Log}[sw]-6(1+10s+9s^2)\text{Log}[(1+s)w]+6\text{Log}[1+\frac{wr_{nuc}^2}{s_0}]+60s\text{Log}[1+\frac{wr_{nuc}^2}{s_0}]+54s^2\text{Log}[1+\frac{wr_{nuc}^2}{s_0}])r_{nuc}^6 s_0^3+$$

$$9w^2(5-s-2s^2+(2+8s+6s^2)\text{Log}[sw]-2(1+4s+3s^2)\text{Log}[(1+s)w]+2\text{Log}[1+\frac{wr_{nuc}^2}{s_0}]+8s\text{Log}[1+\frac{wr_{nuc}^2}{s_0}]+6s^2\text{Log}[1+\frac{wr_{nuc}^2}{s_0}])r_{nuc}^4 s_0^4+$$

$$6w\left(6+2s+3(1+s)^2\text{Log}[sw]-3(1+s)^2\text{Log}[(1+s)w]+3\text{Log}\left[1+\frac{wr_{nuc}^2}{s_0}\right]+6s\text{Log}\left[1+\frac{wr_{nuc}^2}{s_0}\right]+3s^2\text{Log}\left[1+\frac{wr_{nuc}^2}{s_0}\right]\right)r_{nuc}^2 s_0^5+$$

$$6(1+(1+s)\text{Log}[sw]-(1+s)\text{Log}[(1+s)w]+\text{Log}[1+\frac{wr_{nuc}^2}{s_0}]+s\text{Log}[1+\frac{wr_{nuc}^2}{s_0}])s_0^6))/(6(1+s)(swr_{nuc}^2-s_0)^5(wr_{nuc}^2+s_0)^3)-$$

$$\frac{1}{6(swr_{nuc}^2-s_0)^5}s_0^2(24(1-e^{-w}+e^{sw}swE_1[-sw]-e^{sw}swE_1[-(1+s)w])r_{nuc}^2 s_0^2-\frac{1}{1+s}$$

$$6e^{-w}(e^w-s+e^w s+e^{w+sw}(1+s)(1+sw)E_1[-sw]-e^{w+sw}(1+s)(1+sw)E_1[-(1+s)w])(swr_{nuc}^2-s_0)s_0^2-$$

$$24e^{-w}s_0^2((-1+e^w)r_{nuc}^2+e^{w+\frac{s_0}{r_{nuc}^2}}(E_1[-\frac{s_0}{r_{nuc}^2}]-E_1[-w-\frac{s_0}{r_{nuc}^2}])s_0)-\frac{1}{r_{nuc}^2(wr_{nuc}^2+s_0)}$$

$$18e^{-w}(swr_{nuc}^2-s_0)s_0^2(e^w w(1+e^{\frac{s_0}{r_{nuc}^2}}E_1[-\frac{s_0}{r_{nuc}^2}]-e^{\frac{s_0}{r_{nuc}^2}}E_1[-w-\frac{s_0}{r_{nuc}^2}])r_{nuc}^4+$$

$$+e^{w}+e^{w+\frac{s_0}{r_{nuc}^2}}(1+w)E_1[-\frac{s_0}{r_{nuc}^2}]-e^{w+\frac{s_0}{r_{nuc}^2}}(1+w)E_1[-w-\frac{s_0}{r_{nuc}^2}])r_{nuc}^2s_0+e^{w+\frac{s_0}{r_{nuc}^2}}(E_1[-\frac{s_0}{r_{nuc}^2}]-E_1[-w-\frac{s_0}{r_{nuc}^2}])s_0^2)-$$

$$\frac{1}{r_{nuc}^4(wr_{nuc}^2+s_0)^2}6e^{-w}s_0(-swr_{nuc}^2+s_0)^2(e^{w}w^2r_{nuc}^8+w(-2+2e^{w}+e^{w}w+2e^{w+\frac{s_0}{r_{nuc}^2}}wE_1[-\frac{s_0}{r_{nuc}^2}]-2e^{w+\frac{s_0}{r_{nuc}^2}}wE_1[-w-\frac{s_0}{r_{nuc}^2}])r_{nuc}^6s_0+$$

$$(-1+e^{w}-w+2e^{w}w+e^{w+\frac{s_0}{r_{nuc}^2}}w(4+w)E_1[-\frac{s_0}{r_{nuc}^2}]-e^{w+\frac{s_0}{r_{nuc}^2}}w(4+w)E_1[-w-\frac{s_0}{r_{nuc}^2}])r_{nuc}^4s_0^2+$$

$$(-1+e^{w}+2e^{w+\frac{s_0}{r_{nuc}^2}}(1+w)E_1[-\frac{s_0}{r_{nuc}^2}]-2e^{w+\frac{s_0}{r_{nuc}^2}}(1+w)E_1[-w-\frac{s_0}{r_{nuc}^2}])r_{nuc}^2s_0^3+e^{w+\frac{s_0}{r_{nuc}^2}}(E_1[-\frac{s_0}{r_{nuc}^2}]-E_1[-w-\frac{s_0}{r_{nuc}^2}])s_0^4)+\frac{1}{r_{nuc}^6(wr_{nuc}^2+s_0)^3}e^{-w}(swr_{nuc}^2-s_0)^3(e^{w}w^3r_{nuc}^{12}-e^{w}w^2(-3+2w)r_{nuc}^{10}s_0-w(3-3e^{w}-3w+6e^{w}w+e^{w}w^2+3e^{w+\frac{s_0}{r_{nuc}^2}}E_1[-\frac{s_0}{r_{nuc}^2}]-3e^{w+\frac{s_0}{r_{nuc}^2}}w^2E_1[-w-\frac{s_0}{r_{nuc}^2}])r_{nuc}^8s_0^2-$$

$$(1-e^{w}-5w+6e^{w}w-w^2+3e^{w}w^2+e^{w+\frac{s_0}{r_{nuc}^2}}w^2(9+w)E_1[-\frac{s_0}{r_{nuc}^2}]-e^{w+\frac{s_0}{r_{nuc}^2}}w^2(9+w)E_1[-w-\frac{s_0}{r_{nuc}^2}])r_{nuc}^6s_0^3-$$

$$(-2+2e^{w}-2w+3e^{w}w+3e^{w+\frac{s_0}{r_{nuc}^2}}w(3+w)E_1[-\frac{s_0}{r_{nuc}^2}]-3e^{w+\frac{s_0}{r_{nuc}^2}}w(3+w)E_1[-w-\frac{s_0}{r_{nuc}^2}])r_{nuc}^4s_0^4-$$

$$(-1+e^{w}+3e^{w+\frac{s_0}{r_{nuc}^2}}(1+w)E_1[-\frac{s_0}{r_{nuc}^2}]-3e^{w+\frac{s_0}{r_{nuc}^2}}(1+w)E_1[-w-\frac{s_0}{r_{nuc}^2}])r_{nuc}^2s_0^5-e^{w+\frac{s_0}{r_{nuc}^2}}(E_1[-\frac{s_0}{r_{nuc}^2}]-E_1[-w-\frac{s_0}{r_{nuc}^2}])s_0^6))$$

(4.26).

$$2\Lambda_2^{dip}=(s_0^3(s^3(1+s)w^5r_{nuc}^{10}+3s^2w^4(3+2s-$$
$$-2(1+s)Log[sw]+2(1+s)Log[(1+s)w]-2Log[1+\frac{wr_{nuc}^2}{s_0}]$$
$$-2sLog[1+\frac{wr_{nuc}^2}{s_0}])r_{nuc}^8s_0-$$
$$3sw^3\left(3-6s-5s^2+(2+8s+6s^2)Log[sw]\right.$$
$$-2(1+4s+3s^2)Log[(1+s)w]+2Log\left[1+\frac{wr_{nuc}^2}{s_0}\right]$$
$$\left.+8sLog\left[1+\frac{wr_{nuc}^2}{s_0}\right]+6s^2Log\left[1+\frac{wr_{nuc}^2}{s_0}\right]\right)r_{nuc}^6s_0^2-$$
$$w^2\left(1+22s-3s^2-6s^3+18s(1+s)^2Log[sw]\right.$$
$$-18s(1+s)^2Log[(1+s)w]+18sLog\left[1+\frac{wr_{nuc}^2}{s_0}\right]$$
$$+36s^2Log\left[1+\frac{wr_{nuc}^2}{s_0}\right]$$
$$\left.+18s^3Log\left[1+\frac{wr_{nuc}^2}{s_0}\right]\right)r_{nuc}^4s_0^3-$$
$$3w\left(1+5s+2s(3+4s+s^2)Log[sw]\right.$$
$$-2s(3+4s+s^2)Log[(1+s)w]+6sLog\left[1+\frac{wr_{nuc}^2}{s_0}\right]$$
$$\left.+8s^2Log\left[1+\frac{wr_{nuc}^2}{s_0}\right]+2s^3Log\left[1+\frac{wr_{nuc}^2}{s_0}\right]\right)r_{nuc}^2s_0^4-$$
$$3(1+2s+2s(1+s)Log[sw]-2s(1+s)Log[(1+s)w]+2sLog[1$$
$$+\frac{wr_{nuc}^2}{s_0}]+2s^2Log[1+\frac{wr_{nuc}^2}{s_0}])s_0^5))/(3(1$$
$$+s)(swr_{nuc}^2-s_0)^5(wr_{nuc}^2+s_0)^3)-$$

$$\frac{1}{6w(swr_{nuc}^2 - s_0)^5} e^{-w} s_0^3 (-24(1 - e^w + w - sw + e^w sw + e^{w+sw} s^2 w^2 E_1[-sw] - e^{w+sw} s^2 w^2 E_1[-(1 + s)w]) r_{nuc}^2 s_0 +$$

$$\frac{1}{1+s} 6(-1 + e^w - s + e^w s + e^w sw - s^2 w + e^w s^2 w + e^{w+sw} s(1+s)w(2+sw) E_1[-sw] - e^{w+sw} s(1+s)w(2+sw) E_1[-(1+s)w])(swr_{nuc}^2 - s_0)s_0 +$$

$$\frac{1}{r_{nuc}^2} 24 s_0 \left((1 - e^w + w) r_{nuc}^4 + (-1 + e^w) r_{nuc}^2 s_0 + e^{w + \frac{s_0}{r_{nuc}^2}} \left(E_1\left[-\frac{s_0}{r_{nuc}^2}\right] - E_1\left[-w - \frac{s_0}{r_{nuc}^2}\right] \right) s_0^2 \right) +$$

$$\frac{1}{r_{nuc}^4 (wr_{nuc}^2 + s_0)} 18(swr_{nuc}^2 - s_0)s_0 ((-1 + e^w) w r_{nuc}^6 + (-1 + e^w + e^w w + 2e^{w + \frac{s_0}{r_{nuc}^2}} w E_1[-\frac{s_0}{r_{nuc}^2}] - 2e^{w + \frac{s_0}{r_{nuc}^2}} w E_1[-w - \frac{s_0}{r_{nuc}^2}]) r_{nuc}^4 s_0 +$$

$$(-1 + e^w + e^{w + \frac{s_0}{r_{nuc}^2}} (2 + w) E_1[-\frac{s_0}{r_{nuc}^2}] - e^{w + \frac{s_0}{r_{nuc}^2}} (2 + w) E_1[-w - \frac{s_0}{r_{nuc}^2}]) r_{nuc}^2 s_0^2 + e^{w + \frac{s_0}{r_{nuc}^2}} (E_1[-\frac{s_0}{r_{nuc}^2}] - E_1[-w - \frac{s_0}{r_{nuc}^2}]) s_0^3) +$$

$$\frac{1}{r_{nuc}^6 (wr_{nuc}^2 + s_0)^2} 6 s_0 (-swr_{nuc}^2 + s_0)^2 (e^w w^2 (3 + 2e^{\frac{s_0}{r_{nuc}^2}} E_1[-\frac{s_0}{r_{nuc}^2}] - 2e^{\frac{s_0}{r_{nuc}^2}} E_1[-w - \frac{s_0}{r_{nuc}^2}]) r_{nuc}^8 + w(-4 + 6e^w + e^w w + 4e^{w + \frac{s_0}{r_{nuc}^2}} (1 + w) E_1[-\frac{s_0}{r_{nuc}^2}] - 4e^{w + \frac{s_0}{r_{nuc}^2}} (1 + w) E_1[-w - \frac{s_0}{r_{nuc}^2}]) r_{nuc}^6 s_0 + (-3 + 3e^w - w + 2e^w w + e^{w + \frac{s_0}{r_{nuc}^2}} (2 + 8w + w^2) E_1[-\frac{s_0}{r_{nuc}^2}] - e^{w + \frac{s_0}{r_{nuc}^2}} (2 + 8w + w^2) E_1[-w - \frac{s_0}{r_{nuc}^2}]) r_{nuc}^4 s_0^2 +$$

$$
\begin{aligned}
&(-1+e^{w}+2e^{w+\frac{s_0}{r_{nuc}^2}}(2+w)E_1[-\frac{s_0}{r_{nuc}^2}]-2e^{w+\frac{s_0}{r_{nuc}^2}}(2+w)E_1[-w\\
&\quad-\frac{s_0}{r_{nuc}^2}])r_{nuc}^2s_0^3+e^{w+\frac{s_0}{r_{nuc}^2}}(E_1[-\frac{s_0}{r_{nuc}^2}]-E_1[-w\\
&\quad-\frac{s_0}{r_{nuc}^2}])s_0^4)+\\
&\frac{1}{r_{nuc}^8(wr_{nuc}^2+s_0)^3}(swr_{nuc}^2-s_0)^3(2e^{w}w^3r_{nuc}^{12}+w^2(-6+6e^{w}\\
&\quad+5e^{w}w+6e^{w+\frac{s_0}{r_{nuc}^2}}wE_1[-\frac{s_0}{r_{nuc}^2}]-6e^{w+\frac{s_0}{r_{nuc}^2}}wE_1[-w\\
&\quad-\frac{s_0}{r_{nuc}^2}])r_{nuc}^{10}s_0+\\
&w\Big(-6+6e^{w}-6w+15e^{w}w+e^{w}w^2\\
&\quad+6e^{w+\frac{s_0}{r_{nuc}^2}}w(3+w)E_1\left[-\frac{s_0}{r_{nuc}^2}\right]\\
&\quad-6e^{w+\frac{s_0}{r_{nuc}^2}}w(3+w)E_1\left[-w-\frac{s_0}{r_{nuc}^2}\right]\Big)r_{nuc}^8s_0^2+\\
&\Big(-2+2e^{w}-11w+15e^{w}w-w^2+3e^{w}w^2\\
&\quad+e^{w+\frac{s_0}{r_{nuc}^2}}w(18+18w+w^2)E_1\left[-\frac{s_0}{r_{nuc}^2}\right]\\
&\quad-e^{w+\frac{s_0}{r_{nuc}^2}}w(18+18w+w^2)E_1\left[-w-\frac{s_0}{r_{nuc}^2}\right]\Big)r_{nuc}^6s_0^3+\\
&\Big(-5+5e^{w}-2w+3e^{w}w+3e^{w+\frac{s_0}{r_{nuc}^2}}(2+6w+w^2)E_1\left[-\frac{s_0}{r_{nuc}^2}\right]\\
&\quad-3e^{w+\frac{s_0}{r_{nuc}^2}}(2+6w+w^2)E_1\left[-w-\frac{s_0}{r_{nuc}^2}\right]\Big)r_{nuc}^4s_0^4+\\
&(-1+e^{w}+3e^{w+\frac{s_0}{r_{nuc}^2}}(2+w)E_1[-\frac{s_0}{r_{nuc}^2}]-3e^{w+\frac{s_0}{r_{nuc}^2}}(2+w)E_1[-w\\
&\quad-\frac{s_0}{r_{nuc}^2}])r_{nuc}^2s_0^5+e^{w+\frac{s_0}{r_{nuc}^2}}(E_1[-\frac{s_0}{r_{nuc}^2}]-E_1[-w\\
&\quad-\frac{s_0}{r_{nuc}^2}])s_0^6))
\end{aligned}
\tag{4.27}
$$

IV.2. Multi components plasma

Astrophysical plasmas – such in accreted neutron stars - are often a mixture of different ions. Furthermore, ionic crystals may contain

structural defects. In these cases, the formulas (3.56) recorded for the same ionic components are subject to change, which may depend on the state of the plasma, such as inhomogeneities, their number and nature of the location.

To study those plasmas we propose to deal with them by three point of view.

IV.2.1 Formalism of charged impurities in a crystal

Consider the scattering of electrons by charged impurities in the crystal. This case was previously studied in [Flo 76] [Ewa 75] [Ito 94]. Approaches of all the authors are essentially the same, differing only in the choice of shielding function ϕ_q, which slightly depend on the Coulomb logarithm.

Charged impurities in the crystalline crust of neutron stars or a crystalline core of white dwarfs - are ions (atomic nuclei) with the charge number $Z_j \neq Z$, where Z - charge number of ions forming the lattice. It is assumed that they are randomly arranged in the crystal.'' Then the scattering of electrons by impurities can be regarded as Coulomb scattering on the excess charge $(Z_j - Z)$ e.

In essence, this is the same scattering as the scattering of electrons on the ion in the gas phase, and it also can be described in the relaxation time approximation.

Similarly, the expression (3.56), the electronic relaxation time for scattering by impurities is equal:

$$\tau_{imp} = \frac{p_F^2 v_F}{4\pi e^2 \sum_j (Z - Z_j)^2 n_j \Lambda_{imp}^{(j)}} \qquad (4.28).$$

Where the summation is over all sorts of impurities. We will consider uncorrelated impurity, the Coulomb logarithm $\Lambda_{imp}^{(j)}$- is a slow function of plasma parameters, depending on the screening of electron scattering by impurities, described by the function ϕ_q. Shielding is determined by electrons, and possibly also the correlations between the impurities, but the latter are neglected.

We will simply make the transformation: for all j $Z \to (Z_j - Z)\, e$

In the formulas (3.56) - (3.69) then we sum over all j to compute the Coulomb logarithm due to the contribution of impurities putting a Debye-like screening $exp[-w(q)] = 0$, and $G = 1$, then our impurities Coulomb logarithm is given by :

$$\boldsymbol{\Lambda_{imp}^{(j)}} = -\frac{1}{c^2 k_F^2 (4k_F^2 + q_s^2)} \left(Log\left[\frac{q_s^2}{4k_F^2 + q_s^2}\right] q_s^4 v_F^2 + 8k_F^4 \left(c^2 \left(1 + 2Log[q_s] - Log[4k_F^2 + q_s^2]\right) + v_F^2\right) - 2k_F^2 q_s^2 \left(c^2 Log\left[1 + \frac{4k_F^2}{q_s^2}\right] + (-2 - 4Log[q_s] + 2Log[4k_F^2 + q_s^2]) v_F^2\right)\right) D\left(\eta_j\right) \quad \textbf{(4.29).}$$

Where : $\eta_j = \frac{T}{T_{pi}^{(j)}}$.

We define Q_{imp}- The so-called parameter heterogeneity. or impurity parameter as :

$$\boldsymbol{Q_{imp} = \sum_j \left(Z_j - Z\right)^2 n_j / n_{ion}} \quad (4.30).$$

Thus the total frequency will be the sum of the frequency of collision of the domine element ν_{d-el} and the impurity frequency

$$\boldsymbol{\nu = \nu_{d-el} + \nu_{imp}} \quad \textbf{(4.31).}$$

According to [Dal 09] we have:

$$\boldsymbol{\frac{\nu}{\nu_{imp}} = \frac{\langle Z^2 \rangle}{Q_{imp}} \frac{\Lambda}{\Lambda_{imp}}} \quad (4.32).$$

Since Λ and Λ_{imp} have the same order of magnitude $\Lambda \approx \Lambda_{imp}$ we can write:

$$\frac{\boldsymbol{\nu}}{\boldsymbol{\nu_{imp}}} \approx \frac{\langle \mathbf{Z^2} \rangle}{\mathbf{Q_{imp}}} \rightarrow \boldsymbol{\nu} \approx \frac{\langle \mathbf{Z^2} \rangle}{\mathbf{Q_{imp}}} \boldsymbol{\nu_{imp}} \qquad (\mathbf{4.33}).$$

Generally speaking, this assumption may be violated in cases where the impurity ions constitute a significant fraction of the total ion concentration. Recent modeling results by the method of molecular dynamics [Ito 94] indicate that there could be a regular Wigner lattice, consisting of several types of ions. This case requires special study and is not considered here.

We will show the validity of the suggest made by J.Daligault and S.Gupta [Dal 09] -they used the method of molecular dynamics- that for a multicomponents mixture if we deal with this mixture as an amorphous solid or heterogeneous liquid depending on Γ values ,the Scattering by charged impurities method gives good results only for small values of the impurity parameter $Q_{imp} \lesssim 100$.

Since τ_{imp} almost independent of T, the scattering by impurities dominates at sufficiently low temperatures. Therefore, the ionic impurities can be a major source of residual resistivity (nearly independent of T) and heat capacity ($\propto$ T) in the crust of neutron stars at sufficiently low temperatures and high densities (at $T \ll T_{pi}$) - mainly in the inner crust.

IV.2.2 Linear Mixing rule

When there are no dominant-type ions, arranged in a crystal lattice - for example, if we consider the liquid, gas or amorphous alloy, suitable alternative method of calculating the kinetic coefficients. In this case we

can use equation (3.56), having made it to the replacement $Zn_{ion}\Lambda_{ei}$ namenatele $\sum_j Z_j^2 n_j \Lambda_{ei}^j$where the sum is over all ion species j, and the Coulomb logarithm Λ_{ei}^j in general, depend on j. In [Pot 99a], A.Y Potekhin and al proposed a way to approximate calculation of Λ_{ei}^j 'is based on "rule of additivity" for ionic mixtures [Han 77]. It consists in the fact that each of the Λ_{ei}^j i rely on the formulas (3.56) - (3.69), substituting in them Z_j instead of Z and Γ_j, instead, of Γ.

IV.2.3. The effective OCP comportment

Almost as good and much more straightforward approach is that all Coulomb logarithms replaced by one designed by the same formulas, but with the replacement of Z by $\sqrt{\langle Z^2 \rangle}$).

IV.3. Scattering of strongly degenerate Electron by electrons

Despite just shown the inapplicability of relaxation-time approximation to its collisions, comfortable yet provide the transport coefficients in the form of (3.36), which allows us to apply the rule Mattissena in the form of (3.41) for a liquid or (3.42) for the crystal.

The character of thermal conductivity due to collisions between degenerate electrons is different at temperatures $T_{pe} \lesssim T \ll T_F$ and $T \ll T_{pe}$ [Lam 68]: In the first case, the characteristic momentum q ~k_{TF} transferred in the scattering is much smaller than the thermal smearing of the Fermi surface and in the second case the transferred momenta in the collisions exceed the width of the thermal smearing out of the Fermi surface. By the virtue of the Pauli principle for the electron momenta before and after the scattering must be within the thermal width of the Fermi surface.

Consequently, at $T \ll T_{pe}$ the number of transitions $(\vec{p}_1, \vec{p}_2 \rightarrow \vec{p}_1', \vec{p}_2')$ suppressed: there are allowed only transitions in which the directions of

the momenta change, but not their absolute values. When $T_{pe} \lesssim T \ll T_F$ this restriction disappears, as the transfer of momentum in either direction is not able to withdraw the electron outside the thermal width of the Fermi surface.

E. Flowers and N. Itoh [Flo 76] derived a variational expression for τ_{ee} strongly degenerate relativistic electrons at $T \ll T_{pe}$ V Urpin and D. Yakovlev [Urp 80] obtained a more general result that applies also for $T \ll T_F$, but does not require $T \ll T_{pe}$ This result is used in The papers [Pot 97] [Pot 99a], which were calculated by electronic conductivity, due to its scattering, and obtained approximate formula for them, the result can be written in analogy with (3.36) as follows:

$$\boldsymbol{\nu_{ee} = \frac{3\alpha_f^2}{2\pi^3}\frac{(k_B T)^2}{\hbar m_e^* c^2}\left(\frac{2k_F}{k_{TF}}\right)J(x_r, y)} \qquad \textbf{(4.34)}.$$

where $y = \sqrt{3}\, T_{pe} / T$ and $J(x_r, y)$ - analytical approximation function is given by:

$$\boldsymbol{J(x_r, y) \approx \left(1 + \frac{6}{5x_r^2} + \frac{5}{5x_r^4}\right) \times}$$

$$\boldsymbol{\times \left[\frac{y^3}{3(1 + 0.07414y)^3} \ln\left(1 + \frac{2.81}{y} - \frac{0.81}{y}\frac{v_F^2}{c^2}\right)\frac{\pi^5}{6}\frac{y^4}{(13.91 + y)^4}\right]}$$

(4.35).

In our simulation we will deal with the whole electrons of the multicomponent plasma, that require a special consederation of $n_e = \sum_j Z_j n_j$.

B- Simulation

IV.4. Nuclear form factor effects

In order to study the effect of the nuclear form factor on the transport coefficients we like to compute electrical and thermal conductivities against the mass density of several elements at different temperatures, we compute those coefficients from the equation (3.34) , and we substitute the analytical formulae (4.7) (4.8) for the Gaussian form factor, and (4.16) (4.17) for the oscillating form factor , and (4.26) (4.27) in the case of dipolar form factor, precious estimation of the nuclear effect will be shown by computing the relative error from the point like form factor case, a series of MATLAB codes are developed to simulate and illustrate these objectives.

The figure (4.1) illustrate the relation between the radial charge distribution and its corresponding form factor and show some examples from standard nuclear physics.

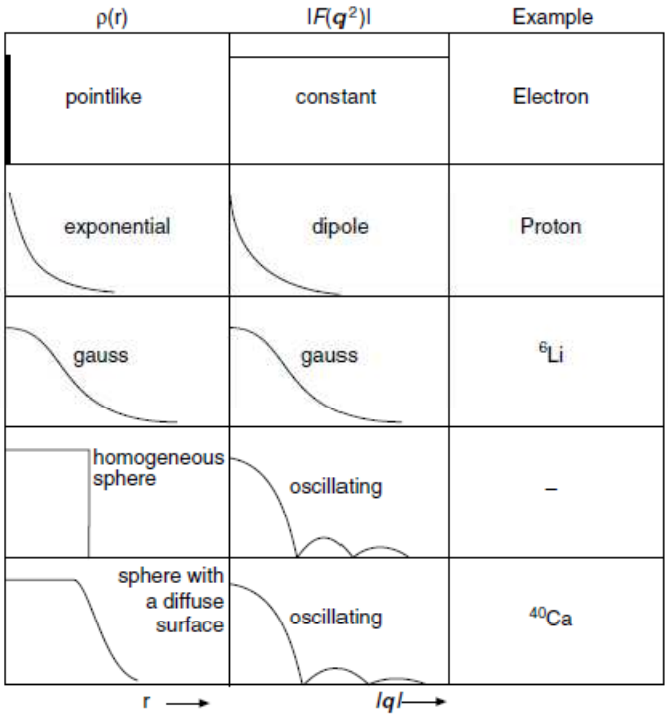

Figure 4.1 : Relation between the radial charge distribution $\varrho(r)$ and the correspondingform factor in Born approximation from [Pov 08].

IV.4.1 Results

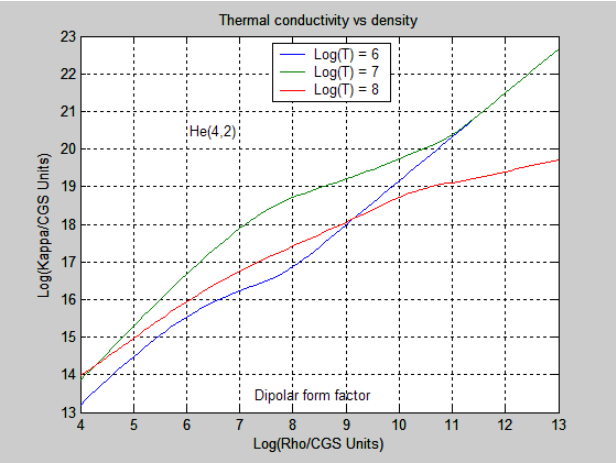

Figure 4.2a : *Thermal conductivity Vs the mass density for* ^4_2He *using dipolar form factor.*

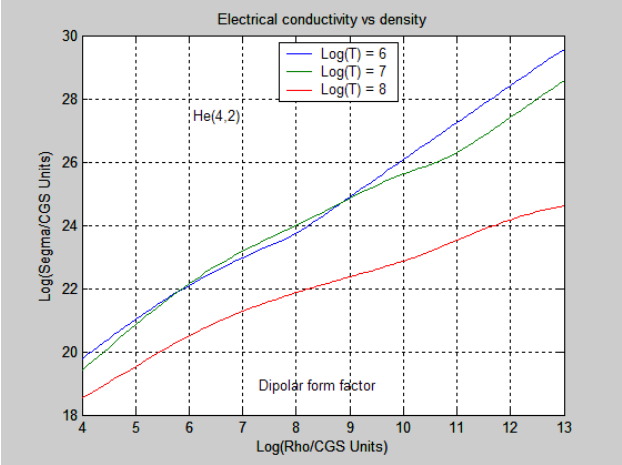

Figure 4.2b : *Electrical conductivity Vs the mass density for* ^4_2He *using dipolar form factor.*

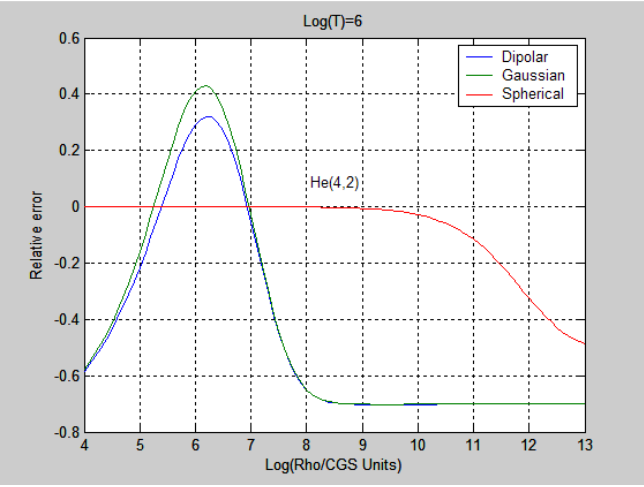

Figure 4.2c : *Relative error (with respect to point like case)Vs the mass density for* ^4_2He.

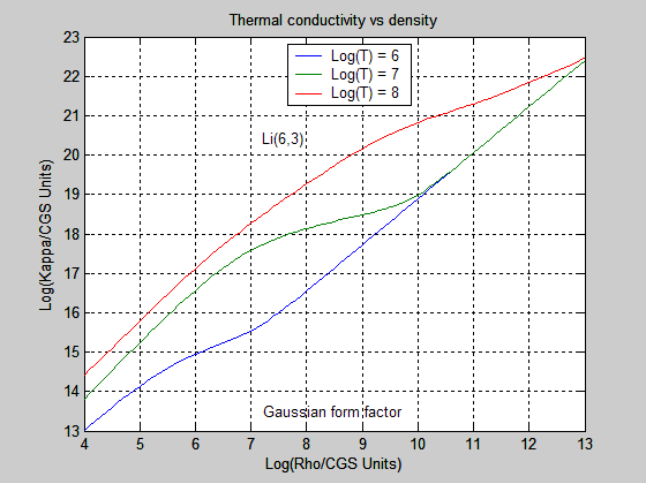

Figure 4.3a : *Thermal conductivity Vs the mass density for* ${}^{6}_{3}Li$ *using Gaussian form factor.*

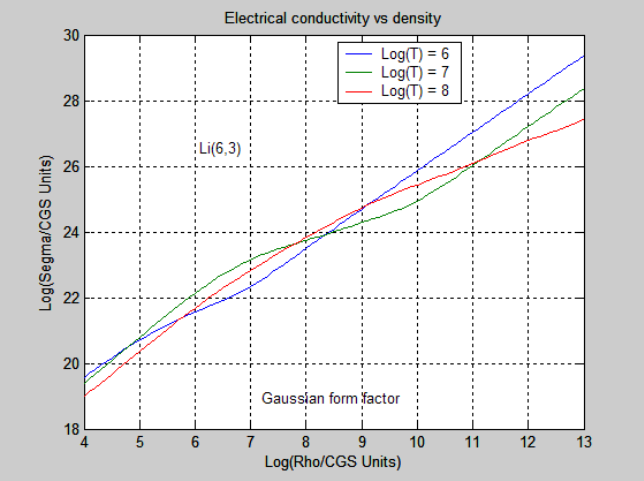

Figure 4.3b : *Electrical conductivity Vs the mass density for* ${}^{6}_{3}Li$ *using Gaussian form factor.*

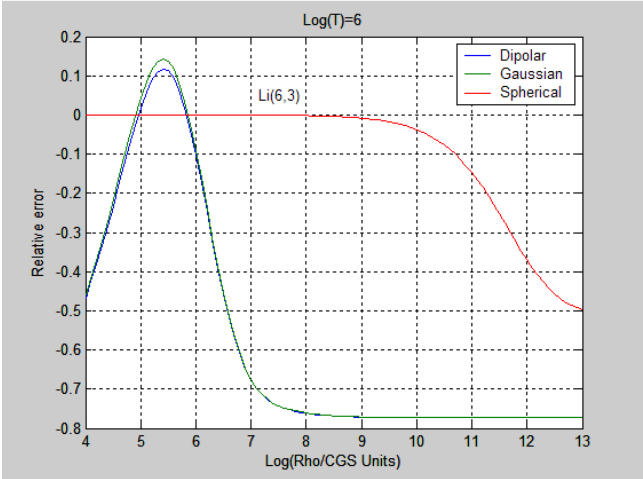

Figure 4.3c : *Relative error (with respect to point like case)Vs the mass density for* ${}^{6}_{3}Li$.

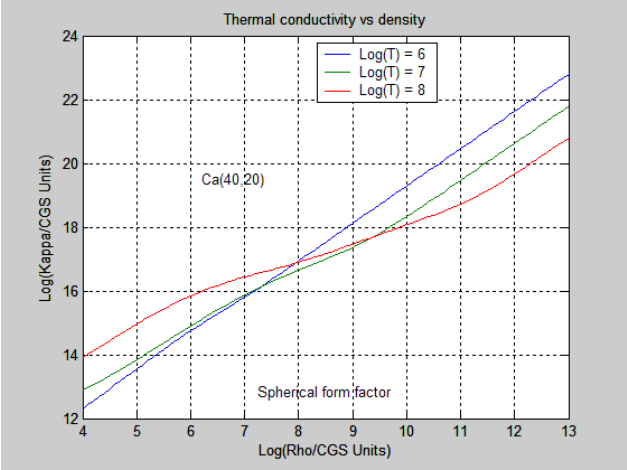

Figure 4.4a : *Thermal conductivity Vs the mass density for* $^{40}_{20}Ca$ *using spherical form factor.*

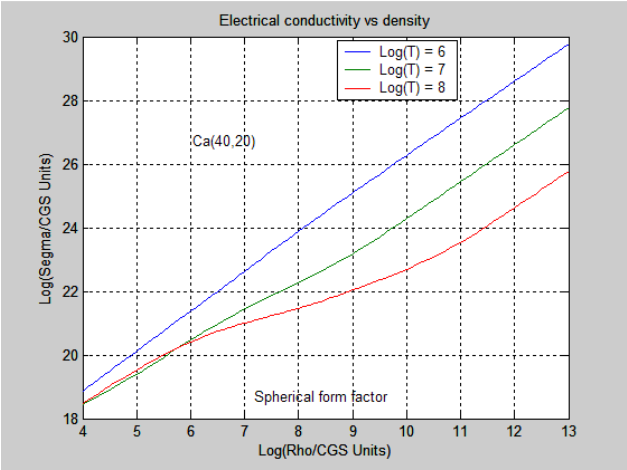

Figure 4.4b : *Electrical conductivity Vs the mass density for* $^{40}_{20}Ca$ *using spherical form factor.*

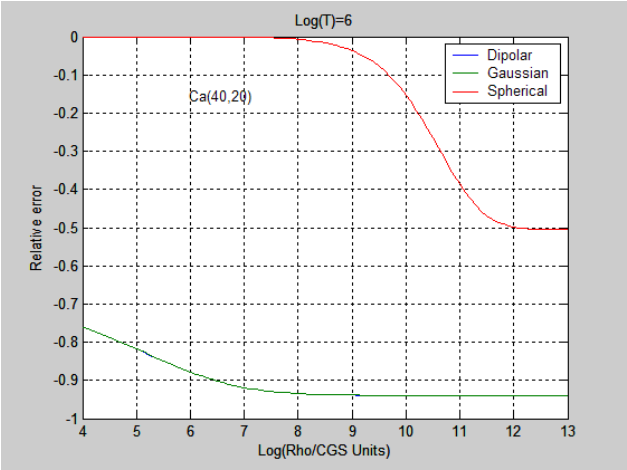

Figure 4.4c : *Relative error (with respect to point like case)Vs the mass density for* $^{40}_{20}Ca$ *.*

IV.4.2 Discussion

Figures(4.2-4.4) type (a ,b) shows the dependence of the Thermal conductivity (a) and electrical conductivity (b) due to electron-ion scattering in fully ionized plasma at different temperatures for different elements on the mass density. the blue line for $T = 10^6 K$, the green line for $T = 10^7 K$, the red line for $T = 10^8 K$, and we use different form factors that ordinary nuclei had in terrestrial conditions, the relative error ie ($\frac{\tau^{FS}-\tau^{PL}}{\tau^{PL}}$) , where the FS: for finite size case, PL: for point like case) on the masse density is shown in Figures(4.2-4.4) type (c), we see that in the spherical form factor case even in our calculation , it still produce the same results as previous studies (eg [Gne 01]) the increasing of the decrease of kinetic coefficients beyond the drip point (until 40% at $\rho = 10^{13} g/cm^3$), but for the case that we studied (the dipolar and the Gaussian form factors) and for physical situations ie $\sim 10^5 - 10^7 g/cm^3$ for light element we see an increasing of the values of kinetic coefficients from few percent to ~40% and a decreasing of the values of kinetic coefficients for $\rho \lesssim 10^5 g/cm^3$ until ~60% and a decreasing of the values of kinetic coefficients for $\rho \gtrsim 10^7 g/cm^3$ until ~60%. for heavy elements like the $^{40}_{20}Ca$ we see an decreasing of the values of kinetic coefficients at $T = 10^6 K$ $\sim 80\% - 95\%$.

IV.5. Multi components plasma

We like to study transport coefficients of plasma systems contains more than one components , and show their comportment against change in the temperature figures (4.2 to 4.11) and in the total mass density figures (4.12 to 4.21) by using different methods introduced in §IV.2.

In order to get this objective we develop a Number of MATLAB codes especially to deal with Data Bases that we need to save our results.

In our work we only consider the point like form factor case and using the high temperature "the fitted" Coulomb logarithm.

Our simulation is based on the consideration that the relative mass density of all elements $X_j = \frac{\rho_j}{\rho}$ is fixed, and we will give these ratios for every figure.

IV.5.1 Results

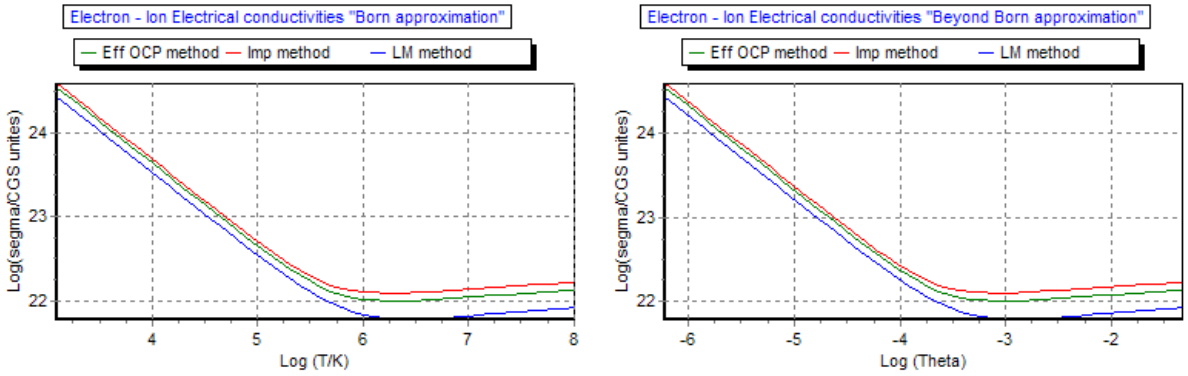

Figure 4.5a : *Electron ion electrical conductivities in the Born approximation (Left panel) and beyond Born approximation (Right panel) , we show different method of computation :Effective OCP method (Green line) ,Impurities method(Red line) , Linear mixing method (Blue line) for the mixture* ${}_1^1H\ \rho_1 = 5 \times 10^5 g/cm^3$, ${}_2^4He\ \rho_2 = 5 \times 10^5 g/cm^3$.

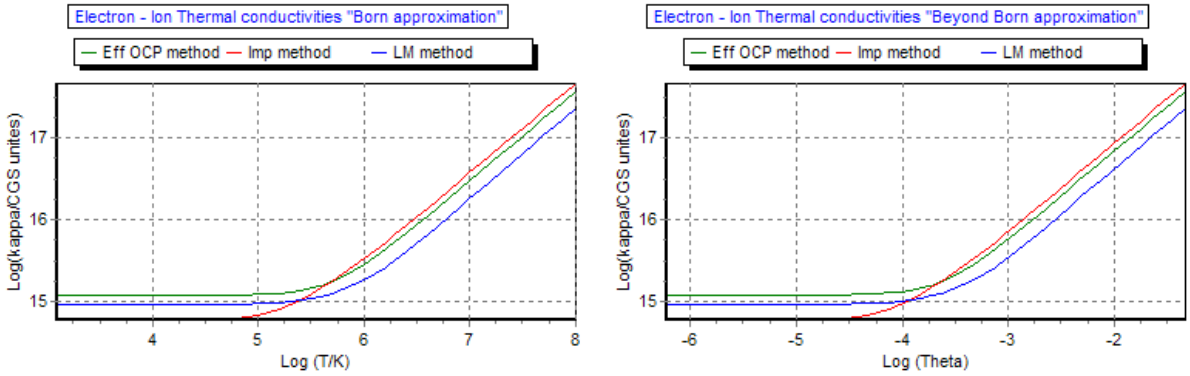

Figure 4.5b : *Electron ion thermal conductivities in the Born approximation (Left panel) and beyond Born approximation (Right panel) , we show different method of computation :Effective OCP method (Green line) ,Impurities method(Red line) , Linear mixing method (Blue line) for the mixture* ${}_1^1H\ \rho_1 = 5 \times 10^5 g/cm^3$, ${}_2^4He\ \rho_2 = 5 \times 10^5 g/cm^3$.

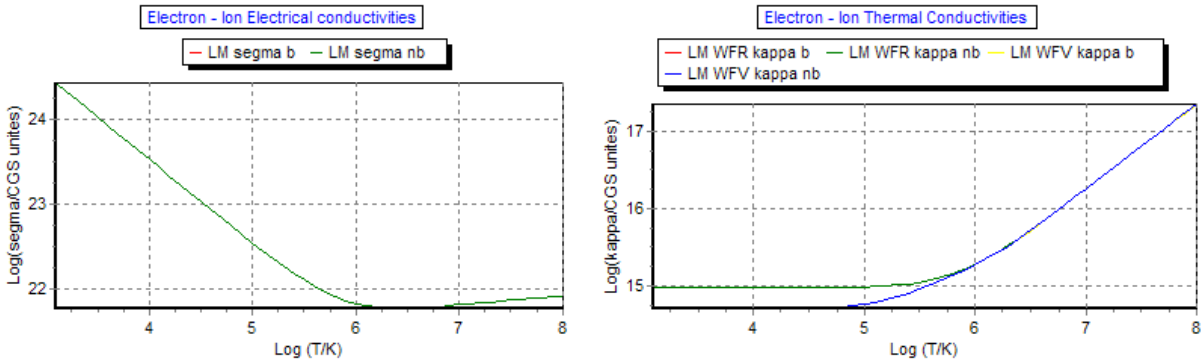

Figure 4.5c : *Electron ion electrical conductivities in the Born and beyond Born approximations (Left panel), and the difference between Thermal conductivities in the case were The Weidermann-Franz Law respected (WFR), and were The Weidermann-Franz Law violated (WFV) (Right panel) for the mixture* ${}_1^1H\ \rho_1 = 5 \times 10^5 g/cm^3$, ${}_2^4He\ \rho_2 = 5 \times 10^5 g/cm^3$.

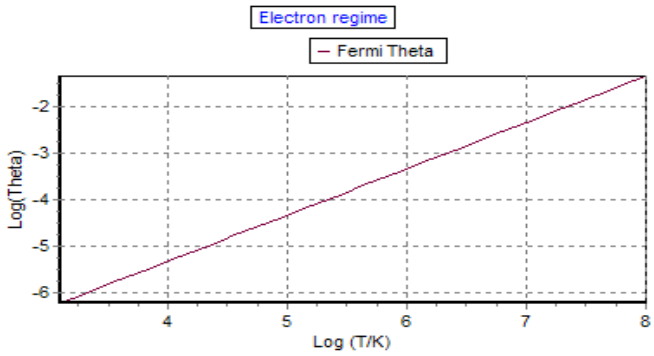

Figure 4.5d : *the Fermi temperature VS the temperature in the logarithmic scale for the mixture* ${}_1^1H\ \rho_1 = 5 \times 10^5 g/cm^3$, ${}_2^4He\ \rho_2 = 5 \times 10^5 g/cm^3$.

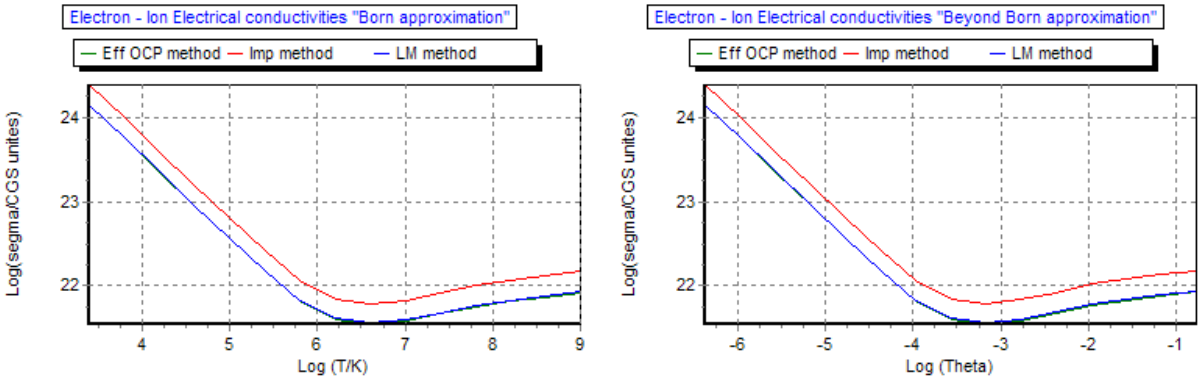

Figure 4.6a : *Electron ion electrical conductivities in the Born approximation (Left panel) and beyond Born approximation (Right panel) , we show different method of computation :Effective OCP method (Green line) ,Impurities method(Red line) , Linear mixing method (Blue line)for the mixture* ${}_6^{12}C\ \rho_1 = 5 \times 10^6 g/cm^3$, ${}_8^{16}O\ \rho_2 = 5 \times 10^6 g/cm^3$.

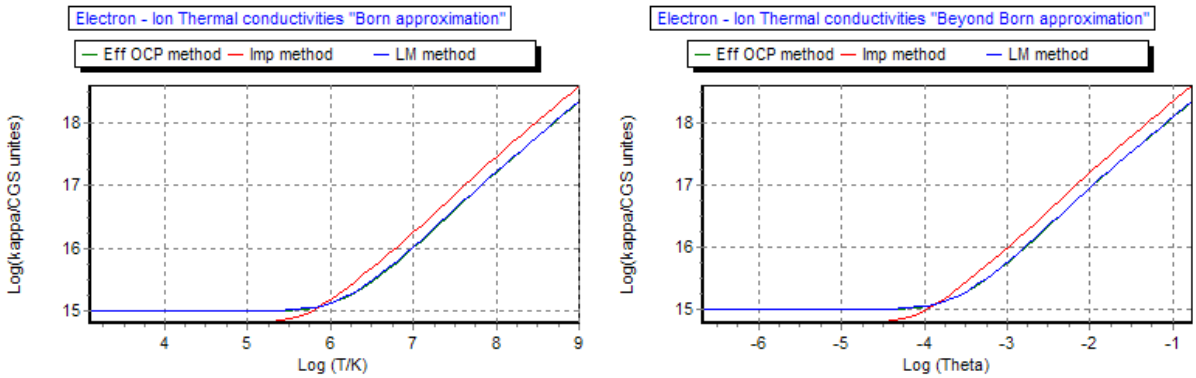

Figure 4.6b : *Electron ion thermal conductivities in the Born approximation (Left panel) and beyond Born approximation (Right panel) , we show different method of computation :Effective OCP method (Green line) ,Impurities method(Red line) , Linear mixing method (Blue line) for the mixture* ${}^{12}_{6}C\ \rho_1 = 5 \times 10^6 g/cm^3$, ${}^{16}_{8}O\ \rho_2 = 5 \times 10^6 g/cm^3$.

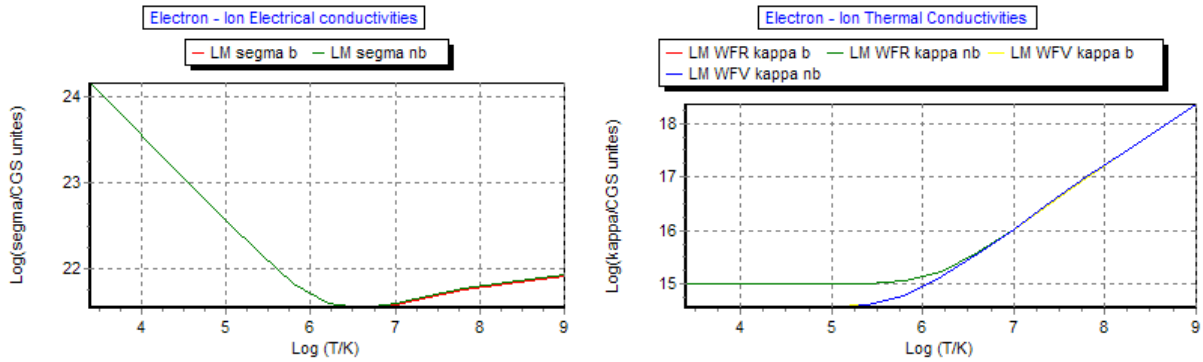

Figure 4.6c *: Electron ion electrical conductivities in the Born and beyond Born approximations (Left panel), and the difference between Thermal conductivities in the case were The Weidermann-Franz Law respected (WFR), and were The Weidermann-Franz Law violated (WFV) (Right panel) for the mixture* ${}^{12}_{6}C\ \rho_1 = 5 \times 10^6 g/cm^3$, ${}^{16}_{8}O\ \rho_2 = 5 \times 10^6 g/cm^3$.

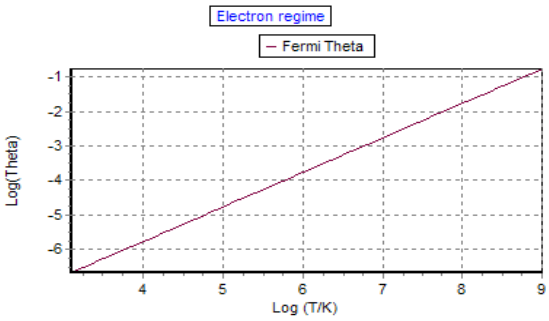

Figure 4.6d: *the Fermi temperature VS the temperature in the logarithmic scale for the mixture* ${}^{12}_{6}C\ \rho_1 = 5 \times 10^6 g/cm^3$, ${}^{16}_{8}O\ \rho_2 = 5 \times 10^6 g/cm^3$.

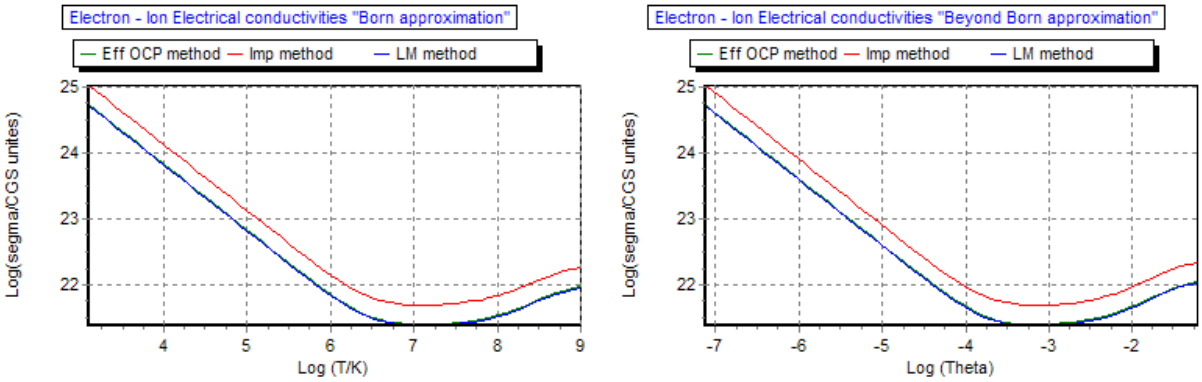

Figure 4.7a : *Electron ion electrical conductivities in the Born approximation (Left panel) and beyond Born approximation (Right panel) , we show different method of computation :Effective OCP method (Green line) ,Impurities method(Red line) , Linear mixing method (Blue line) for the mixture* $^{12}_{6}C\ \rho_1 = 5 \times 10^6 g/cm^3$, $^{16}_{8}O\ \rho_2 = 5 \times 10^6 g/cm^3$.

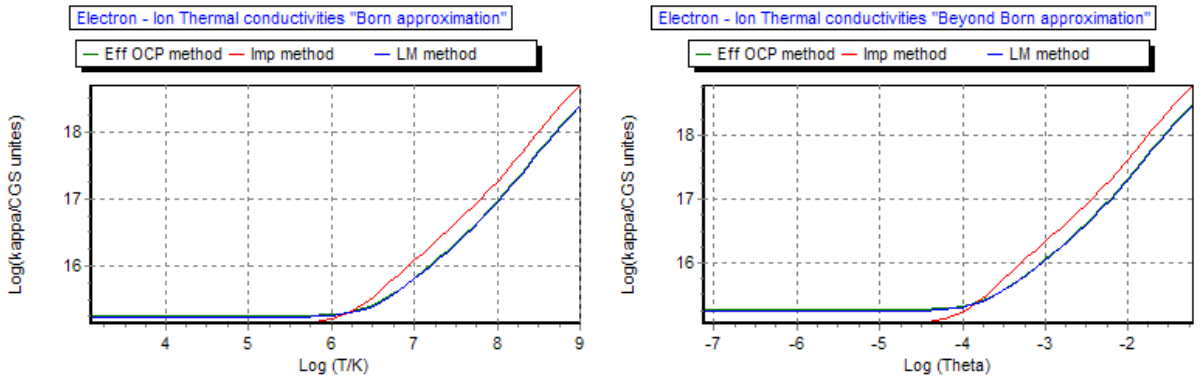

Figure 4.7b : *Electron ion thermal conductivities in the Born approximation (Left panel) and beyond Born approximation (Right panel) , we show different method of computation :Effective OCP method (Green line) ,Impurities method(Red line) , Linear mixing method (Blue line) for the mixture* $^{12}_{6}C\ \rho_1 = 5 \times 10^6 g/cm^3$, $^{16}_{8}O\ \rho_2 = 5 \times 10^6 g/cm^3$.

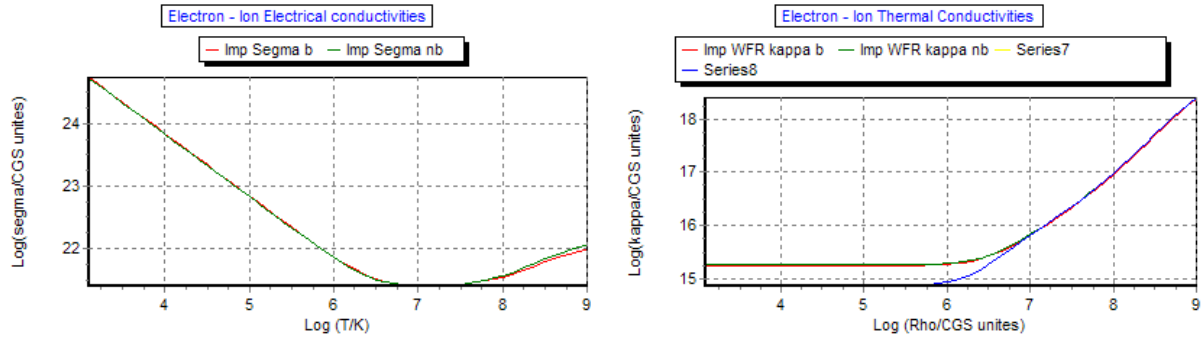

Figure 4.7c: *Electron ion electrical conductivities in the Born and beyond Born approximations (Left panel), and the difference between Thermal conductivities in the case were The Weidermann-Franz Law respected (WFR), and were The Weidermann-Franz Law violated (WFV) (Right panel)) for the mixture* $^{12}_{6}C\ \rho_1 = 5 \times 10^6 g/cm^3$, $^{16}_{8}O\ \rho_2 = 5 \times 10^6 g/cm^3$.

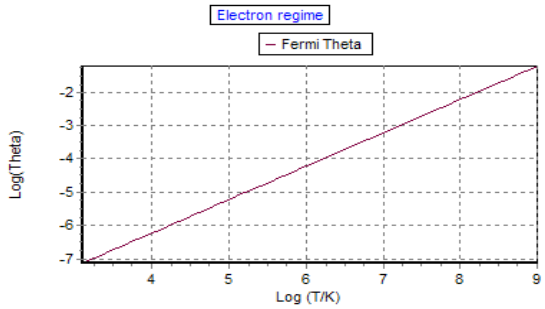

Figure 4.7d *: the Fermi temperature VS the temperature in the logarithmic scale) for the mixture* ${}^{12}_{6}C\ \rho_1 = 5 \times 10^6 g/cm^3$, ${}^{16}_{8}O\ \rho_2 = 5 \times 10^6 g/cm^3$.

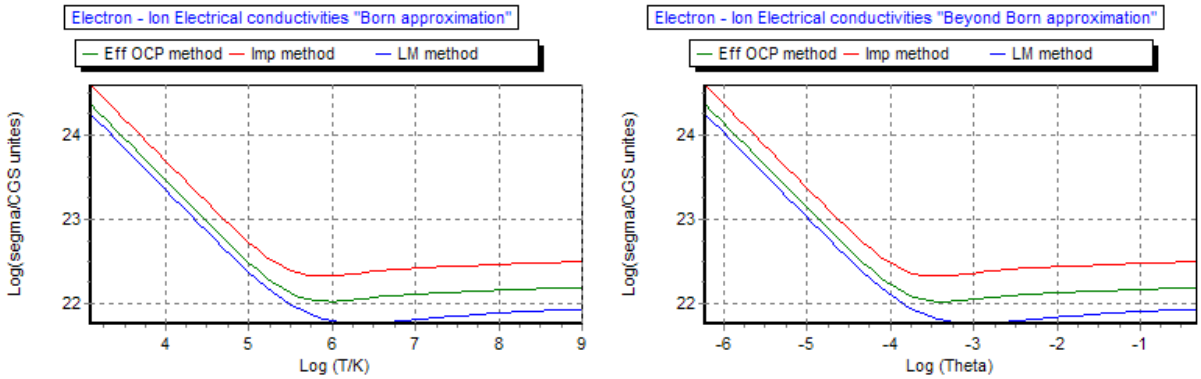

Figure 4.8a *: Electron ion thermal conductivities in the Born approximation (Left panel) and beyond Born approximation (Right panel) , we show different method of computation :Effective OCP method (Green line) ,Impurities method(Red line) , Linear mixing method (Blue line) for the mixture* ${}^{1}_{1}H\ \rho_1 = 5 \times 10^5 g/cm^3$, ${}^{4}_{2}He\ \rho_2 = 3 \times 10^5 g/cm^3$, ${}^{6}_{3}Li\ \rho_3 = 2 \times 10^5 g/cm^3$.

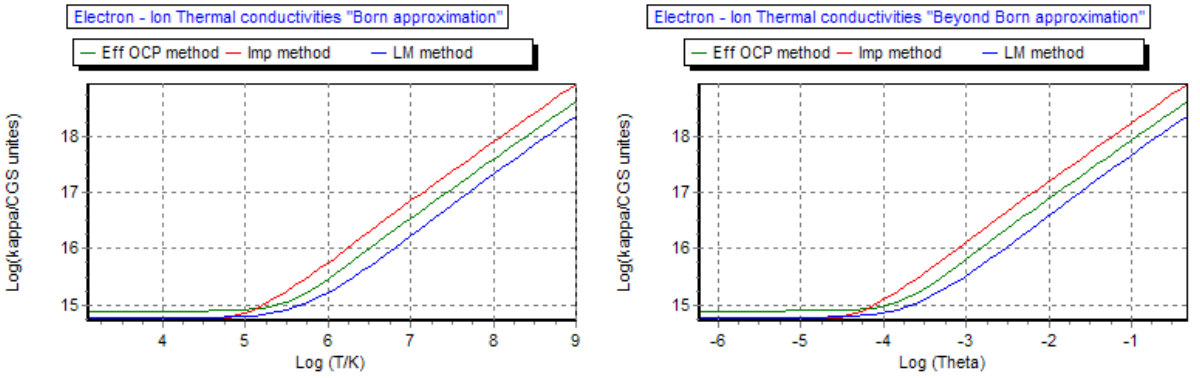

Figure 4.8b *: Electron ion thermal conductivities in the Born approximation (Left panel) and beyond Born approximation (Right panel) , we show different method of computation :Effective OCP method (Green line) ,Impurities method(Red line) , Linear mixing method (Blue line) for the mixture* ${}^{1}_{1}H\ \rho_1 = 5 \times 10^5 g/cm^3$, ${}^{4}_{2}He\ \rho_2 = 3 \times 10^5 g/cm^3$, ${}^{6}_{3}Li\ \rho_3 = 2 \times 10^5 g/cm^3$.

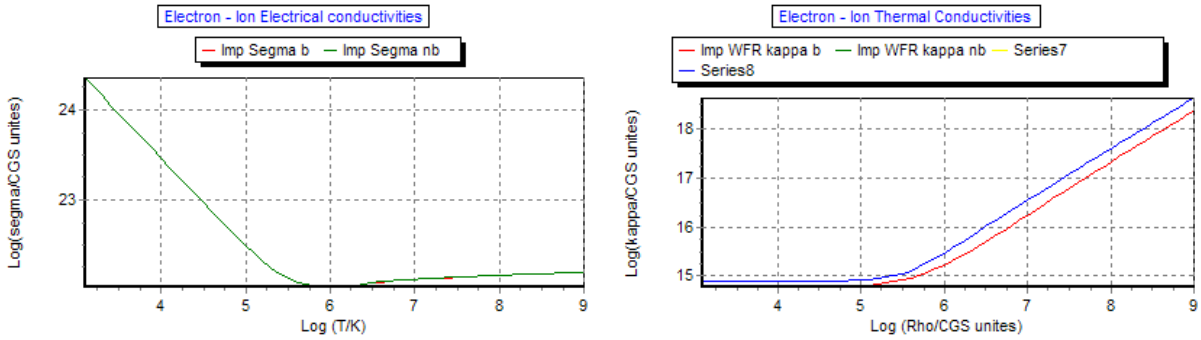

Figure 4.8c : *Electron ion electrical conductivities in the Born and beyond Born approximations (Left panel), and the difference between Thermal conductivities in the case were The Weidermann-Franz Law respected (WFR), and were The Weidermann-Franz Law violated (WFV) (Right panel) for the mixture* ${}_1^1H\ \rho_1 = 5 \times 10^5 g/cm^3$, ${}_2^4He\ \rho_2 = 3 \times 10^5 g/cm^3$, ${}_3^6Li\ \rho_3 = 2 \times 10^5 g/cm^3$.

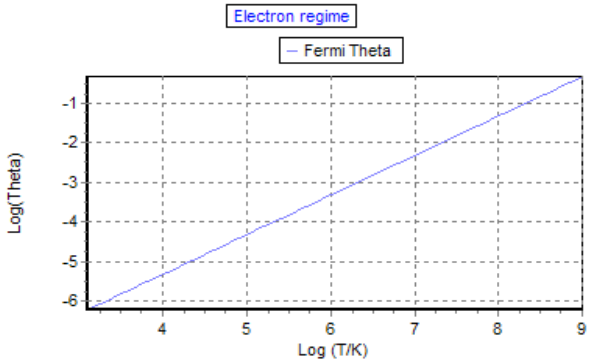

Figure 4.8d : *the Fermi temperature VS the temperature in the logarithmic scale for the mixture* ${}_1^1H\ \rho_1 = 5 \times 10^5 g/cm^3$, ${}_2^4He\ \rho_2 = 3 \times 10^5 g/cm^3$, ${}_3^6Li\ \rho_3 = 2 \times 10^5 g/cm^3$.

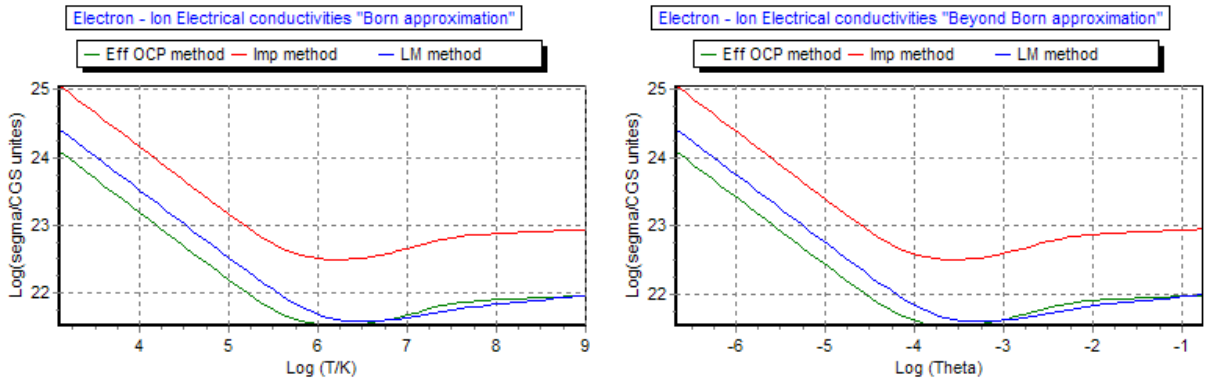

Figure 4.9a : *Electron ion thermal conductivities in the Born approximation (Left panel) and beyond Born approximation (Right panel) , we show different method of computation :Effective OCP method (Green line) ,Impurities method(Red line) , Linear mixing method (Blue line), for the mixture* ${}_6^{12}C\ \rho_1 = 5 \times 10^6 g/cm^3$, ${}_7^{14}N\ \rho_2 = 4 \times 10^6 g/cm^3$, ${}_8^{16}O\ \rho_3 = 10^6 g/cm^3$.

.

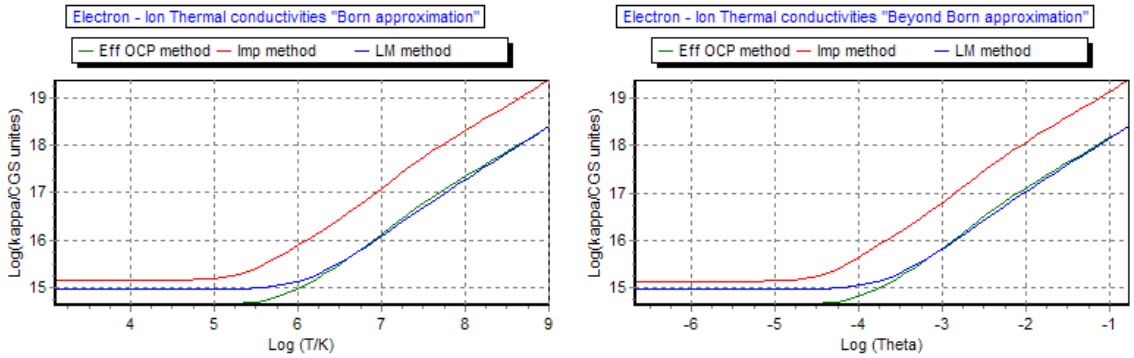

Figure 4.9b : *Electron ion electrical (upper panel) and thermal (lower panel) conductivities in the Born approximation (Left panel) and beyond Born approximation (Right panel) , we show different method of computation :Effective OCP method (Green line) ,Impurities method(Red line) , Linear mixing method (Blue line), For the mixture* ${}^{12}_{6}C$ $\rho_1 = 5 \times 10^6 g/cm^3$, ${}^{14}_{7}N$ $\rho_2 = 4 \times 10^6 g/cm^3$, ${}^{16}_{8}O$ $\rho_3 = 10^6 g/cm^3$.

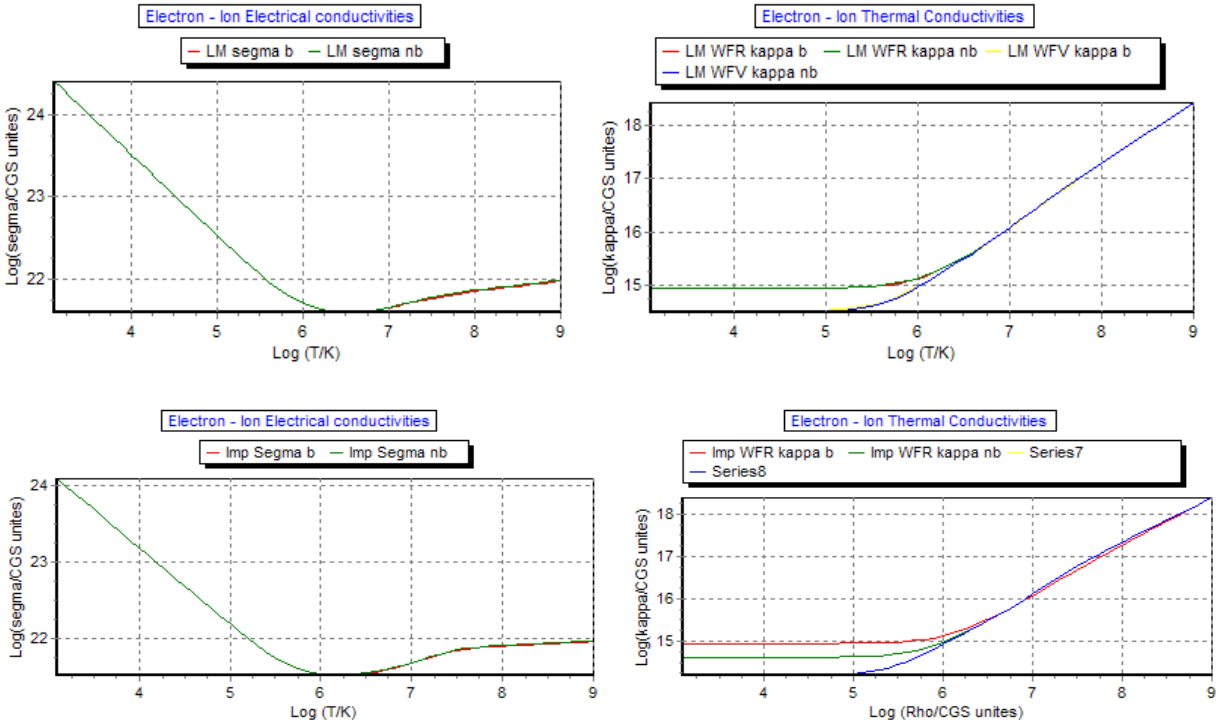

Figure 4.9c : *Electron ion electrical conductivities in the Born and beyond Born approximations (Left panel), and the difference between Thermal conductivities in the case were The Weidermann-Franz Law respected (WFR), and were The Weidermann-Franz Law violated (WFV) (Right panel), For the mixture* ${}^{12}_{6}C$ $\rho_1 = 5 \times 10^6 g/cm^3$, ${}^{14}_{7}N$ $\rho_2 = 4 \times 10^6 g/cm^3$, ${}^{16}_{8}O$ $\rho_3 = 10^6 g/cm^3$.

.

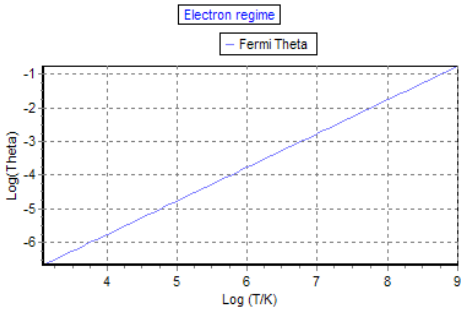

Figure 4.9d : *the Fermi temperature VS the temperature in the logarithmic scale, for the mixture* ${}^{12}_{6}C\ \rho_1 = 5 \times 10^6 g/cm^3$, ${}^{14}_{7}N\ \rho_2 = 4 \times 10^6 g/cm^3$, ${}^{16}_{8}O\ \rho_3 = 10^6 g/cm^3$.

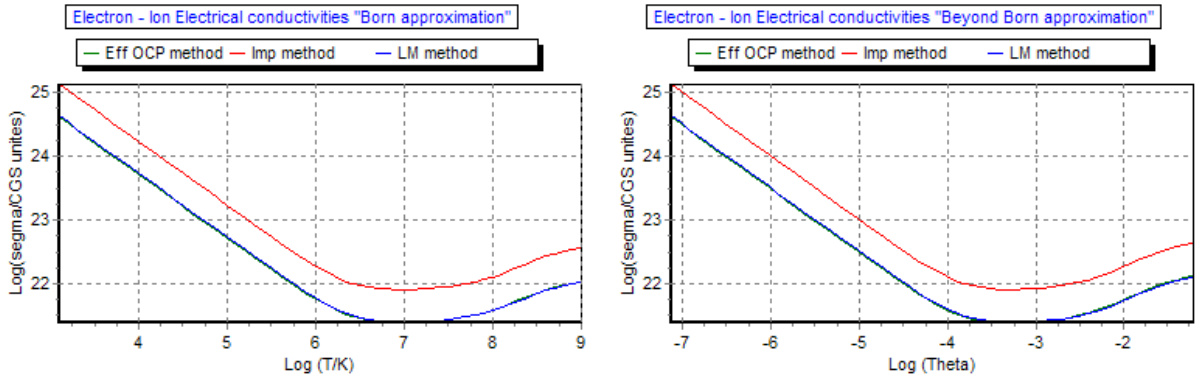

Figure 4.10a : *Electron ion thermal conductivities in the Born approximation (Left panel) and beyond Born approximation (Right panel) , we show different method of computation :Effective OCP method (Green line) ,Impurities method(Red line) , Linear mixing method (Blue line), for the mixture* ${}^{50}_{24}Cr\ \rho_1 = 4 \times 10^7 g/cm^3$, ${}^{52}_{25}Mn\ \rho_2 = 3 \times 10^7 g/cm^3$, ${}^{56}_{26}Fe\ \rho_3 = 3 \times 10^7 g/cm^3$.

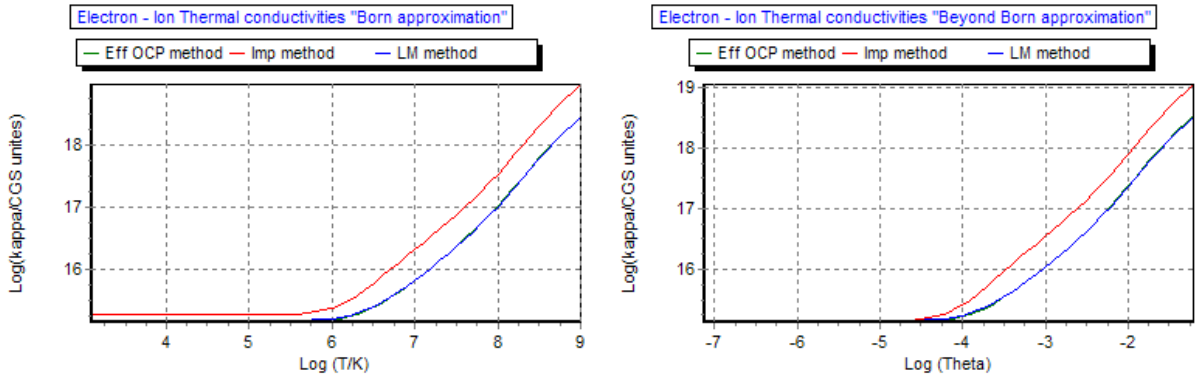

Figure 4.10b : *Electron ion electrical (upper panel) and thermal (lower panel) conductivities in the Born approximation (Left panel) and beyond Born approximation (Right panel) , we show different method of computation :Effective OCP method (Green line) ,Impurities method(Red line) , Linear mixing method (Blue line) for the mixture* ${}^{50}_{24}Cr\ \rho_1 = 4 \times 10^7 g/cm^3$, ${}^{52}_{25}Mn\ \rho_2 = 3 \times 10^7 g/cm^3$, ${}^{56}_{26}Fe\ \rho_3 = 3 \times 10^7 g/cm^3$

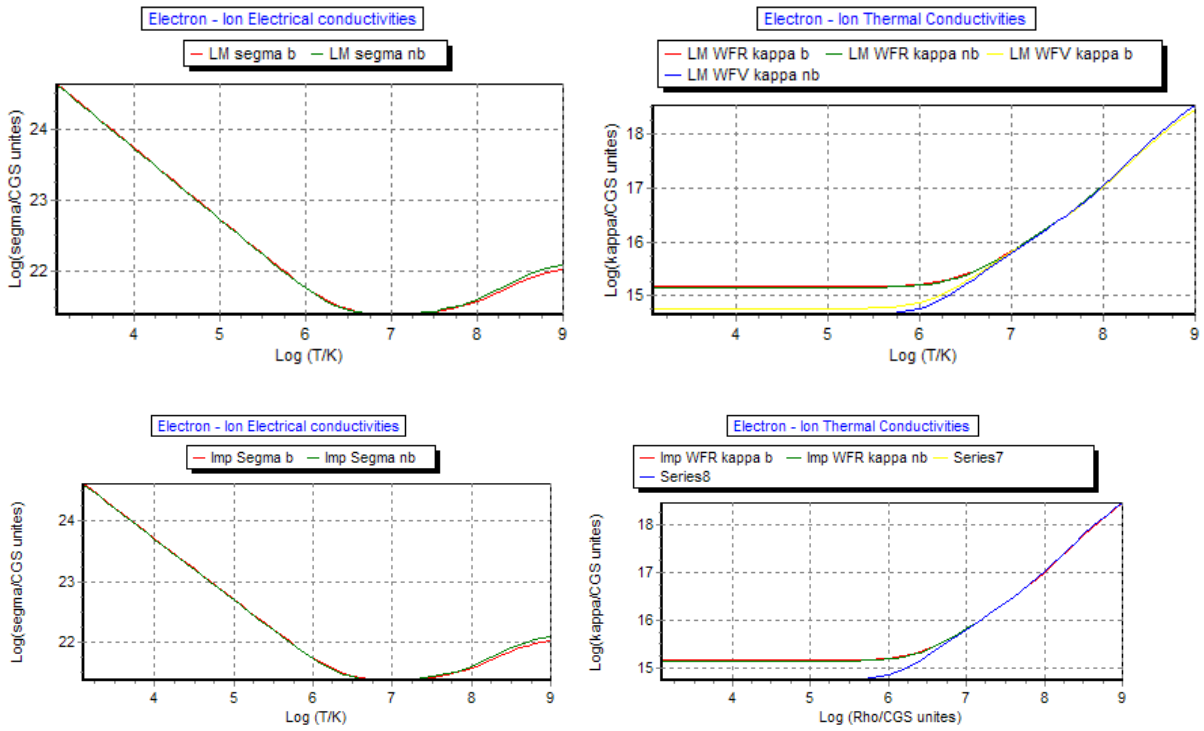

Figure 4.10c : *Electron ion electrical conductivities in the Born and beyond Born approximations (Left panel), and the difference between Thermal conductivities in the case were The Weidermann-Franz Law respected (WFR), and were The Weidermann-Franz Law violated (WFV) (Right panel) for the mixture* ${}^{50}_{24}Cr\ \rho_1 = 4 \times 10^7 g/cm^3$, ${}^{52}_{25}Mn\ \rho_2 = 3 \times 10^7 g/cm^3$, ${}^{56}_{26}Fe\ \rho_3 = 3 \times 10^7 g/cm^3$.

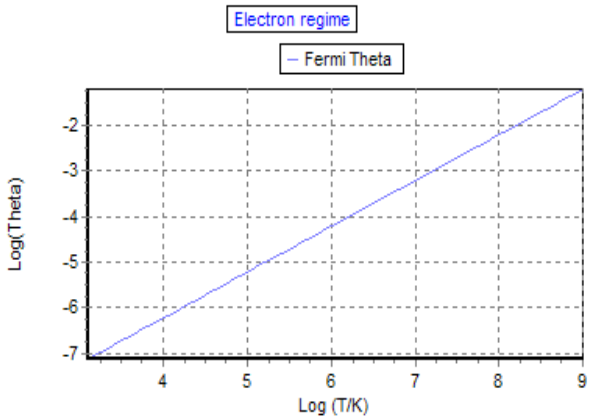

Figure 4.10d : *the Fermi temperature VS the temperature in the logarithmic scale , for the mixture* ${}^{50}_{24}Cr\ \rho_1 = 4 \times 10^7 g/cm^3$, ${}^{52}_{25}Mn\ \rho_2 = 3 \times 10^7 g/cm^3$, ${}^{56}_{26}Fe\ \rho_3 = 3 \times 10^7 g/cm^3$.

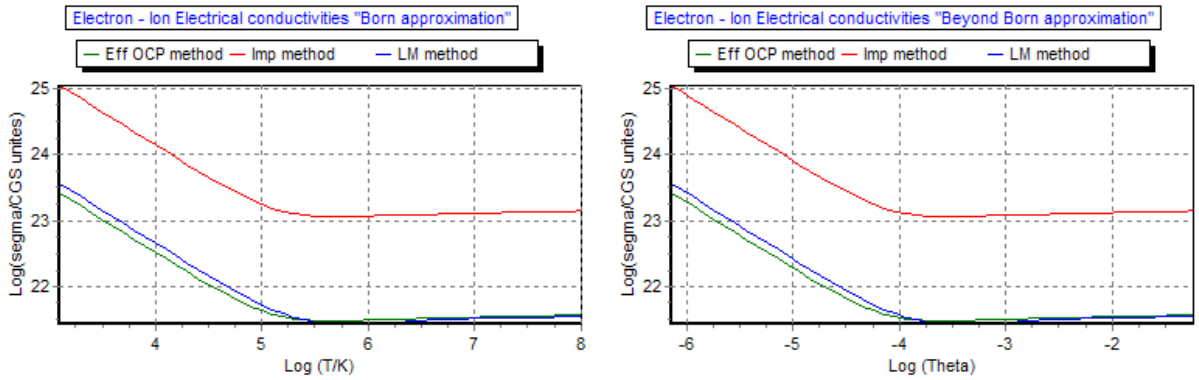

Figure 4.11a : *Electron ion thermal conductivities in the Born approximation (Left panel) and beyond Born approximation (Right panel) , we show different method of computation :Effective OCP method (Green line) ,Impurities method(Red line) , Linear mixing method (Blue line),for the mixture* ${}_1^1H\ \rho_1 = 10^5 g/cm^3$, ${}_1^2H\ \rho_2 = 10^5 g/cm^3$, ${}_1^3H\ \rho_3 = 10^5 g/cm^3$, ${}_2^3He\ \rho_4 = 10^5 g/cm^3$, ${}_2^4He\ \rho_5 = 10^5 g/cm^3$, ${}_3^6Li\ \rho_6 = 10^5 g/cm^3$, ${}_3^7Li\ \rho_7 = 10^5 g/cm^3$, ${}_4^7Be\ \rho_8 = 10^5 g/cm^3$, ${}_4^9Be\ \rho_9 = 10^5 g/cm^3$, ${}_4^{10}Be\ \rho_{10} = 10^5 g/cm^3$

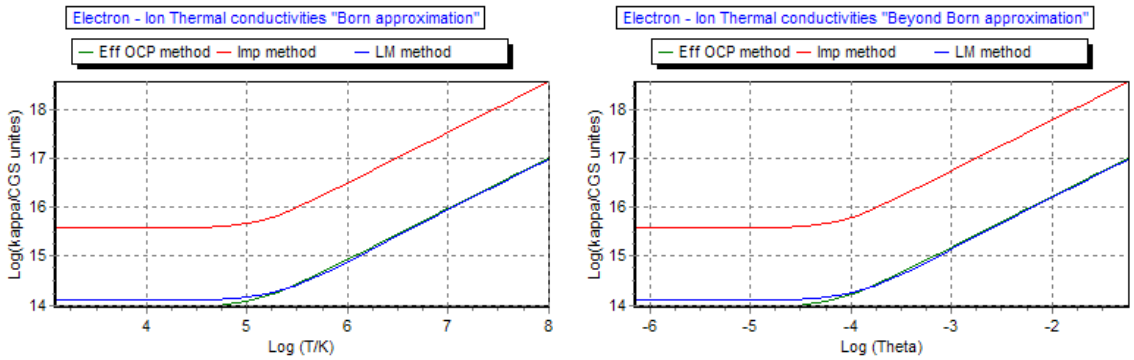

Figure 4.11b *: Electron ion electrical (upper panel) and thermal (lower panel) conductivities in the Born approximation (Left panel) and beyond Born approximation (Right panel) , we show different method of computation :Effective OCP method (Green line) ,Impurities method(Red line) , Linear mixing method (Blue line), for the mixture:* ${}_1^1H\ \rho_1 = 10^5 g/cm^3$, ${}_1^2H\ \rho_2 = 10^5 g/cm^3$, ${}_1^3H\ \rho_3 = 10^5 g/cm^3$, ${}_2^3He\ \rho_4 = 10^5 g/cm^3$, ${}_2^4He\ \rho_5 = 10^5 g/cm^3$, ${}_3^6Li\ \rho_6 = 10^5 g/cm^3$, ${}_3^7Li\ \rho_7 = 10^5 g/cm^3$, ${}_4^7Be\ \rho_8 = 10^5 g/cm^3$, ${}_4^9Be\ \rho_9 = 10^5 g/cm^3$, ${}_4^{10}Be\ \rho_{10} = 10^5 g/cm^3$

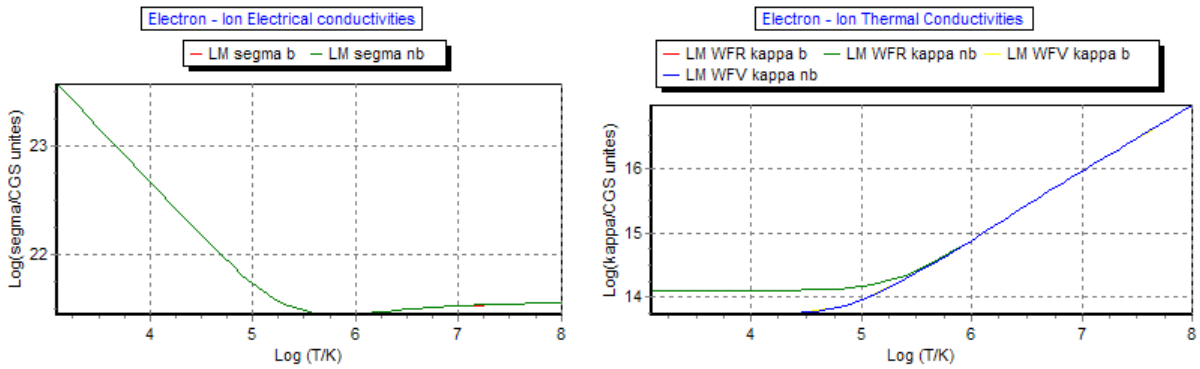

Figure 4.11c :*Electron ion electrical conductivities in the Born and beyond Born approximations (Left panel), and the difference between Thermal conductivities in the case were The Weidermann-Franz Law respected (WFR), and were The Weidermann-Franz Law violated (WFV) (Right panel), for the mixture* ${}_1^1H\ \rho_1 = 10^5 g/cm^3$, ${}_1^2H\ \rho_2 = 10^5 g/cm^3$, ${}_1^3H\ \rho_3 = 10^5 g/cm^3$, ${}_2^3He\ \rho_4 = 10^5 g/cm^3$, ${}_2^4He\ \rho_5 = 10^5 g/cm^3$, ${}_3^6Li\ \rho_6 = 10^5 g/cm^3$, ${}_3^7Li\ \rho_7 = 10^5 g/cm^3$, ${}_4^7Be\ \rho_8 = 10^5 g/cm^3$, ${}_4^9Be\ \rho_9 = 10^5 g/cm^3$, ${}_4^{10}Be\ \rho_{10} = 10^5 g/cm^3$

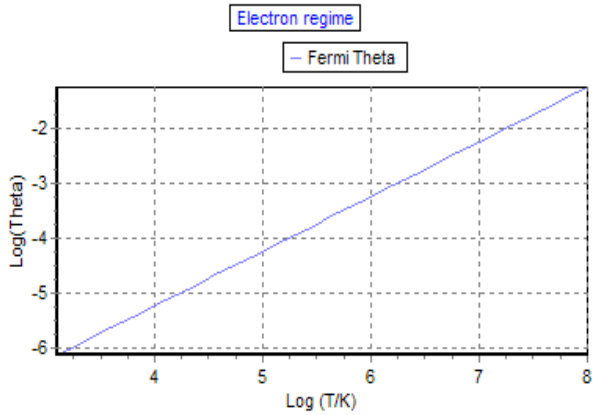

Figure 4.11d : *the Fermi temperature VS the temperature in the logarithmic scale, for the mixture:* ${}_1^1H\ \rho_1 = 10^5 g/cm^3$, ${}_1^2H\ \rho_2 = 10^5 g/cm^3$, ${}_1^3H\ \rho_3 = 10^5 g/cm^3$, ${}_2^3He\ \rho_4 = 10^5 g/cm^3$, ${}_2^4He\ \rho_5 = 10^5 g/cm^3$, ${}_3^6Li\ \rho_6 = 10^5 g/cm^3$, ${}_3^7Li\ \rho_7 = 10^5 g/cm^3$, ${}_4^7Be\ \rho_8 = 10^5 g/cm^3$, ${}_4^9Be\ \rho_9 = 10^5 g/cm^3$, ${}_4^{10}Be\ \rho_{10} = 10^5 g/cm^3$

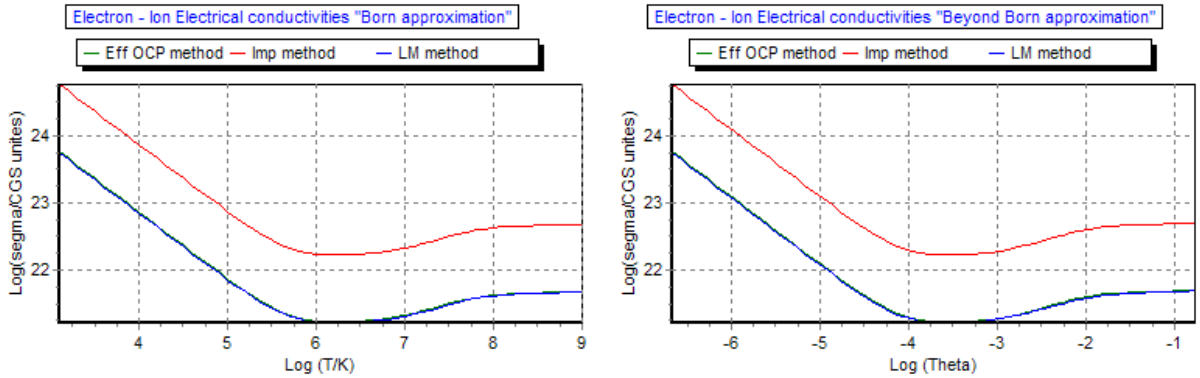

Figure 4.12a *: Electron ion thermal conductivities in the Born approximation (Left panel) and beyond Born approximation (Right panel) , we show different method of computation :Effective OCP method (Green line) ,Impurities method(Red line) , Linear mixing method (Blue line), for the mixture* $^{20}_{10}Ne\ \rho_1 = 10^6 g/cm^3$, $^{22}_{11}Na\ \rho_2 = 10^6 g/cm^3$, $^{24}_{12}Mg\ \rho_3 = 10^6 g/cm^3$, $^{26}_{13}Al\ \rho_4 = 10^6 g/cm^3$, $^{28}_{14}Si\ \rho_5 = 10^6 g/cm^3$, $^{31}_{15}P\ \rho_6 = 10^6 g/cm^3$, $^{33}_{16}S\ \rho_7 = 10^6 g/cm^3$, $^{35}_{17}Cl\ \rho_8 = 10^5 g/cm^3$, $^{36}_{18}Ar\ \rho_9 = 10^5 g/cm^3$, $^{39}_{19}K\ \rho_{10} = 10^5 g/cm^3$

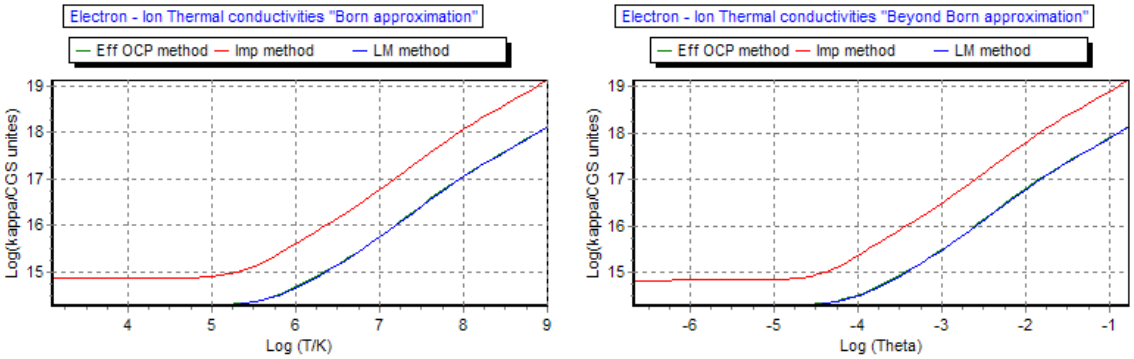

Figure 4.12b *: Electron ion electrical (upper panel) and thermal (lower panel) conductivities in the Born approximation (Left panel) and beyond Born approximation (Right panel) , we show different method of computation :Effective OCP method (Green line) ,Impurities method(Red line) , Linear mixing method (Blue line), for the mixture* $^{20}_{10}Ne\ \rho_1 = 10^6 g/cm^3$, $^{22}_{11}Na\ \rho_2 = 10^6 g/cm^3$, $^{24}_{12}Mg\ \rho_3 = 10^6 g/cm^3$, $^{26}_{13}Al\ \rho_4 = 10^6 g/cm^3$, $^{28}_{14}Si\ \rho_5 = 10^6 g/cm^3$, $^{31}_{15}P\ \rho_6 = 10^6 g/cm^3$, $^{33}_{16}S\ \rho_7 = 10^6 g/cm^3$, $^{35}_{17}Cl\ \rho_8 = 10^5 g/cm^3$, $^{36}_{18}Ar\ \rho_9 = 10^5 g/cm^3$, $^{39}_{19}K\ \rho_{10} = 10^5 g/cm^3$

.

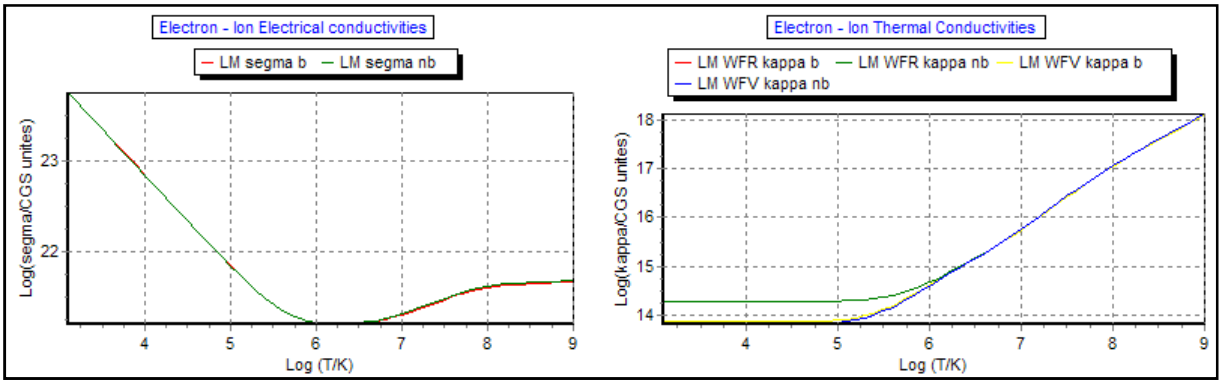

Figure 4.12c : *Electron ion electrical conductivities in the Born and beyond Born approximations (Left panel), and the difference between Thermal conductivities in the case were The Weidermann-Franz Law respected (WFR), and were The Weidermann-Franz Law violated (WFV) (Right panel), for the mixture* $^{20}_{10}Ne\ \rho_1 = 10^6 g/cm^3$, $^{22}_{11}Na\ \rho_2 = 10^6 g/cm^3$, $^{24}_{12}Mg\ \rho_3 = 10^6 g/cm^3$, $^{26}_{13}Al\ \rho_4 = 10^6 g/cm^3$, $^{28}_{14}Si\ \rho_5 = 10^6 g/cm^3$, $^{31}_{15}P\ \rho_6 = 10^6 g/cm^3$, $^{33}_{16}S\ \rho_7 = 10^6 g/cm^3$, $^{35}_{17}Cl\ \rho_8 = 10^5 g/cm^3$, $^{36}_{18}Ar\ \rho_9 = 10^5 g/cm^3$, $^{39}_{19}K\ \rho_{10} = 10^5 g/cm^3$

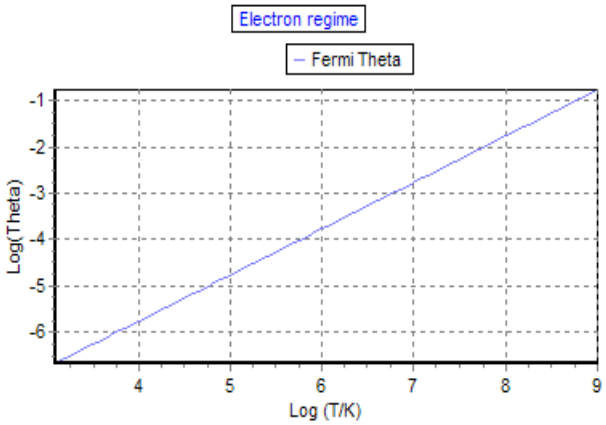

Figure 4.12d : *the Fermi temperature VS the temperature in the logarithmic scale , for the mixture* $^{20}_{10}Ne\ \rho_1 = 10^6 g/cm^3$, $^{22}_{11}Na\ \rho_2 = 10^6 g/cm^3$, $^{24}_{12}Mg\ \rho_3 = 10^6 g/cm^3$, $^{26}_{13}Al\ \rho_4 = 10^6 g/cm^3$, $^{28}_{14}Si\ \rho_5 = 10^6 g/cm^3$, $^{31}_{15}P\ \rho_6 = 10^6 g/cm^3$, $^{33}_{16}S\ \rho_7 = 10^6 g/cm^3$, $^{35}_{17}Cl\ \rho_8 = 10^5 g/cm^3$, $^{36}_{18}Ar\ \rho_9 = 10^5 g/cm^3$, $^{39}_{19}K\ \rho_{10} = 10^5 g/cm^3$

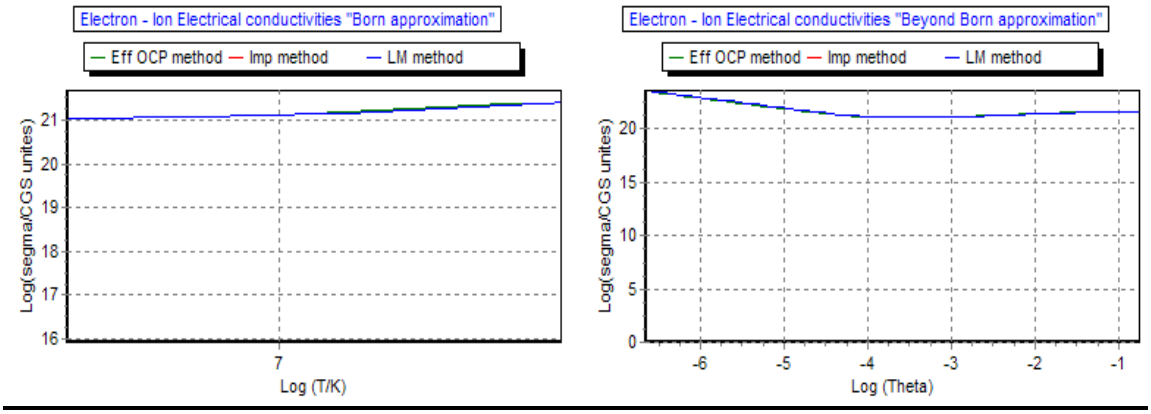

Figure 4.13a : *Electron ion thermal conductivities in the Born approximation (Left panel) and beyond Born approximation (Right panel) , we show different method of computation :Effective OCP method (Green line) ,Impurities method(Red line) , Linear mixing method (Blue line), for ten Ca's isotopes at fixed mass density ratio .*

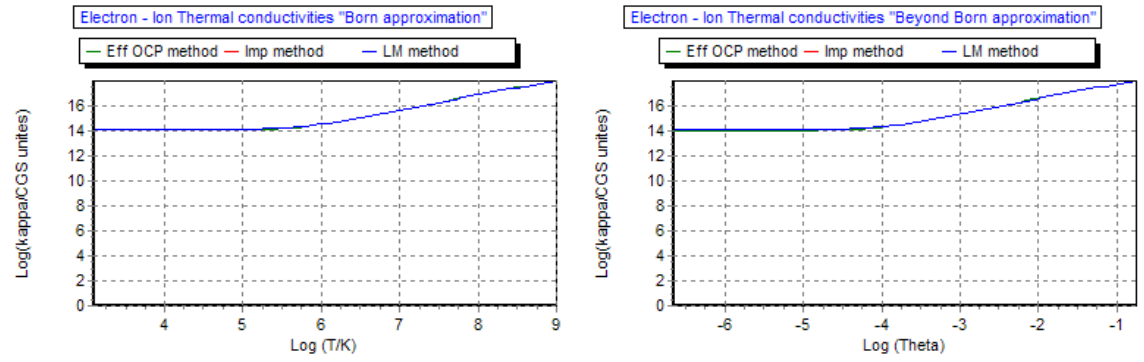

Figure 4.13b: *Electron ion electrical (upper panel) and thermal (lower panel) conductivities in the Born approximation (Left panel) and beyond Born approximation (Right panel) , we show different method of computation :Effective OCP method (Green line) ,Impurities method(Red line), Linear mixing method (Blue line) for ten Ca's isotopes at fixed mass density ratio.*

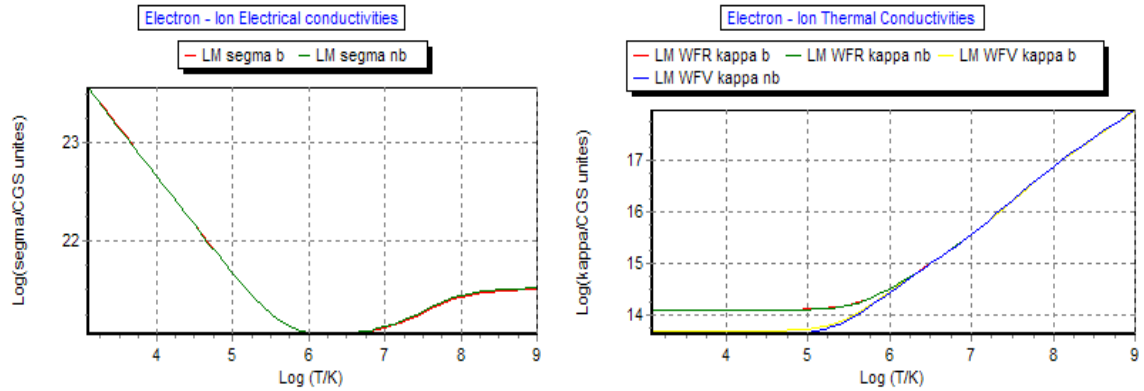

Figure 4.13c : *Electron ion electrical conductivities in the Born and beyond Born approximations (Left panel), and the difference between Thermal conductivities in the case were The Weidermann-Franz Law respected (WFR), and were The Weidermann-Franz Law violated (WFV) (Right panel) for ten Ca's isotopes at fixed mass density ratio.*

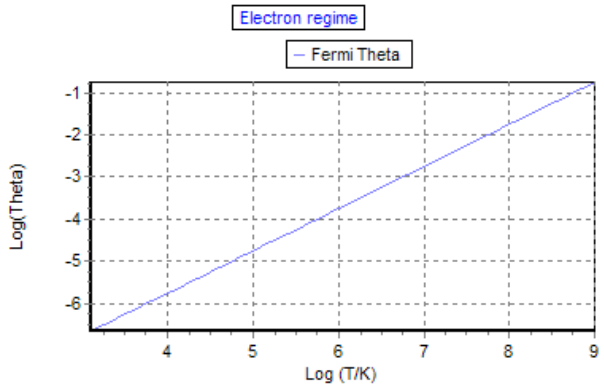

Figure 4.13d : *the Fermi temperature VS the temperature in the logarithmic scale for ten Ca's isotopes at fixed mass density ratio .*

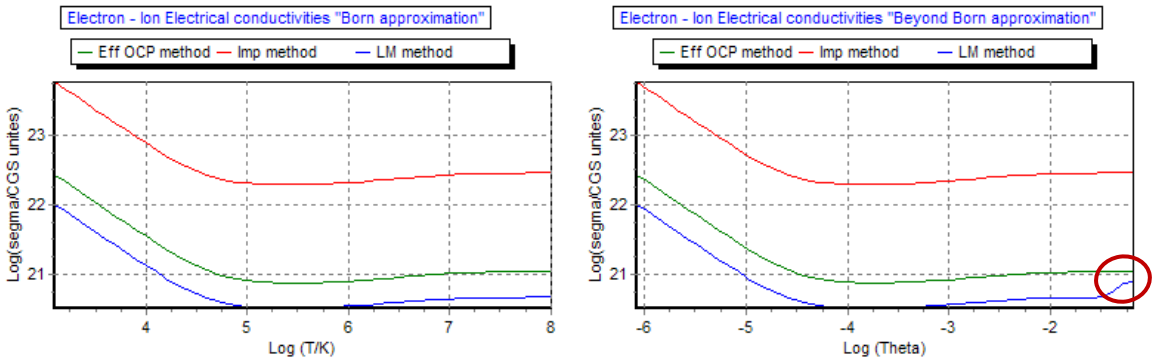

Figure 4.14a *: Electron ion electrical conductivities in the Born approximation (Left panel) and beyond Born approximation (Right panel) , we show different method of computation :Effective OCP method (Green line) ,Impurities method(Red line) , Linear mixing method (Blue line), for 89 elements from the hydrogen to the iron at fixed mass density ratio.*

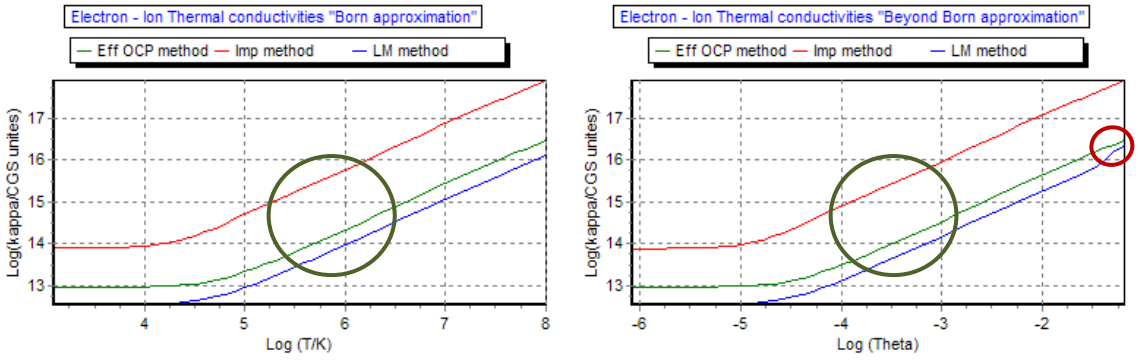

Figure 4.14b *: Electron ion thermal conductivities in the Born approximation (Left panel) and beyond Born approximation (Right panel) , we show different method of computation :Effective OCP method (Green line) ,Impurities method(Red line) , Linear mixing method (Blue line) , for 89 elements from the hydrogen to the iron at fixed mass density ratio.*

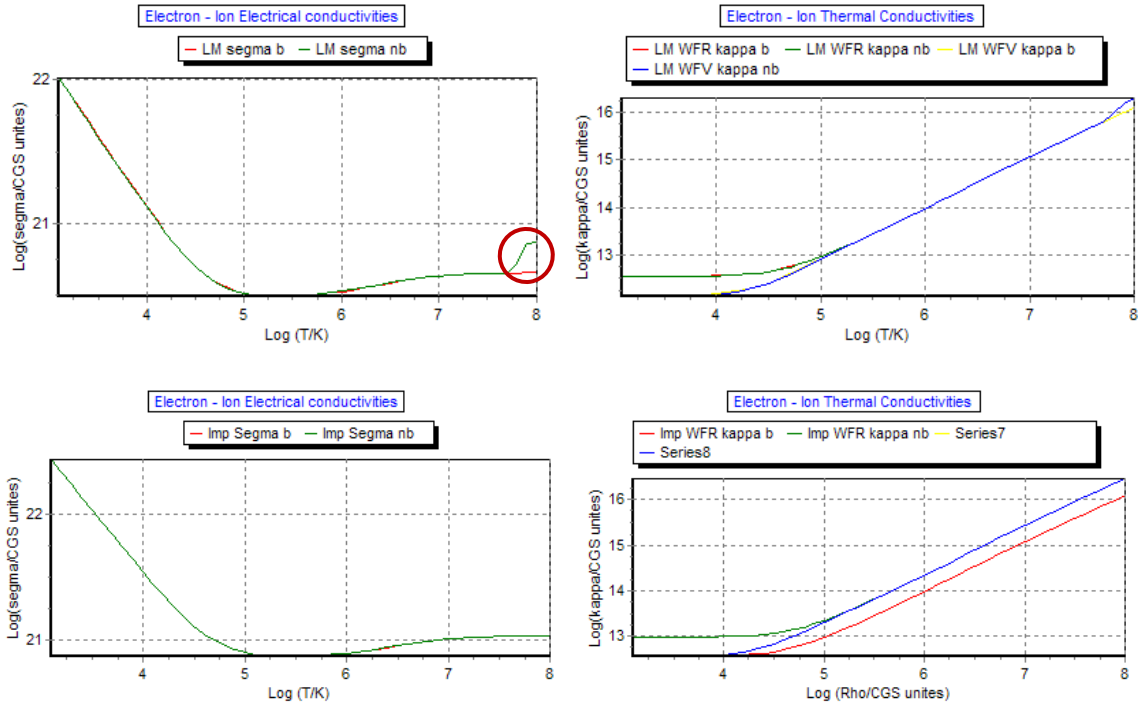

Figure 4.14c*: Electron ion electrical conductivities in the Born and beyond Born approximations (Left panel), and the difference between Thermal conductivities in the case were The Weidermann-Franz Law respected (WFR), and were The Weidermann-Franz Law violated (WFV) (Right panel) , for 89 elements from the hydrogen to the iron at fixed mass density ratio.*

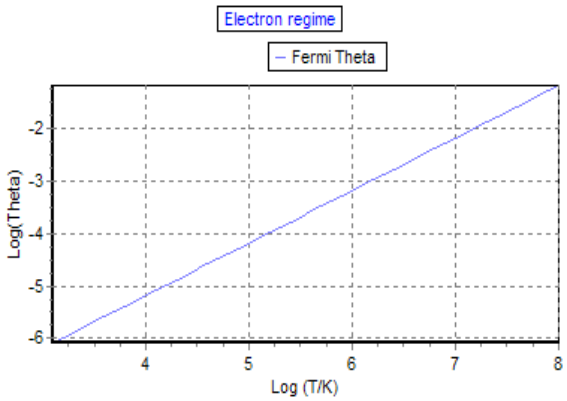

Figure 4.14d : *the Fermi temperature VS the temperature in the logarithmic scale, for 89 elements from the hydrogen to the iron at fixed mass density ratio .*

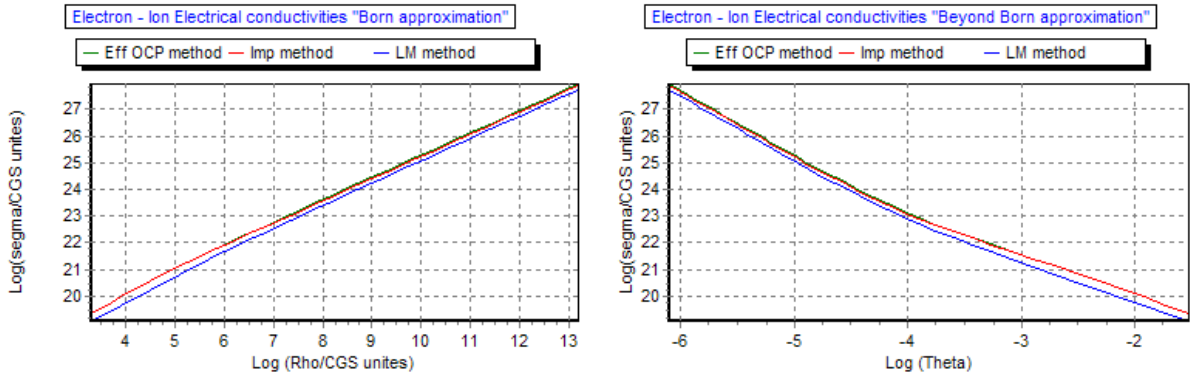

Figure 4.15a : *Electron ion electrical conductivities in the Born approximation (Left panel) and beyond Born approximation (Right panel) , we show different method of computation :Effective OCP method (Green line) ,Impurities method(Red line) , Linear mixing method (Blue line) , for the mixture* ${}_1^1H$, ${}_2^4He$, $X_j = 0.5, j = 1,2$ *at* $T = 10^6 K$.

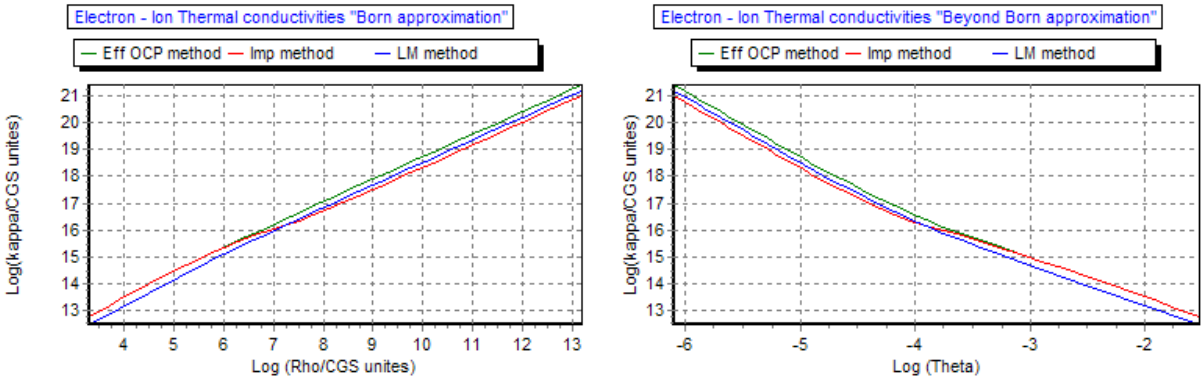

Figure 4.15b : *Electron ion thermal conductivities in the Born approximation (Left panel) and beyond Born approximation (Right panel) , we show different method of computation :Effective OCP method (Green line) ,Impurities method(Red line) , Linear mixing method (Blue line) , for the mixture* ${}_1^1H$, ${}_2^4He$, $X_j = 0.5, j = 1,2$ *at* $T = 10^6 K$.

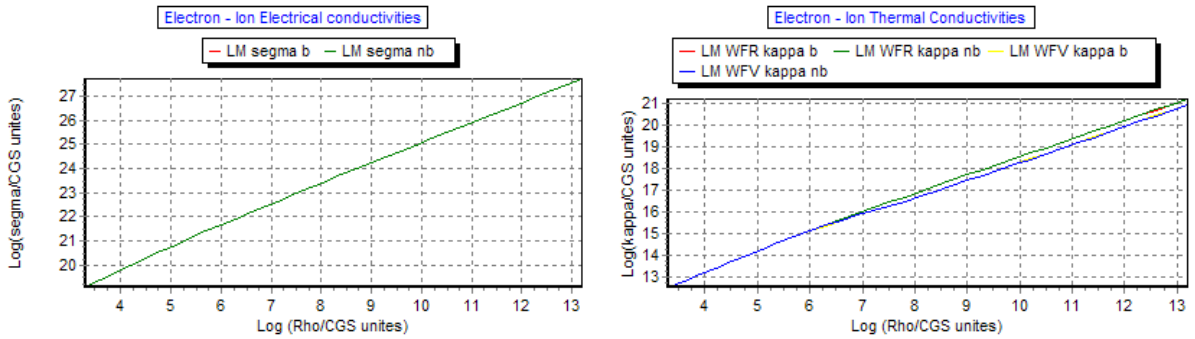

Figure 4.15c : *Electron ion electrical conductivities in the Born and beyond Born approximations (Left panel), and the difference between Thermal conductivities in the case were The Weidermann-Franz Law respected (WFR), and were The Weidermann-Franz Law violated (WFV) (Right panel) , for the mixture* ${}_1^1H$, ${}_2^4He$, $X_j = 0.5, j = 1,2$ *at* $T = 10^6 K$.

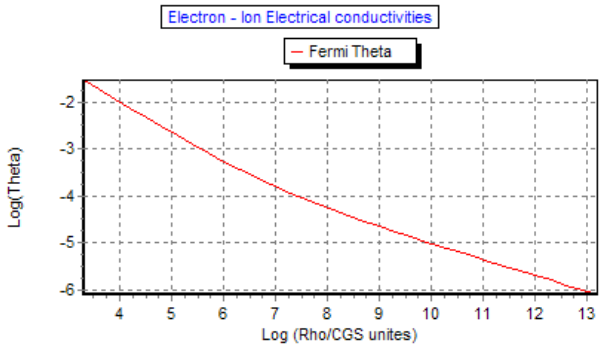

Figure 4.15d: *the Fermi temperature VS the total mass density in the logarithmic scale, for the mixture* ${}_1^1H$, ${}_2^4He$, $X_j = 0.5, j = 1{,}2$ *at* $T = 10^6 K$.

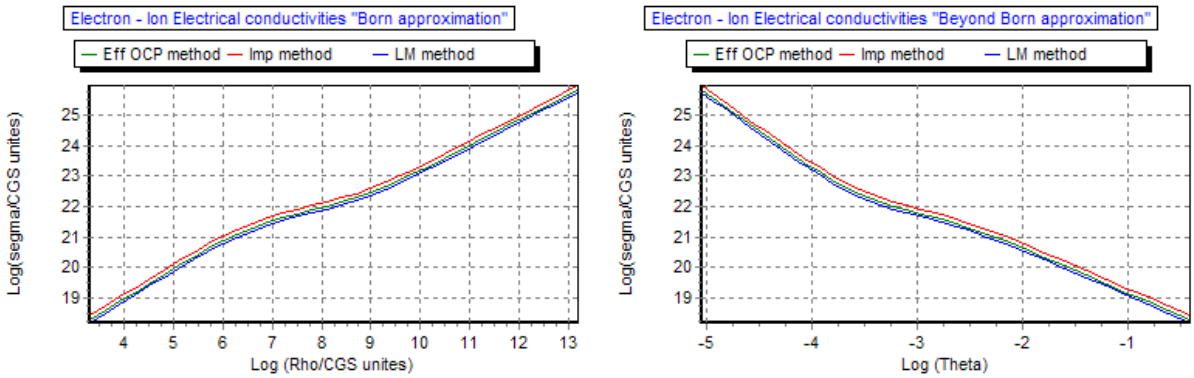

Figure 4.16a : *Electron ion electrical conductivities in the Born approximation (Left panel) and beyond Born approximation (Right panel) , we show different method of computation :Effective OCP method (Green line) ,Impurities method(Red line) , Linear mixing method (Blue line) , for the mixture* ${}_6^{12}C$, ${}_8^{16}O$, $X_j = 0.5, j = 1{,}2$ *at* $T = 10^7 K$.

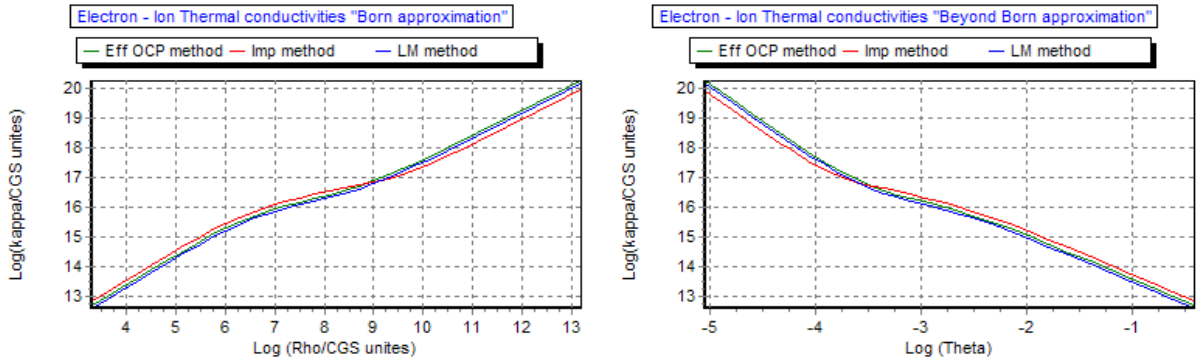

Figure 4.16b: *Electron ion thermal conductivities in the Born approximation (Left panel) and beyond Born approximation (Right panel) , we show different method of computation :Effective OCP method (Green line) ,Impurities method(Red line) , Linear mixing method (Blue line) , , for the mixture* ${}_6^{12}C$, ${}_8^{16}O$, $X_j = 0.5, j = 1{,}2$ *at* $T = 10^7 K$.

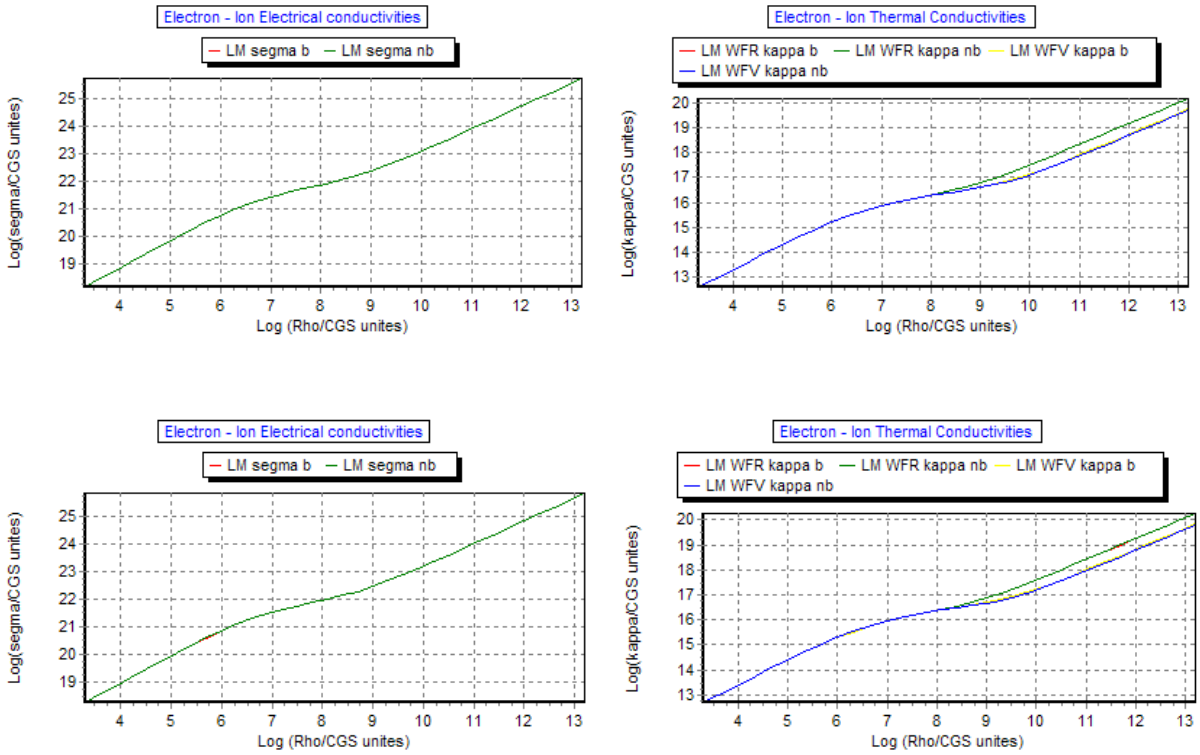

Figure 4.16c : *Electron ion electrical conductivities in the Born and beyond Born approximations (Left panel), and the difference between Thermal conductivities in the case were The Weidermann-Franz Law respected (WFR), and were The Weidermann-Franz Law violated (WFV) (Right panel) , for the mixture* ${}^{12}_{6}C$, ${}^{16}_{8}O$, $X_j = 0.5, j = 1{,}2$ *at* $T = 10^7 K$.

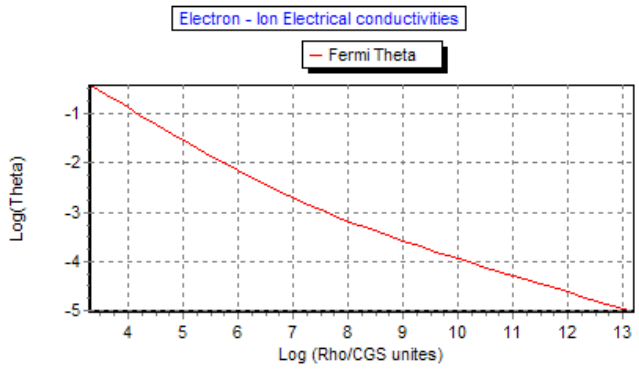

Figure 4.16d : *the Fermi temperature VS the total mass density in the logarithmic scale ,for the mixture* ${}^{12}_{6}C$, ${}^{16}_{8}O$, $X_j = 0.5, j = 1{,}2$ *at* $T = 10^7 K$.

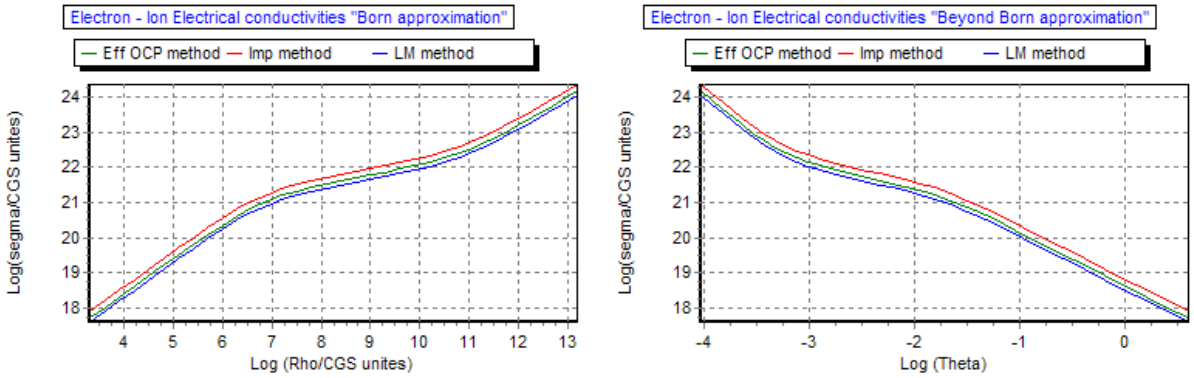

Figure 4.17a : *Electron ion electrical conductivities in the Born approximation (Left panel) and beyond Born approximation (Right panel) , we show different method of computation :Effective OCP method (Green line) ,Impurities method(Red line) , Linear mixing method (Blue line) ,for the mixture* $^{52}_{25}Mn$ *,* $^{54}_{26}Fe$ *,* $X_j = 0.5, j = 1,2$ *at* $T = 10^8 K$.

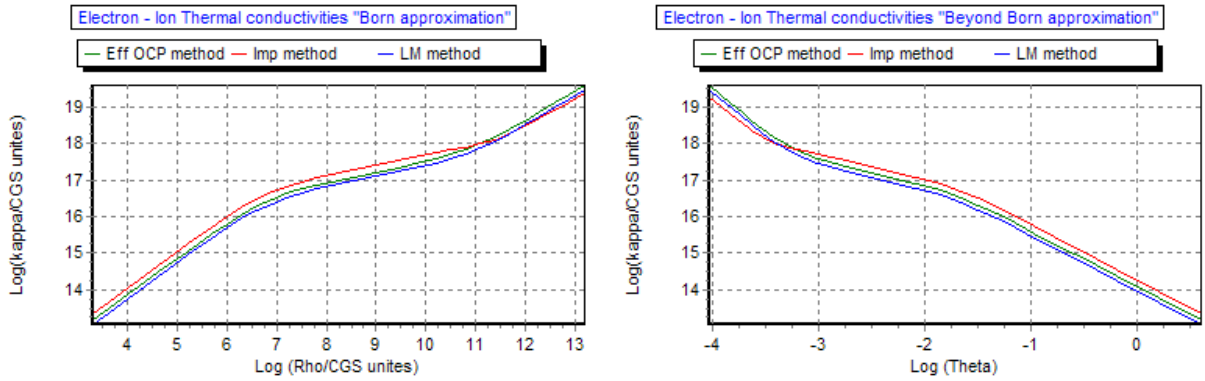

Figure 4.17b : *Electron ion thermal conductivities in the Born approximation (Left panel) and beyond Born approximation (Right panel) , we show different method of computation :Effective OCP method (Green line) ,Impurities method(Red line) , Linear mixing method (Blue line) ,for the mixture* $^{52}_{25}Mn$ *,* $^{54}_{26}Fe$ *,* $X_j = 0.5, j = 1,2$ *at* $T = 10^8 K$.

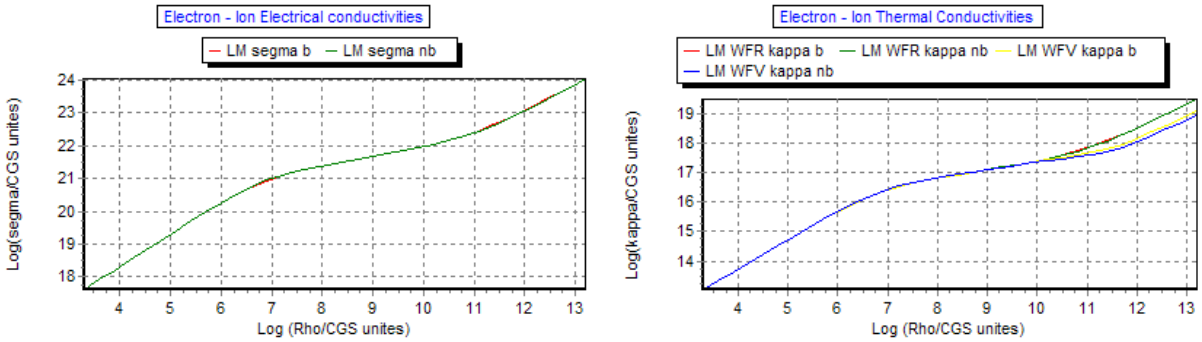

Figure 4.17c : *Electron ion electrical conductivities in the Born and beyond Born approximations (Left panel), and the difference between Thermal conductivities in the case were The Weidermann-Franz Law respected (WFR), and were The Weidermann-Franz Law violated (WFV) (Right panel) ,for the mixture* $^{52}_{25}Mn$ *,* $^{54}_{26}Fe$ *,* $X_j = 0.5, j = 1,2$ *at* $T = 10^8 K$.

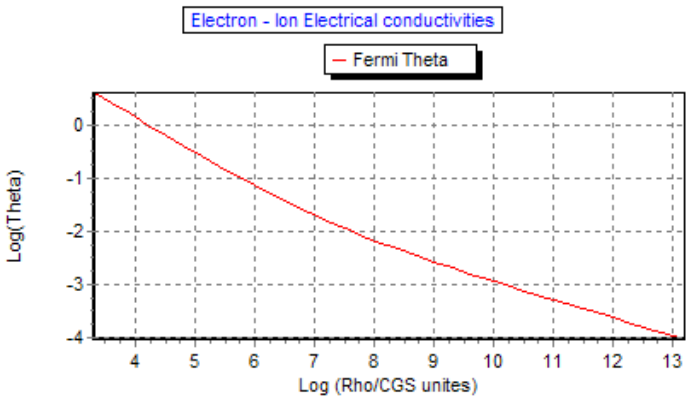

Figure 4.17d: *the Fermi temperature VS the total mass density in the logarithmic scale,for the mixture* ${}^{52}_{25}Mn$, ${}^{54}_{26}Fe$ $, X_j = 0.5, j = 1,2$ *at* $T = 10^8 K$.

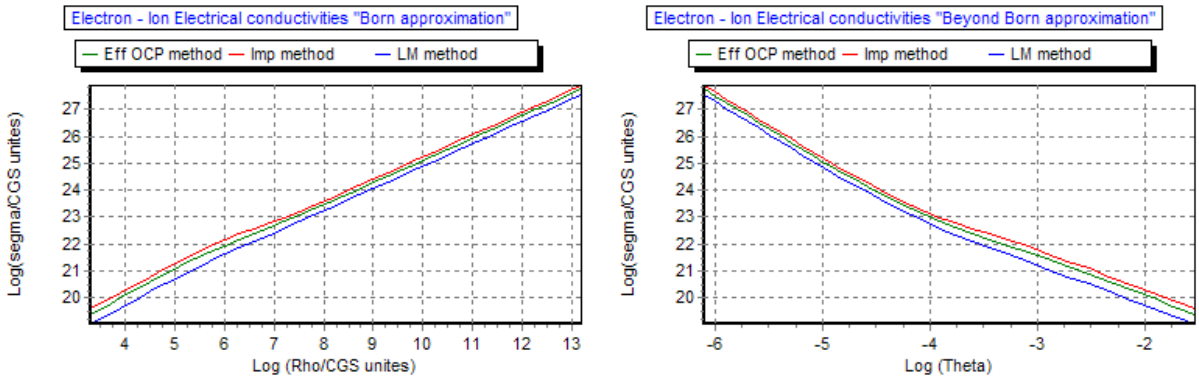

Figure 4.18a: *Electron ion electrical conductivities in the Born approximation (Left panel) and beyond Born approximation (Right panel) , we show different method of computation :Effective OCP method (Green line) ,Impurities method(Red line) , Linear mixing method (Blue line) ,for the mixture* ${}^{1}_{1}H$, ${}^{4}_{2}He, {}^{6}_{3}Li, X_j = 1/3, j = 1,2,3$ *at* $T = 10^6 K$.

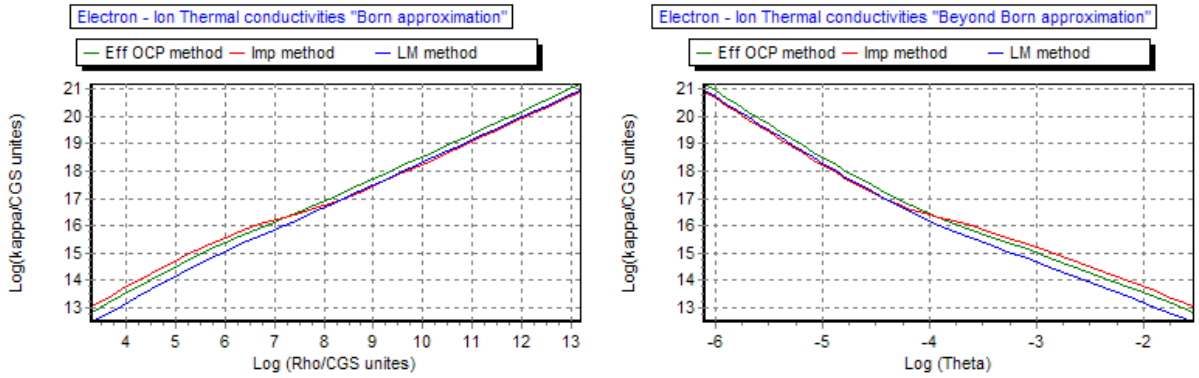

Figure 4.18b : *Electron ion thermal conductivities in the Born approximation (Left panel) and beyond Born approximation (Right panel) , we show different method of computation :Effective OCP method (Green line) ,Impurities method(Red line) , Linear mixing method (Blue line) ,for the mixture* ${}^{1}_{1}H$, ${}^{4}_{2}He, {}^{6}_{3}Li, X_j = 1/3, j = 1,2,3$ *at* $T = 10^6 K$.

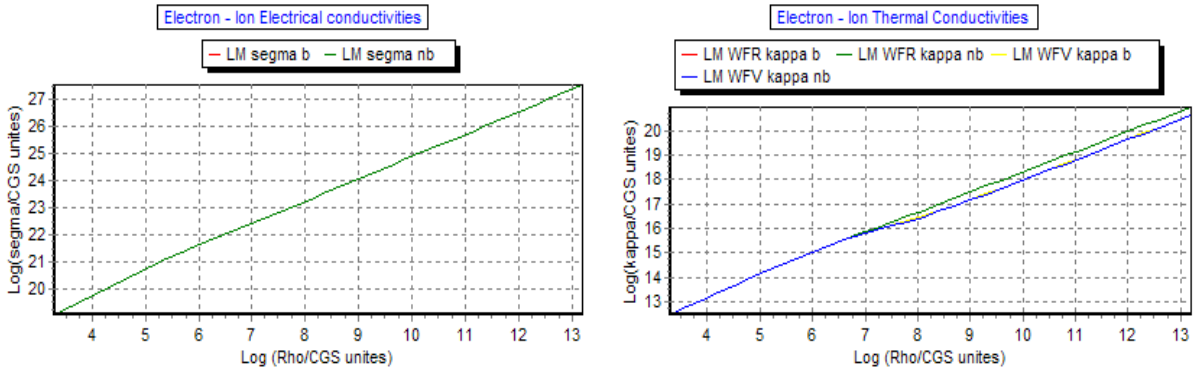

Figure 4.18c *: Electron ion electrical conductivities in the Born and beyond Born approximations (Left panel), and the difference between Thermal conductivities in the case were The Weidermann-Franz Law respected (WFR), and were The Weidermann-Franz Law violated (WFV) (Right panel) ,for the mixture* ${}_{1}^{1}H$, ${}_{2}^{4}He, {}_{3}^{6}Li, X_j = 1/3, j = 1,2,3$ *at* $T = 10^6 K$.

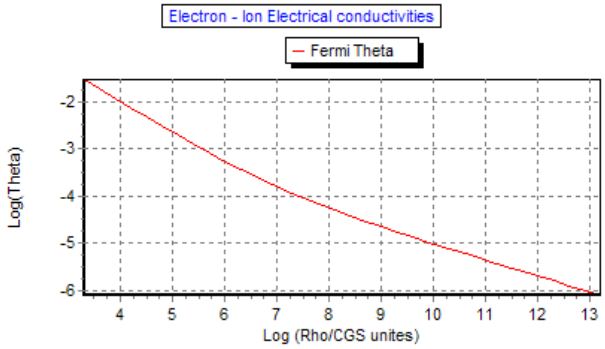

Figure 4.18d *: the Fermi temperature VS the total mass density in the logarithmic scale, for the mixture* ${}_{1}^{1}H$, ${}_{2}^{4}He, {}_{3}^{6}Li, X_j = 1/3, j = 1,2,3$ *at* $T = 10^6 K$.

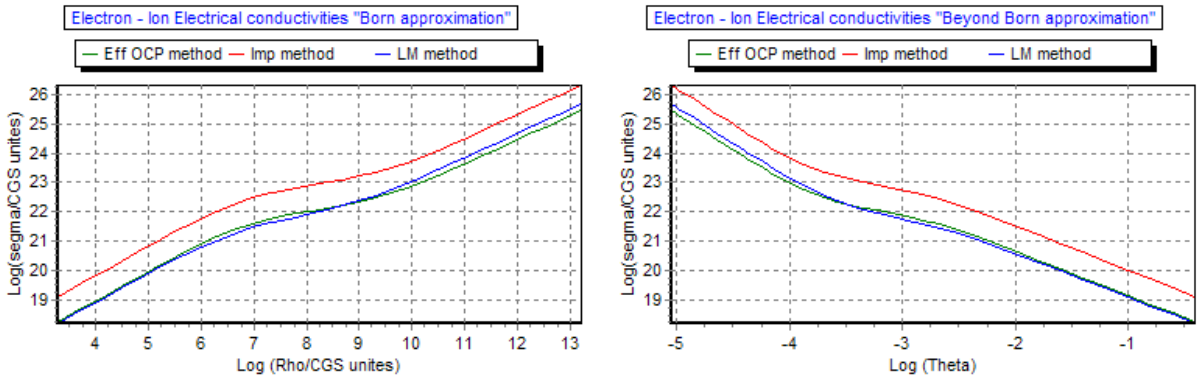

Figure 4.19a *: Electron ion electrical conductivities in the Born approximation (Left panel) and beyond Born approximation (Right panel) , we show different method of computation :Effective OCP method (Green line) ,Impurities method(Red line) , Linear mixing method (Blue line) ,for the mixture* ${}_{6}^{12}C$, ${}_{7}^{14}N$, ${}_{8}^{16}O, X_j = 1/3, j = 1,2,3$ *at* $T = 10^7 K$.

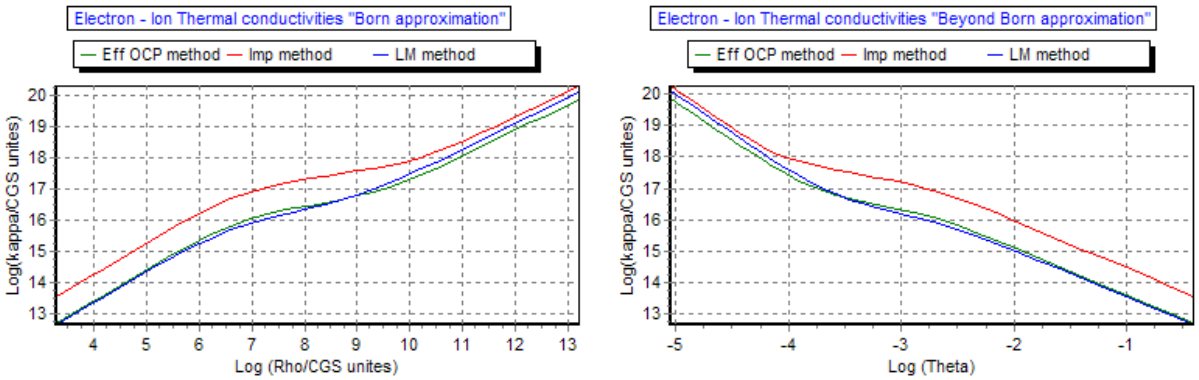

Figure 4.19b : *Electron ion thermal conductivities in the Born approximation (Left panel) and beyond Born approximation (Right panel) , we show different method of computation :Effective OCP method (Green line) ,Impurities method(Red line) , Linear mixing method (Blue line) ,for the mixture* ${}^{12}_{6}C$, ${}^{14}_{7}N$, ${}^{16}_{8}O, X_j = 1/3, j = 1,2,3$ *at* $T = 10^7 K$.

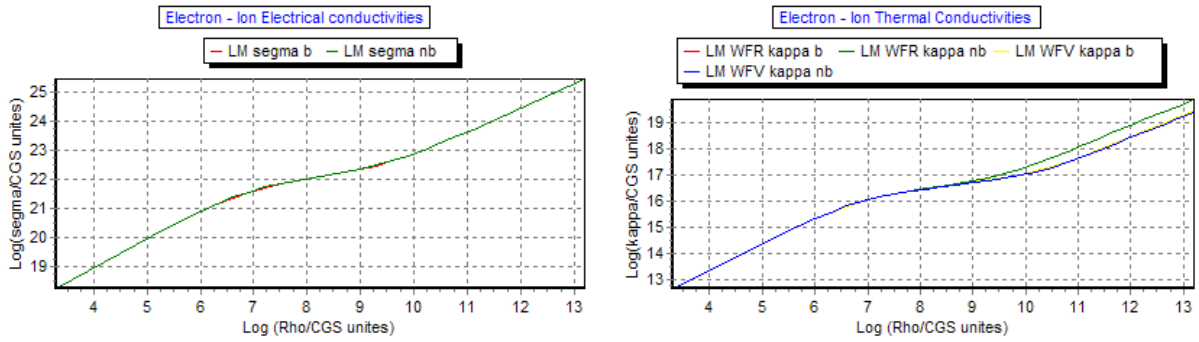

Figure 4.19c : *Electron ion electrical conductivities in the Born and beyond Born approximations (Left panel), and the difference between Thermal conductivities in the case were The Weidermann-Franz Law respected (WFR), and were The Weidermann-Franz Law violated (WFV) (Right panel) ,for the mixture* ${}^{12}_{6}C$, ${}^{14}_{7}N$, ${}^{16}_{8}O, X_j = 1/3, j = 1,2,3$ *at* $T = 10^7 K$.

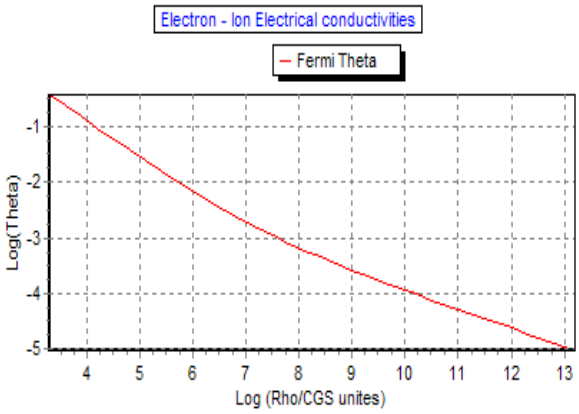

Figure 4.19d : *the Fermi temperature VS the total mass density in the logarithmic scale ,for the mixture* ${}^{12}_{6}C$, ${}^{14}_{7}N$, ${}^{16}_{8}O, X_j = 1/3, j = 1,2,3$ *at* $T = 10^7 K$.

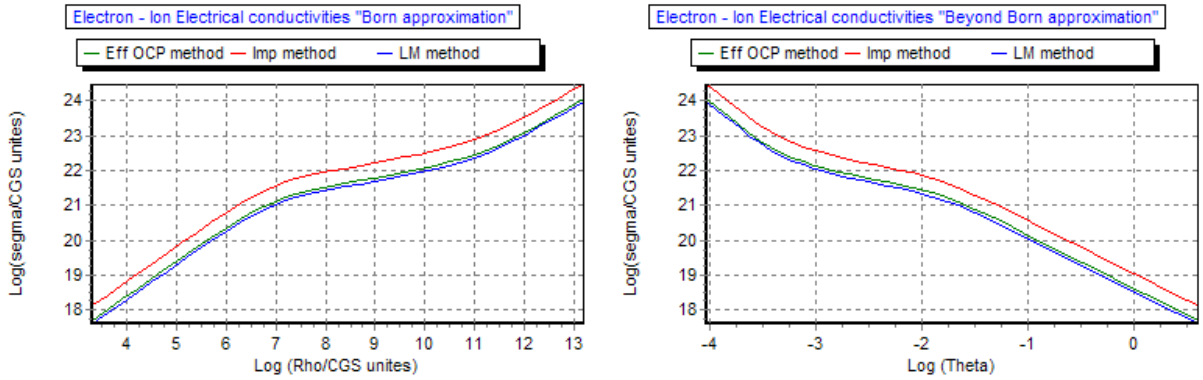

Figure 4.20a : *Electron ion electrical conductivities in the Born approximation (Left panel) and beyond Born approximation (Right panel) , we show different method of computation :Effective OCP method (Green line) ,Impurities method(Red line) , Linear mixing method (Blue line) ,for the mixture* $^{50}_{24}Cr$, $^{52}_{25}Mn, ^{56}_{26}Fe, X_j = 1/3$, $j = 1,2,3$ *at* $T = 10^7 K$.

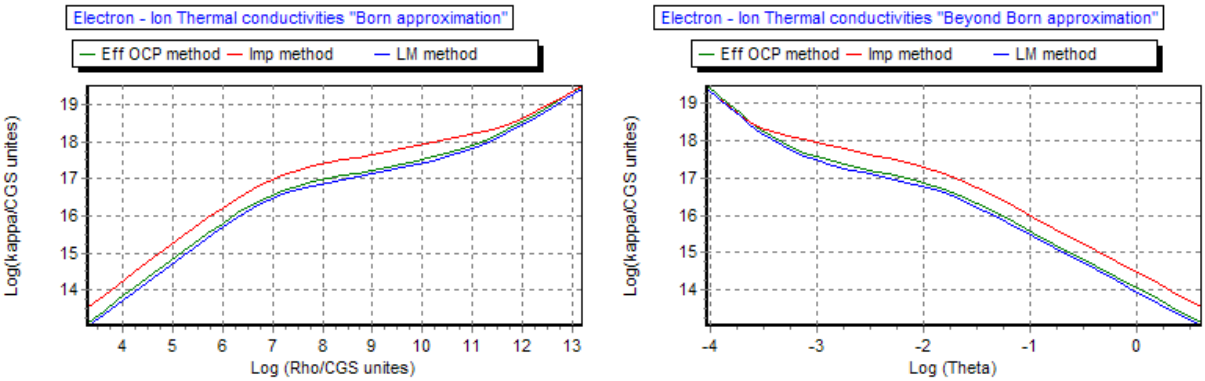

Figure 4.20b : *Electron ion thermal conductivities in the Born approximation (Left panel) and beyond Born approximation (Right panel) , we show different method of computation :Effective OCP method (Green line) ,Impurities method(Red line) , Linear mixing method (Blue line) ,for the mixture* $^{50}_{24}Cr$, $^{52}_{25}Mn, ^{56}_{26}Fe, X_j = 1/3$, $j = 1,2,3$ *at* $T = 10^7 K$.

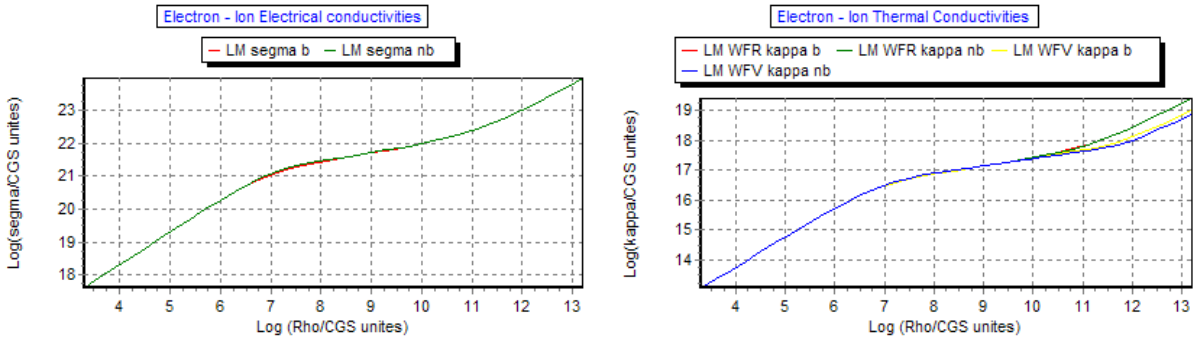

Figure 4.20c : *Electron ion electrical conductivities in the Born and beyond Born approximations (Left panel), and the difference between Thermal conductivities in the case were The Weidermann-Franz Law respected (WFR), and were The Weidermann-Franz Law violated (WFV) (Right panel), for the mixture* $^{50}_{24}Cr$, $^{52}_{25}Mn, ^{56}_{26}Fe, X_j = 1/3$, $j = 1,2,3$ *at* $T = 10^7 K$.

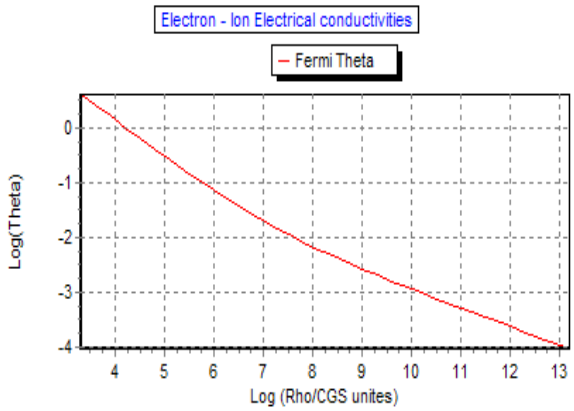

Figure 4.20d : *the Fermi temperature VS the total mass density in the logarithmic scale ,for the mixture* $^{50}_{24}Cr$, $^{52}_{25}Mn, ^{56}_{26}Fe, X_j = 1/3$, $j = 1,2,3$ *at* $T = 10^7 K$.

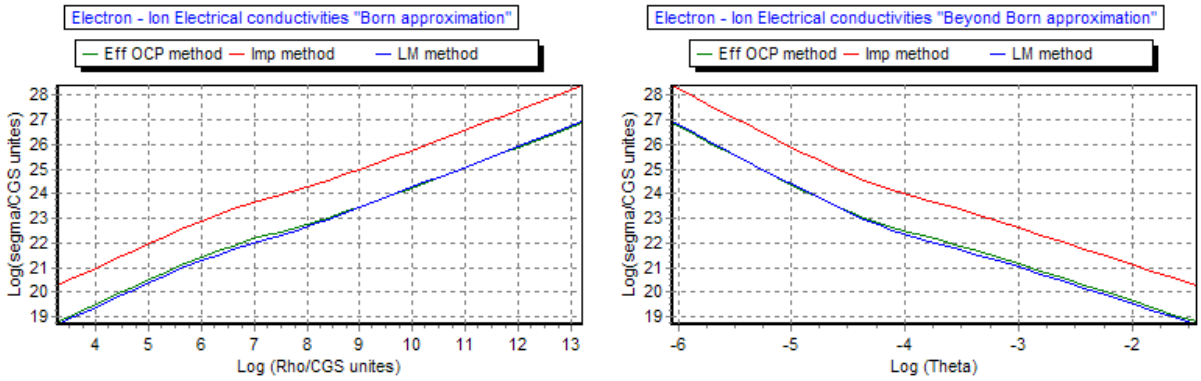

Figure 4.21a : *Electron ion electrical conductivities in the Born approximation (Left panel) and beyond Born approximation (Right panel) , we show different method of computation :Effective OCP method (Green line) ,Impurities method(Red line) , Linear mixing method (Blue line) ,for the mixture:* $^{1}_{1}H$, $^{2}_{1}H$, $^{3}_{1}H$, $^{3}_{2}He$, $^{4}_{2}He, ^{6}_{3}Li, ^{7}_{3}Li$, $^{7}_{4}Be, ^{9}_{4}Be, ^{10}_{4}Be$, $X_j = \frac{1}{10}, j = 1..10$ *at* $T = 10^6 K$.

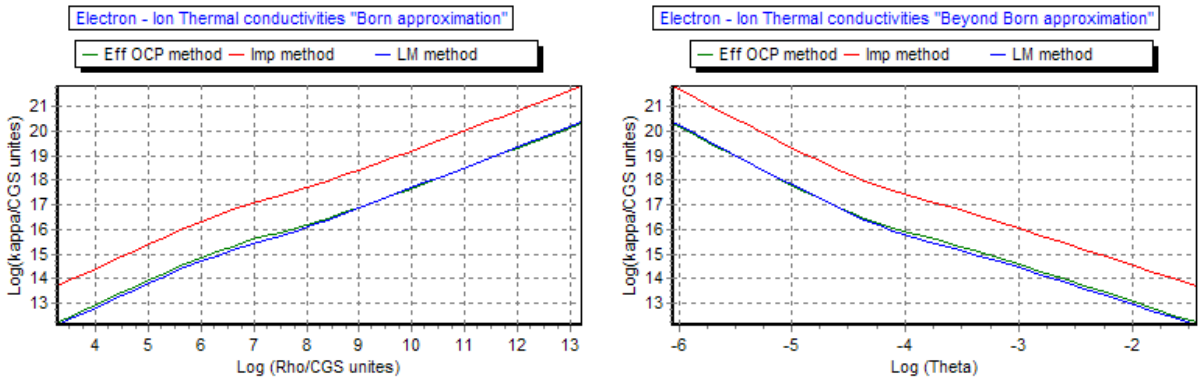

Figure 4.21b : *Electron ion thermal conductivities in the Born approximation (Left panel) and beyond Born approximation (Right panel) , we show different method of computation :Effective OCP method (Green line) ,Impurities method(Red line) , Linear mixing method (Blue line) ,for the mixture* ${}_1^1H$, ${}_1^2H$, ${}_1^3H$, ${}_2^3He$, ${}_2^4He$, ${}_3^6Li$, ${}_3^7Li$, ${}_4^7Be$, ${}_4^9Be$, ${}_4^{10}Be$, $X_j = \frac{1}{10}, j = 1..10$ *at* $T = 10^6 K$.

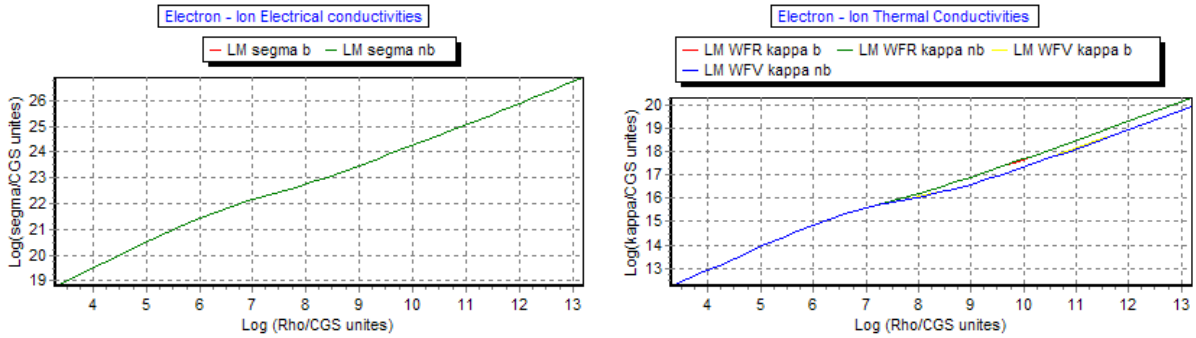

Figure 4.21c : *Electron ion electrical conductivities in the Born and beyond Born approximations (Left panel), and the difference between Thermal conductivities in the case were The Weidermann-Franz Law respected (WFR), and were The Weidermann-Franz Law violated (WFV) (Right panel) ,for the mixture:*
${}_1^1H$, ${}_1^2H$, ${}_1^3H$, ${}_2^3He$, ${}_2^4He$, ${}_3^6Li$, ${}_3^7Li$, ${}_4^7Be$, ${}_4^9Be$, ${}_4^{10}Be$, $X_j = \frac{1}{10}, j = 1..10$ *at* $T = 10^6 K$..

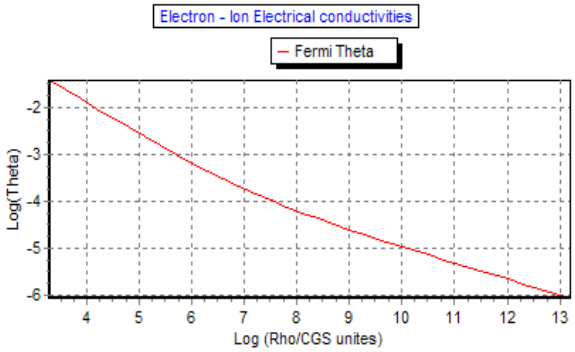

Figure 4.21d : *the Fermi temperature VS the total mass density in the logarithmic scale ,for the mixture* ${}_1^1H$, ${}_1^2H$, ${}_1^3H$, ${}_2^3He$, ${}_2^4He$, ${}_3^6Li$, ${}_3^7Li$, ${}_4^7Be$, ${}_4^9Be$, ${}_4^{10}Be$, $X_j = \frac{1}{10}, j = 1..10$ *at* $T = 10^6 K$.

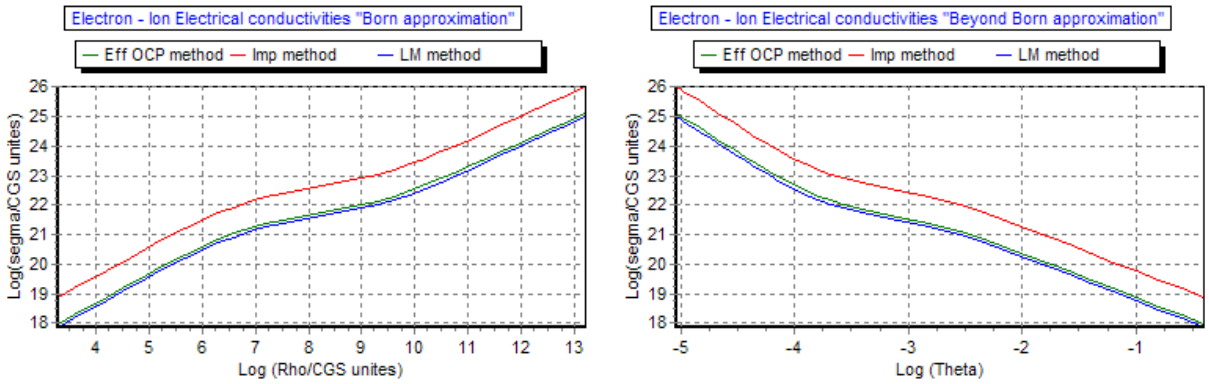

Figure 4.22a : *Electron ion electrical conductivities in the Born approximation (Left panel) and beyond Born approximation (Right panel) , we show different method of computation :Effective OCP method (Green line) ,Impurities method(Red line) , Linear mixing method (Blue line) ,for the mixture* ${}^{20}_{10}Ne$, ${}^{22}_{11}Na$, ${}^{24}_{12}Mg$, ${}^{26}_{13}Al$, ${}^{28}_{14}Si$, ${}^{31}_{15}P$, ${}^{33}_{16}S$, ${}^{35}_{17}Cl$, ${}^{36}_{18}Ar$, ${}^{39}_{19}K$, $X_j = \frac{1}{10}, j = 1..10$ *at* $T = 10^7 K$.

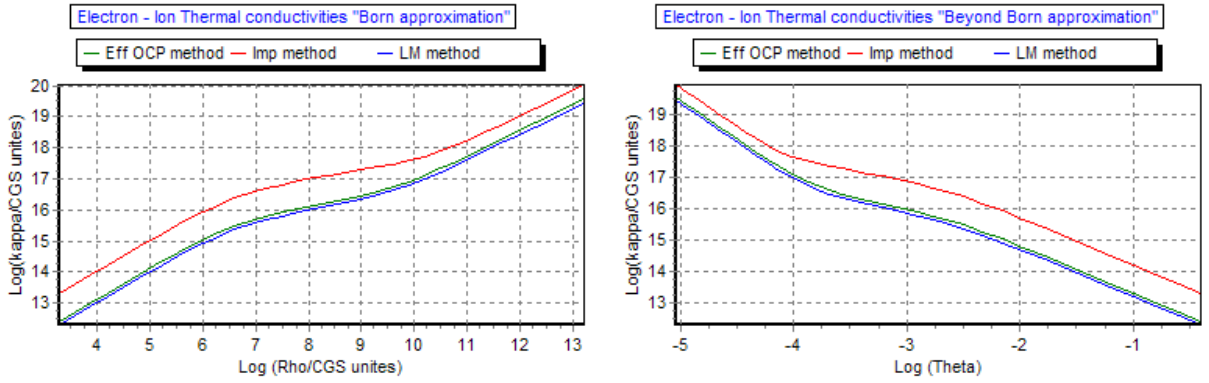

Figure 4.22b : *Electron ion thermal conductivities in the Born approximation (Left panel) and beyond Born approximation (Right panel) , we show different method of computation :Effective OCP method (Green line) ,Impurities method(Red line) , Linear mixing method (Blue line) ,for the mixture:*

${}^{20}_{10}Ne$, ${}^{22}_{11}Na$, ${}^{24}_{12}Mg$, ${}^{26}_{13}Al$, ${}^{28}_{14}Si$, ${}^{31}_{15}P$, ${}^{33}_{16}S$, ${}^{35}_{17}Cl$, ${}^{36}_{18}Ar$, ${}^{39}_{19}K$, $X_j = \frac{1}{10}, j = 1..10$ *at* $T = 10^7 K$.

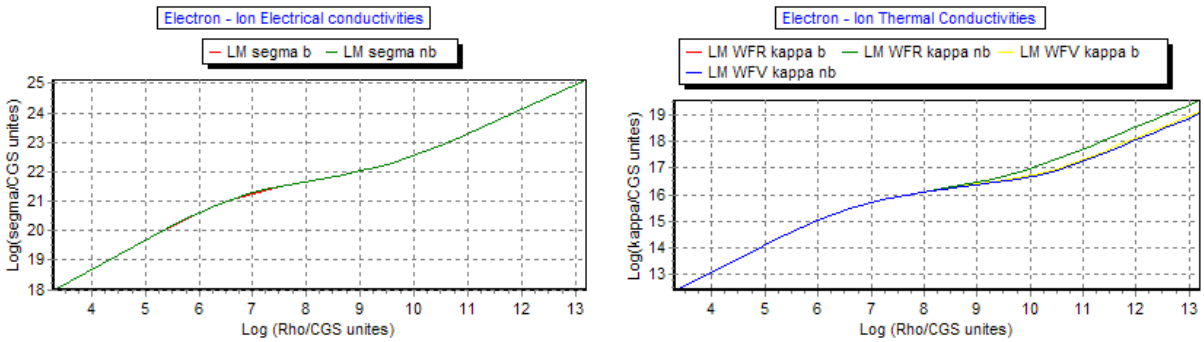

Figure 4.22c : *Electron ion electrical conductivities in the Born and beyond Born approximations (Left panel), and the difference between Thermal conductivities in the case were The Weidermann-Franz Law respected (WFR), and were The Weidermann-Franz Law violated (WFV) (Right panel) ,for the mixture* ${}^{20}_{10}Ne$, ${}^{22}_{11}Na$, ${}^{24}_{12}Mg$, ${}^{26}_{13}Al$, ${}^{28}_{14}Si$, ${}^{31}_{15}P$, ${}^{33}_{16}S$, ${}^{35}_{17}Cl$, ${}^{36}_{18}Ar$, ${}^{39}_{19}K$, $X_j = \frac{1}{10}, j = 1..10$ *at* $T = 10^7 K$.

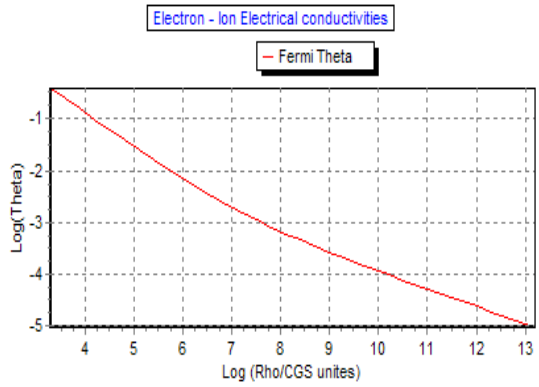

Figure 4.22d : *the Fermi temperature VS the total mass density in the logarithmic scale ,for the mixture* ${}^{20}_{10}Ne$, ${}^{22}_{11}Na$, ${}^{24}_{12}Mg$, ${}^{26}_{13}Al$, ${}^{28}_{14}Si$, ${}^{31}_{15}P$, ${}^{33}_{16}S$, ${}^{35}_{17}Cl$, ${}^{36}_{18}Ar$, ${}^{39}_{19}K$, $X_j = \frac{1}{10}, j = 1..10$ *at* $T = 10^7 K$.

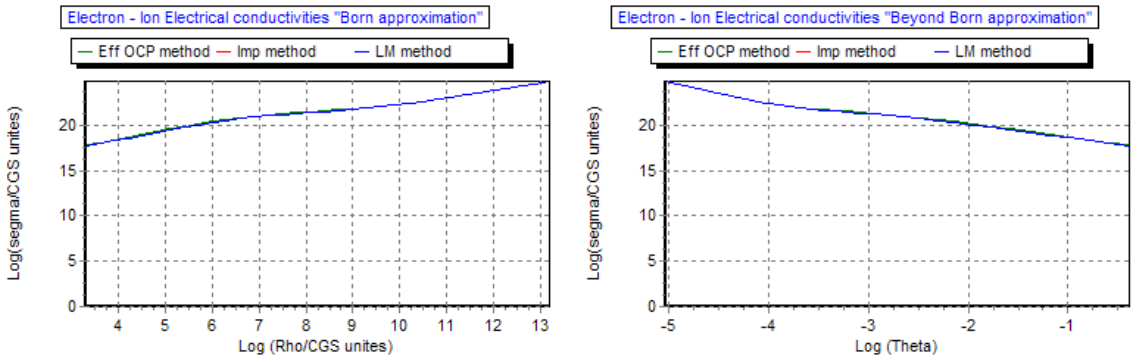

Figure 4.23a : *Electron ion electrical conductivities in the Born approximation (Left panel) and beyond Born approximation (Right panel) , we show different method of computation :Effective OCP method (Green line) ,Impurities method(Red line) , Linear mixing method (Blue line) ,for the mixture* ${}^{40}_{20}Ca$, ${}^{41}_{20}Ca$, ${}^{42}_{20}Ca$, ${}^{43}_{20}Ca$, ${}^{44}_{20}Ca$, ${}^{45}_{20}Ca$, ${}^{46}_{20}Ca$, ${}^{47}_{20}Ca$, ${}^{48}_{20}Ca$, $X_j = \frac{1}{10}, j = 1..10$ *at* $T = 10^7 K$.

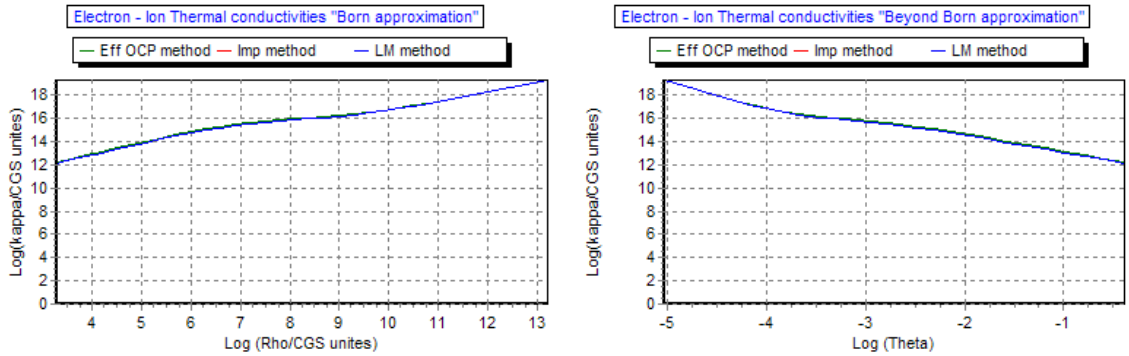

Figure 4.23b *: Electron ion thermal conductivities in the Born approximation (Left panel) and beyond Born approximation (Right panel) , we show different method of computation :Effective OCP method (Green line) ,Impurities method(Red line) , Linear mixing method (Blue line) ,for the mixture:* ${}^{40}_{20}Ca$, ${}^{41}_{20}Ca$, ${}^{42}_{20}Ca$, ${}^{43}_{20}Ca$, ${}^{44}_{20}Ca$, ${}^{45}_{20}Ca$, ${}^{46}_{20}Ca$, ${}^{47}_{20}Ca$, ${}^{48}_{20}Ca$, $X_j = \frac{1}{10}, j = 1..10$ *at* $T = 10^7 K$. .

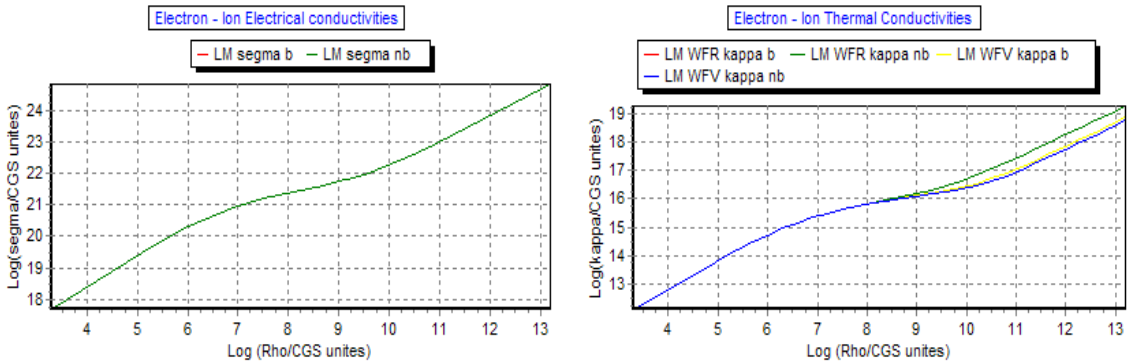

Figure 4.23c *: Electron ion electrical conductivities in the Born and beyond Born approximations (Left panel), and the difference between Thermal conductivities in the case were The Weidermann-Franz Law respected (WFR), and were The Weidermann-Franz Law violated (WFV) (Right panel) ,for the mixture:*

${}^{40}_{20}Ca$, ${}^{41}_{20}Ca$, ${}^{42}_{20}Ca$, ${}^{43}_{20}Ca$, ${}^{44}_{20}Ca$, ${}^{45}_{20}Ca$, ${}^{46}_{20}Ca$, ${}^{47}_{20}Ca$, ${}^{48}_{20}Ca$, $X_j = \frac{1}{10}, j = 1..10$ *at* $T = 10^7 K$.

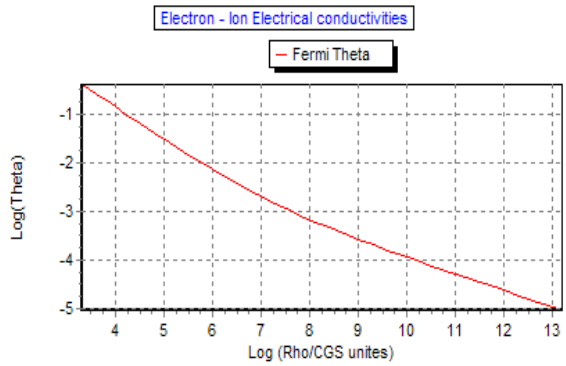

Figure 4.23d *: the Fermi temperature VS the total mass density in the logarithmic scale ,for the mixture* ${}^{40}_{20}Ca$, ${}^{41}_{20}Ca$, ${}^{42}_{20}Ca$, ${}^{43}_{20}Ca$, ${}^{44}_{20}Ca$, ${}^{45}_{20}Ca$, ${}^{46}_{20}Ca$, ${}^{47}_{20}Ca$, ${}^{48}_{20}Ca$, $X_j = \frac{1}{10}, j = 1..10$ *at* $T = 10^7 K$.

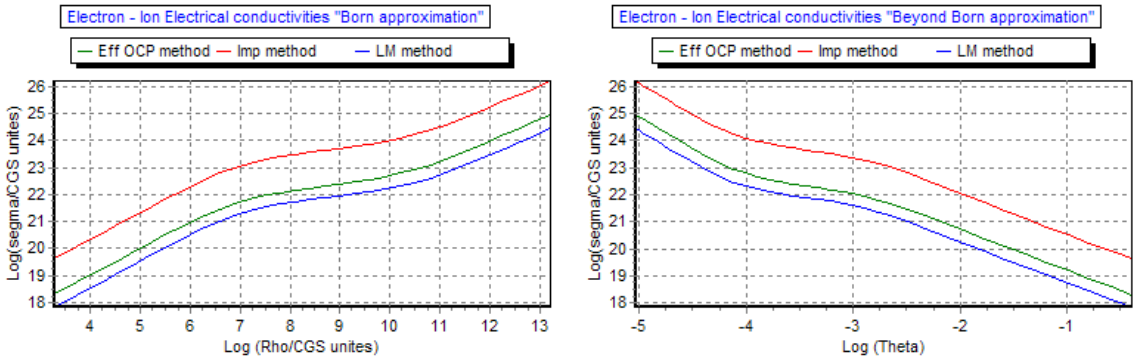

Figure 4.24a : *Electron ion electrical conductivities in the Born approximation (Left panel) and beyond Born approximation (Right panel) , we show different method of computation :Effective OCP method (Green line) ,Impurities method(Red line) , Linear mixing method (Blue line), for 89 elements from the hydrogen to the iron at fixed mass density ratio at* $T = 10^7 K$.

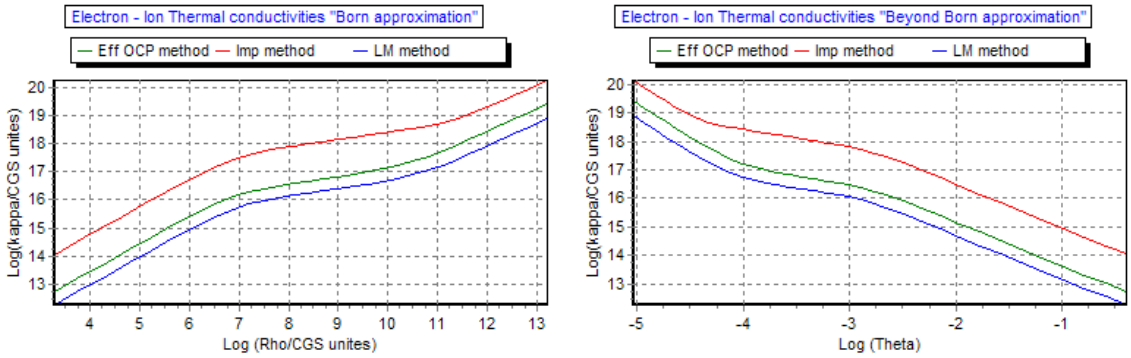

Figure 4.24b : *Electron ion thermal conductivities in the Born approximation (Left panel) and beyond Born approximation (Right panel) , we show different method of computation :Effective OCP method (Green line) ,Impurities method(Red line) , Linear mixing method (Blue line) , for 89 elements from the hydrogen to the iron at fixed mass density ratio at* $T = 10^7 K$.

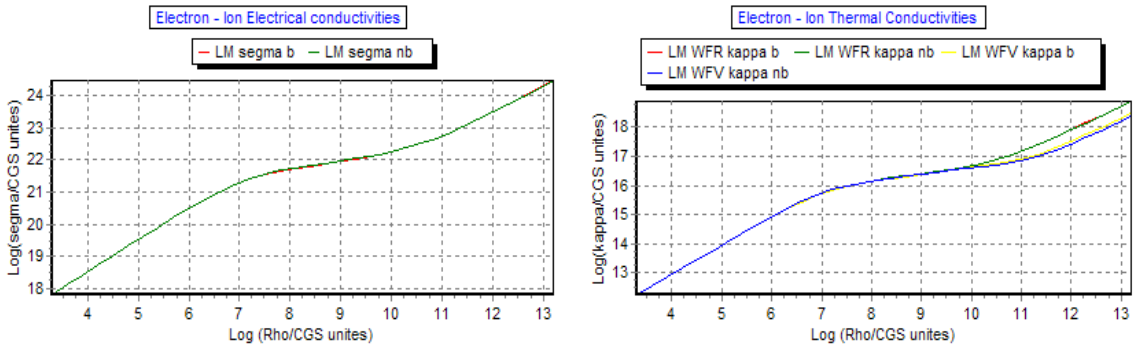

Figure 4.24c : *Electron ion electrical conductivities in the Born and beyond Born approximations (Left panel), and the difference between Thermal conductivities in the case were The Weidermann-Franz Law respected (WFR), and were The Weidermann-Franz Law violated (WFV) (Right panel) , for 89 elements from the hydrogen to the iron at fixed mass density ratio at* $T = 10^7 K$.

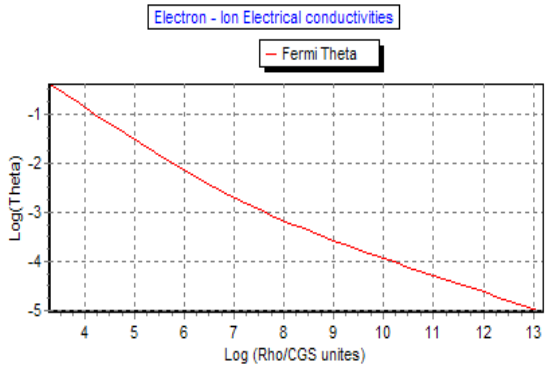

Figure 4.24d *: the Fermi temperature VS the total mass density in the logarithmic scale , for 89 elements from the hydrogen to the iron at fixed mass density ratio at* $T = 10^7 K$.

IV.5. 2. Discussion

a) Figures. (4.5 to 4.14) and (4.15 to 4.24) Type 'a' and 'b'

In the figures (4.5 to 4.14) we show the dependence of the Electrical conductivity and thermal conductivity due to electron-ion scattering on temperature in fully ionized plasma mixtures of different elements at different densities and mass densities ratios , and In the figures (4.15 to 4.24) we show the dependence of the Electrical conductivity and thermal conductivity due to electron-ion scattering on the total mass density in fully ionized plasma mixtures of different elements at different temperature and mass densities ratios , we find that the points of view used to compute kinetic coefficient are approximately the same as it already expected in [Pot 99a], but this is true in the case were the impurity parameter is small as it was mentioned by Daligault & Grupta [Dal 09](see green circles) , the fundamental difference between the two approach that in the Ioffe model we don't need the knowledge of the point of melting which give us a great advantage of unification between liquid and solid states , which is the major results of Baiko's et al work [Bai 98] : The Modification of the structural factors improves the calculation of the conductivities in liquid and in the solid phase, and virtually eliminates the jumps for the different chemical elements in a wide range of density in the OCP case and then The modified structural factor is physically accepted for [Bai 98] , but Itoh et al [Ito 93] Suggest that in the field of condensed matter physics, however, the correctness of the original Ziman [Zim 61] method with the use of the full liquid structure factor has long been established (Ashcroft and Lekner [Ash 66]; Rosenfeld and Stott [Ros 90]). Part of the motivation for the introduction of the suggestion in [Bai 98]

appears to be the finding by Itoh et al [Ito 93] that the conductivity of astrophysical dense matter typically increases by $2-4$ times upon crystallization. Regarding this finding, one should note that simple metals in the laboratory show similar phenomena. The electrical conductivity of the simple metals in the laboratory shows significant ($2-4$ times) jumps upon crystallization (Iida and Guthrie [Lid 1993]). For these reasons they follow the method in which they used the full liquid structure factor, which is in accord with the method used in condensed matter physics (Ashcroft and Lekner [Ash 1966];Rosenfeld and Stott [Ros 90]).

Interestingly, for the multi-component systems found in the crusts of accreting neutron stars, the jump may be much less important than suggested by the calculations of Itoh et al. [Ito 93]. However in our work we don't treat the problem of the physical meaning : if this is likely due to the reason proposed by Baiko et al [Bai 98], or because of the lack of long-range order for those complex mixtures and the high degree of impurity-like disorder that those systems possess as suggested by J. Daligault and S. Gupta [Dal 09] .

b) Figures. (4.5 to 4.24) Type 'c'

Figures (4.5 to 4.14) shows the dependence of the Electrical conductivity in the Born and beyond Born approximations due to electron-ion scattering in fully ionized plasma mixtures of different elements at different densities and mass densities ratios (left panels) and and the difference between Thermal conductivities in the case were The Weidermann-Franz Law respected (WFR) on temperature , and were The Weidermann-Franz Law violated (WFV) (Right panel).and Figures (4.15 to 4.24) the same but the dependence was in the total mass density at different temperature and mass densities ratios For comparison, and numerical results does not differ from previous works that we discuss in chapter 3.

c) **Figures. (4.5 to 4.24) Type 'd'**

Show the dependence of the Fermi temperature on the temperature or on the total density , we see that the approximation of strongly degenerate electrons break down practically when $\theta > 10^{-3}$, red circles gives us those situations , the theoretical treatment of the problem will be discuss in the next chapter.

IV.6. Scattering of strongly degenerate Electron by electrons

Now we like to add the electron-electron scattering effects for multi-components plasma systems as we explained in §IV.3, for that we will simulate the electron-electron (ee) and the total (ee+ei) thermal conductivity against the temperature for different elements, we will use a MATLAB codes to make the simulated figures, and in all our work we consider the relative mass density for each specie as a fixed quantity.

IV.6. 1. Results

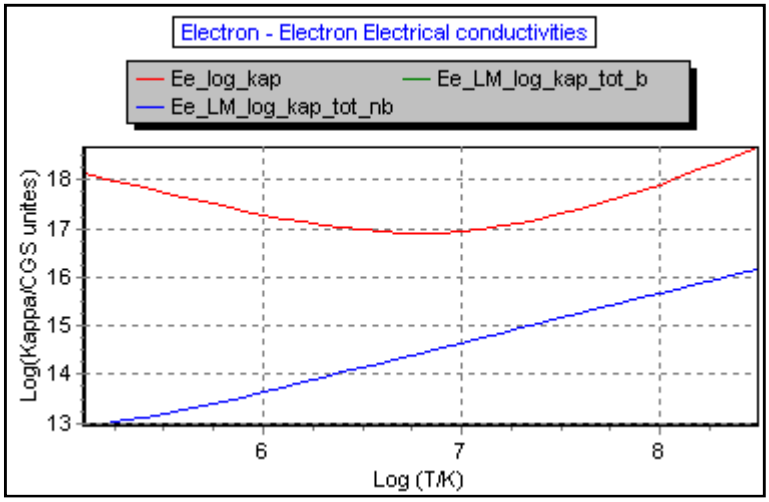

Figure 4.25 *: Electron electron thermal conductivity Vs Temperature (Red line)and the total (ei+ee) in the non-Born approximation beyond thermal conductivity (Blue line), for the* $^{1}_{1}H$ *with* $\rho_1 = 10^4 g/cm^3$.

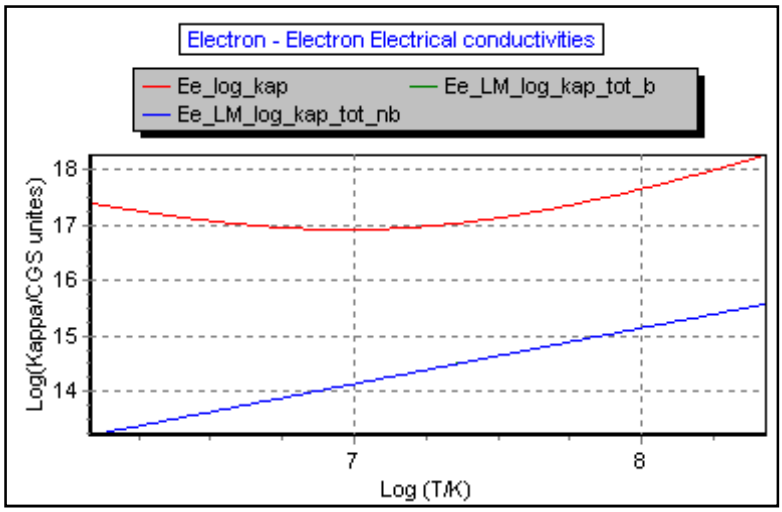

Figure 4.26 *: Electron electron thermal conductivity Vs Temperature (Red line)and the total (ei+ee)in the non-Born approximation beyond thermal conductivity (Blue line), for the mixture* $^{1}_{1}H$, $^{12}_{6}C$, $^{16}_{8}O$, $^{56}_{26}Fe$ *with* $\rho_j = 10^3 g/cm^3$.

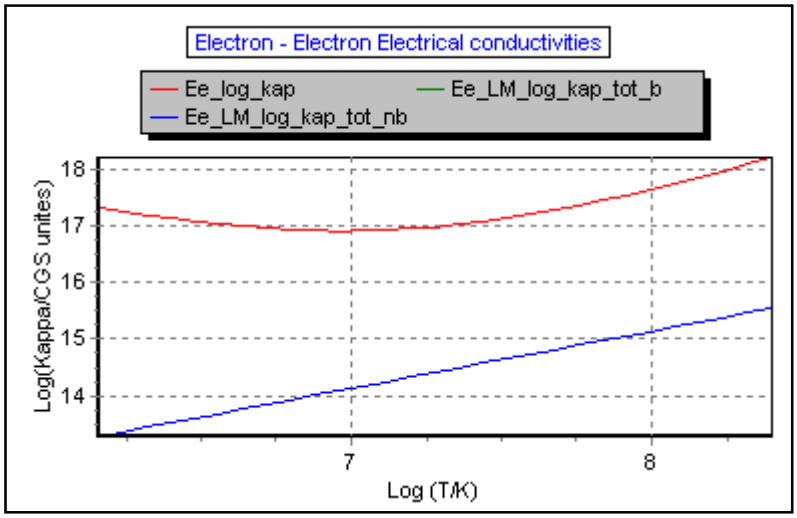

Figure 4.27 *: Electron electron thermal conductivity Vs Temperature(Red line)and the total (ei+ee)in the non-Born approximation beyond thermal conductivity (Blue line), , for 89 elements from the hydrogen to the iron at fixed mass density ratio.*

IV.6. 2. Discussion

Figures (4.25 to 4.27) shows the dependence of the thermal conductivity on the temperature : the Electron electron thermal conductivity (Red line) and the total (ei+ee)in the non-Born approximation beyond thermal conductivity (Blue line). As one can expect no thing new differ from old studies eg [Pot 99b] since one does not need to know from which atom come the electrons and as a result the electron-electron scattering influence be considerable at light values of Z_{eff} and sufficient high temperature.

CHAPTER V

Viscosity coefficients and thermal and magnetic effects

A- Theoretical contribution

V.1. Viscosity

V.1.1. On the theory of viscosity

We take on consideration the viscosity of the crust in this paragraph, the crust may be in a liquid or a solid phase. For strongly coupled ($\Gamma \gg 1$) and solid plasma the transport is assured principally by the electrons. We will consider only this case, and by the power of the ioffe model computations may be generalized to the liquid plasma case. For the solid crust, we suppose that we have a polycrystal structure therefore that on a macroscopic scale the crust acts as an isotropic medium.

Let us symbolize a stationary macroscopic hydrodynamic velocity field, on the plasma, by $\vec{V}(\vec{r})$. The viscous part of the stress tensor in the isotropic medium given by:

$$\Pi_{ij}^{vis} = \eta\left(\frac{\partial V_i}{\partial x_j} + \frac{\partial V_j}{\partial x_i} - \frac{2}{3}\delta_{ij}\vec{\nabla}\cdot\vec{V}\right) + \zeta\delta_{ij}\vec{\nabla}\cdot\vec{V} \qquad (5.1).$$

Where ζ , η are the bulk and the the shear viscosity respectivly. Thouse component of the stress tensor come into the equations of neutron star hydrodynamics and are related to the pulsations of the neutron stars.

First, let us take on consideration the conservative flows, described by$\vec{\nabla}\cdot\vec{V}=\vec{0}$. The figure (5.1) shows us a schematic representation of characteristic of torsional oscillations of the crust flow in the solid crust.

The shear viscosity η produces the dissipation resulting in the entropy production. In the outer crust, η is a summation of the electrons and ions contributions, $\eta_e+\eta_i$, however for $\rho>10^5 g/cm^3$ η_e become much larger than η_i and $\eta\approx\eta_e$.In the inner crust, the dripped neutrons contribution should be took on consederation and it must be added.

The electrons are scattered on ions, on impurity nuclei, and on electrons themselves, therefore the total frequency of the collision is specified by the summation $\nu_e=\nu_{ei}^{\eta}+\nu_{e\,imp}^{\eta}+\nu_{ee}^{\eta}$. but, as long as the temperature is not too low, the approximation $\nu_e\approx\nu_{ei}$ is statisfory.

To compute η_e from the Boltzmann equation for electrons, one must to find out $\delta f=f-f^{(0)}$ due to the presence of a weak plasma velocity field, $\vec{V}$. linearizing in $\vec{V}$ and in δf, The solution of the Boltzmann equation, take the form:

$$\boldsymbol{\delta f=A_{\eta}(\epsilon)\left[\vec{v}\cdot\vec{\nabla}\left(\vec{p}\cdot\vec{V}\right)\right]\frac{\partial f^{(0)}}{\partial\epsilon}} \qquad (\mathbf{5.2}).$$

Where $A_\eta(\epsilon)$ is a function to be founded from the Boltzmann equation. For strongly degenerate electrons and in the relaxation time approximation $A_\eta=\tau_{ei}^{\eta}=1/\nu_{ei}^{\eta}$ is the effective relaxation time appropriate for ei scattering, evaluated at the electronic Fermi surface.

The collision frequency ν_{ei}^{η}, can be written in terms of the effective Coulomb logarithm Λ_{ei}^{η} by :

$$\boldsymbol{\nu_{ei}^{\eta}=12\pi\frac{Z^2e^4n_{ion}}{p_F^2v_F}\Lambda_{ei}^{\eta}} \qquad (\mathbf{5.3}).$$

on obtain the electron viscosity using a standard formula:

$$\boldsymbol{\eta_e=\frac{n_ep_Fv_F}{5\nu_{ei}^{\eta}}} \qquad (\mathbf{5.4}).$$

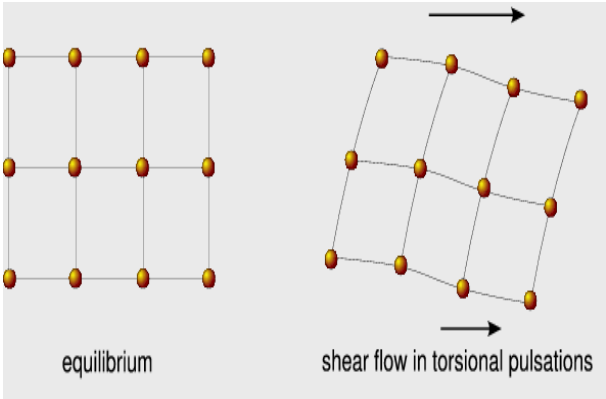

Figure (5.1): *representation of torsional oscillations in neutron star crust. Left: equilibrium arrangement of the crust, as a two-dimensional square lattice. Right: shear flow in the crust [Hae 08].*

The effective Coulomb logarithm for the electron viscosity is given by [Bai 98]:

$$\left(\Lambda_{ei}^{\eta}\right)_{PL} = 3\int_{q_{BZ}}^{2k_F} q^3 \left|\phi_q^{eff}\right|^2_{PL,\sigma}\left[1-\frac{v_F^2}{c^2}\left(\frac{q}{2k_F}\right)^2\right]\left[1-\frac{1}{4}\left(\frac{\hbar q}{m_e^* c^2}\right)^2\right]dq \qquad (5.5).$$

Then we see obviously that we can write it in the form

$$\left(\Lambda_{ei}^{\eta}\right)_{PL} = 3\left[\left(\Lambda_1^{\eta}\right)_{PL} - \left(\frac{v_F^2}{c^2}\right)\left(\Lambda_2^{\eta}\right)_{PL}\right] G_\sigma D \qquad (5.6).$$

Where $\Lambda_1^{\eta}, \Lambda_2^{\eta}$; defined as :

$$\left(\Lambda_1^{\eta}\right)_{PL} = \int_{q_0}^{2k_F} q^3 \frac{1}{(q^2+q_s^2)^2}\left[1-e^{-s_0 q^2}\right]\left[1-\frac{1}{4}\left(\frac{\hbar q}{m_e^* c^2}\right)^2\right]dq = (\Lambda_1)_{PL} - \Delta(\Lambda_1)_{PL} (5.7).$$

$$\Lambda_2^{\eta} = \int_{q_0}^{2k_F} q^3 \frac{1}{(q^2+q_s^2)^2}\left[1-e^{-s_0 q^2}\right]\left(\frac{q}{2k_F}\right)^2\left[1-\frac{1}{4}\left(\frac{\hbar q}{m_e^* c^2}\right)^2\right]dq = (\Lambda_2)_{PL} - \Delta(\Lambda_2)_{PL} \quad (5.8).$$

Where :

$$\Delta(\Lambda_1)_{PL} = \frac{1}{4}\int_{q_0}^{2k_F} q^3 \frac{1}{(q^2+q_s^2)^2}\left[1-e^{-s_0 q^2}\right]\left(\frac{\hbar q}{m_e^* c^2}\right)^2 dq \quad (5.9).$$

$$\Delta(\Lambda_2)_{PL} = \frac{1}{4}\int_{q_0}^{2k_F} q^3 \frac{1}{(q^2+q_s^2)^2}\left[1-e^{-s_0 q^2}\right]\left(\frac{q}{2k_F}\right)^2\left(\frac{\hbar q}{m_e^* c^2}\right)^2 dq \quad (5.10).$$

We like to call $\Delta\Lambda_1, \Delta\Lambda_2$ correctives terms of the viscosity Coulomb logarithm.

V.1.2. Determination of the correctives terms

Thus by integrating (5.9),(5.10 we have:

$$\begin{aligned}
2\Delta(\Lambda_1)_{PL} = {} & \frac{1}{12(1+s)s_0^3}\left(\frac{\hbar}{m_e^* c^2}\right)^2 \times \\
& \times (w^3(1+2s(-1+3s+6s^2)) - 24s^3(1+s)\mathbf{ArcCoth}[1+2s]) - \\
& -3e^{-w}(-2+2e^w-2s+2e^w s-2w-2e^w sw+2s^2 w - \\
& -2e^w s^2 w - w^2 + sw^2 - s^2 w^2 + 3e^w s^2 w^2 - \\
& -3s^3 w^2 + 3e^w s^3 w^2 + e^w s^3 w^3 - s^4 w^3 + e^w s^4 w^3 - \\
& -e^{w+sw} s^3 (1+s) w^3 (4+sw)\mathbf{E_1}[sw] + \\
& +e^{w+sw} s^3 (1+s) w^3 (4+sw)\mathbf{E_1}[(1+s)w] \quad (5.11).
\end{aligned}$$

$$2\Delta(\Lambda_2)_{PL} = \frac{1}{48(1+s)s_0^5}\left(\frac{\hbar}{m_e^* c^2}\right)^2 w \times$$

$$\times \left(w^4\left(3-5s\left(1+2s(-1+3s+6s^2)\right)\right)+ +120s^4(1+s)\coth^{-1}[1+2s]\right.$$

$$+12e^{-w}\,(6-6e^w+6s-6e^w s+6w+2sw+$$

$$+4e^w sw-4s^2 w+4e^w s^2 w)$$

$$+3w^2-sw^2-s^2w^2-3e^w s^2 w^2+3s^3 w^2-3e^w s^3 w^2+w^3+$$

$$-sw^3+s^2w^3-s^3w^3+4e^w s^3 w^3-4s^4 w^3+$$

$$+4e^w s^4 w^3+e^w s^4 w^4-s^5 w^4+e^w s^5 w^4+$$

$$-e^{w+sw}s^4(1+s)w^4(5+sw)E_1[sw]+$$

$$+e^{w+sw}s^4(1+s)w^4(5+sw)E_1[(1+s)w])$$

(5.12)

As one may expect we can compute the analogue coulomb logarithms for other king of form factors, but we will not go further to discuss the viscosity phenomena.

V.2. Thermal and magnetic effects on kinetic coefficients

In this section we shall study thermal effects of nonzero temperature on the neutron star's plasma, using a simple physical picture leads to an appropriate interpolation formula.

V.1.1. Problema One " magnetic fields"

Properties of shells changed consederaly by strong magnetic fields that's in the order of $\sim 10^{12}$G for pulstars and higher for magnetostars, the atomic magnetic field is given B_0 by:

$$B_0 = \frac{m_e^2 e^3 c}{\hbar^3} = 2.35 \times 10^9 G \qquad (5.19).$$

It is the value of B for which the electron cyclotron energy is identical to $e^2/a_0 = 2 \times 13.6\,\text{eV}$ (where a_0 is the Bohr radius). setting it differently, at $B = B_0$ the characteristic magnetic length $a_m = (\hbar c/eB)^{1/2}$ equals the Bohr radius. For usual pulsars and magnetars the surface magnetic field is considerably stronger than B_0. As a result, the atomic structure at low pressure is estimated to be changed radicaly. The electrons motion perpendiculy to B is quantized into Landau levels.

If one consider only the z component of the magnetic field ie $\vec{B} = [0, 0, B]$, the electron energy levels are specified by the relation $\epsilon_n(p_z) = c(m_e c^2 + 2\hbar\omega_c m_e n + p_z^2)^{1/2}$, where p_z the $z-$component of the electron momentum and n is the Landau quantum number.

The ground state of the Landau's level $n = 0$ is nondegenerate with respect to the spin (the spin and B are antiparallel, with spin projection $s = -1$), but the upper levels $n > 0$ are degenerate two times ($s = \pm 1$). The cyclotron frequency for electrons is given $\omega_c = \frac{eB}{m_e c}$; and it is 1836 times bigger than its values for protons. The Coulomb binding energy of electrons in the nucleus is considerably less effective along B, while in the plane perpendicular to B the electron motion is restricted to the $n = 0$ Landau level. so atoms get a cylindrical form and can form linear chains along B.

A phase transition into a "magnetically condensed" phase can be made by this attraction between these chains is (eg [Med 08]).

We now in a few words examine the effects of the magnetic field on plasma properties at finite pressure $P > 0$. The magnetic field strongly quantizes the motion of electrons, if it confines most of them to the ground Landau state $n = 0$. The parameters related to a strong quantization regime are :

$$\boldsymbol{T_{ce} = \frac{\hbar\omega_c}{k_B} \approx 1.343 \times B_{12}K\,,\rho_B = \frac{m_{ion}n_B}{Z} \approx \frac{7045\left(\frac{A}{Z}\right)B_{12}^{\frac{3}{2}}g}{cm^3}} \quad (5.20).$$

And

$$\boldsymbol{T_B = \begin{cases} T_{ce} & if\ \ \rho < \rho_B \\ \frac{T_{ce}}{\gamma_r} & if\ \ \rho > \rho_B \end{cases}} \quad (5.21).$$

The field B is said to be strongly quantizing if $\rho < \rho_B$ and $T \ll T_{ce}$. On the contrary, a magnetic field will be weakly quantizing if many Landau orbitals are occupied, but still $T \ll T_B$. to end with, B is said to be nonquantizing if $T \gg T_B$. The temperature T_B and density ρ_B are shown in Figure 5.2.

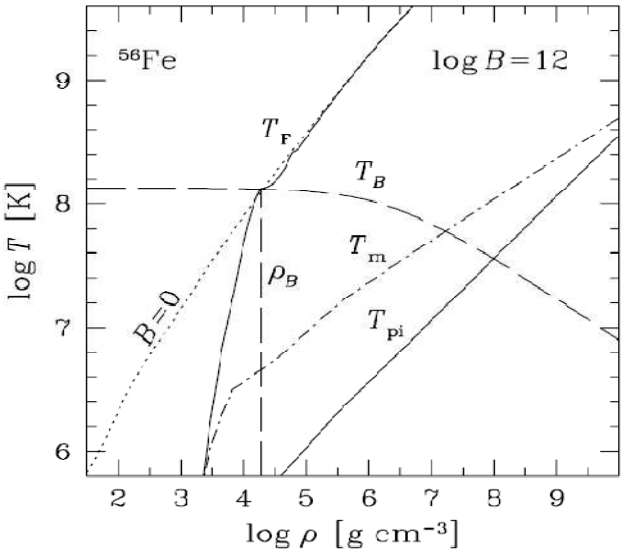

Figure 5.2: *Different domains in the $\rho - T$ plane for ^{56}Fe with magnetic field B = 10^{12} G.Dash-dot line: melting temperature T_m. Solid lines: T_F – Fermi temperature for the electrons; T_{pi} – ion plasma temperature. Long-dash lines: T_B and ρ_B appropriate for the quantized regime of the electrons; for comparison we also show, by dotted lines, TF, Tm and Tpi for B = 0. For further explanation see the text. From [Hae 06].*

We say that a surface magnetic field to be strong if $B \ll 10^9 G$. Such magnetic fields change the accretion of plasma in the neutron star and change the main properties of atoms in the atmosphere.

On the opposite, a magnetic field in the range $B \lesssim 10^9 G$, such as related to most X-ray bursters or with millisecond pulsars, is taken to be weak. almost pulsars are magnetized neutron stars, with the value of B near the magnetic pole $B \sim 10^{12} G$. Much higher magnetic fields are typical for magnetars, $B \sim 10^{14} - 10^{15} G$; such magnetic fields with $B \gtrsim 10^{14}$ are often called "super-strong". These magnetic fields can strongly affect transport processes in neutron star shelles. Electron transport coeffitions in magnetized neutron star crusts are reviewed in [Pot 99b]. In this section we only show to a very short indications.

A magnetic field is regard as uniform, locally. We take the z axis of a coordinate system along B, ie $\vec{B} = [0, 0, B]$. We examine only the strongly degenerate electrons case and we suppose that the relaxation time approximation is valid. Let relaxation time for $B = 0$ be τ_0. The electron gyromagnetic frequency is a central timescale related with magnetic fields:

$$\boldsymbol{\omega_B = \frac{eB}{m_e^* c}} \qquad (\mathbf{5.22}).$$

The electron trajectories in the plane (x,y) are bended magnetic field, and restraines the electron transport across B. as a result, the transport properties will be anisotropic, and one must take tensors σ_{ij} and κ_{ij}, in consideration which can be written as:

$$\boldsymbol{\sigma = \frac{n_e e^2}{m_e^*} \xi_{ij}^{\sigma}} \qquad (\mathbf{5.23}).$$

$$\boldsymbol{\kappa = \frac{\pi^2 k_B^2 T n_e}{3 m_e^*} \xi_{ij}^{\kappa}} \qquad (\mathbf{5.24}).$$

In what follows we will have three basic regimes of transport in magnetic fields.

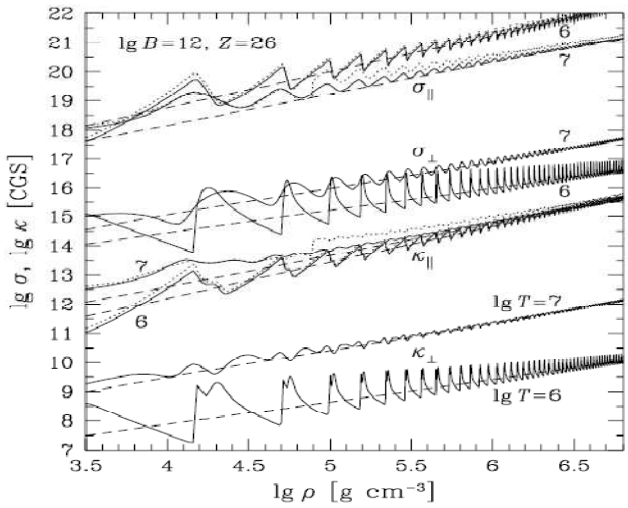

Figure 5.3 T*ransport coefitions: longitudinal (∥) and transverse (⊥)in the outer envelope composed of* Fe^{56} *for* $B = 10^{12}G$ *and* $log\,T\,[K] = 6,7$. *Quantum calculations (solid lines) are compared with classical ones (dash lines). Vertical bars: liquid-solid transition at* $T = 10^7\ K$. *Based on Figure 5 from [Pot 99b].*

V.2.1.a. Nonquantizing magnetic fields

A lot of Landau levels are occupied, and because $k_B T > \hbar\omega_c$ the quantum effects are smeared by thermal effects. The magnetic field B does not affect the transport properties along the magnetic field, while the Hall magnetization parameters $\omega_B\tau_0^{\sigma,\kappa}$ characterises totaly the transport across B :

$$\boldsymbol{\omega_B\tau_0^{\sigma,\kappa} = 1760\frac{B_{12}}{\gamma_r}\frac{\tau_0^{\sigma,\kappa}}{10^{-16}s}} \qquad (\mathbf{5.25}).$$

where $\tau_0^{\sigma,\kappa}$ are the effective relaxation times at B = 0 for the transport coeffitions. The nonzero components of the $\xi_{ij}^{\sigma,\kappa}$ tensors are:

$$\xi_{zz}^{\sigma,\kappa} = \tau_0^{\sigma,\kappa}, \xi_{xx}^{\sigma,\kappa} = \xi_{yy}^{\sigma,\kappa} = \frac{\tau_0^{\sigma,\kappa}}{1 + \left(\omega_B \tau_0^{\sigma,\kappa}\right)^2}, \xi_{xy}^{\sigma,\kappa} = \xi_{xy}^{\sigma,\kappa} = \frac{\left(\omega_B \tau_0^{\sigma,\kappa}\right)^2}{1 + \left(\omega_B \tau_0^{\sigma,\kappa}\right)^2} \qquad (5.26).$$

V.2.1.b. Weakly-quantizing magnetic fields

Electrons occupe a lot of Landau orbitals, however because $k_B T < \hbar\omega_c$ the quantization effects are well pronounced. There are two relaxation times, $\tau_{\parallel}^{\sigma,\kappa}$, and $\tau_{\perp}^{\sigma,\kappa}$, which oscillate with with respect to the density. As shown by Potekhin [Pot 99b], the nonzero tensors components $\xi_{ij}^{\sigma,\kappa}$ are specified by a equations similar to the precedent one:

$$\xi_{zz}^{\sigma,\kappa} = \tau_0^{\sigma,\kappa}, \xi_{xx}^{\sigma,\kappa} = \xi_{yy}^{\sigma,\kappa} = \frac{\tau_0^{\sigma,\kappa}}{1 + \left(\omega_B \tau_0^{\sigma,\kappa}\right)^2}, \xi_{xy}^{\sigma,\kappa} = \xi_{xy}^{\sigma,\kappa} = \frac{\left(\omega_B \tau_0^{\sigma,\kappa}\right)^2}{1 + \left(\omega_B \tau_0^{\sigma,\kappa}\right)^2} \qquad (5.27).$$

The density dependence of the components of the transport coeffitions exhibits characteristic oscillations around the nonquantized (classical) values , if the temperature is constant and in the presence of a weakly quantizing B. every oscillation represents to the filling of a new Landau orbitale. The amplitude of these oscillations diminishs with decreasing of the mass density.

As we see in Figure 5.3, the oscillation amplitude increase with decreasing T ,the “density period” of oscillation decreases with increasing ρ, and the. At $T = 10^7$K, a magnetic field of 10^{12}G consider to be weakly quantizing at $\rho > 10^{4.2}\,\mathrm{g\,cm^{-3}}$.

V.2.1.c. Strongly-quantizing magnetic fields

If $k_B T < \hbar\omega_c$, and the majority of the electrons are occuping the ground Landau orbital. the σ_{ij} and κ_{ij} and their density dependence are significantly different from those of the nonquantizing one.

In [Pot 99b], the formulae for $\tau_{\parallel}^{\sigma,\kappa}$ and $\tau_{\perp}^{\sigma,\kappa}$ are governed by equations (5.27). the fitting formulae for $\tau_{\parallel}^{\sigma,\kappa}$ and $\tau_{\perp}^{\sigma,\kappa}$ are derived in [Pot 99b], which we will use it in our work.

the Figure 5.3,show us that at $T = 10^6$K a field of 10^{12}G is strongly quantizing for $\rho > 10^{4.2}\,\mathrm{g\,cm^{-3}}$.

V.1.2. Problema Two: " partially degenerate electrons"

The strongly degenerate electron approximation (3.36) break down when the temperature become comparable to the Fermi temperature. The figues 5.4, 5.5 illustrate the situation:

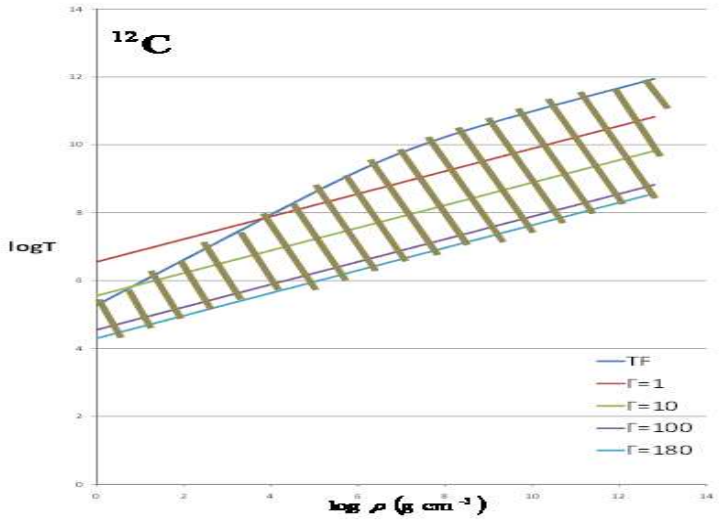

Figure 5.4*: T Vs ρ graphs for the ^{12}C, the dashed region is the region where we should take quantum corrections.*

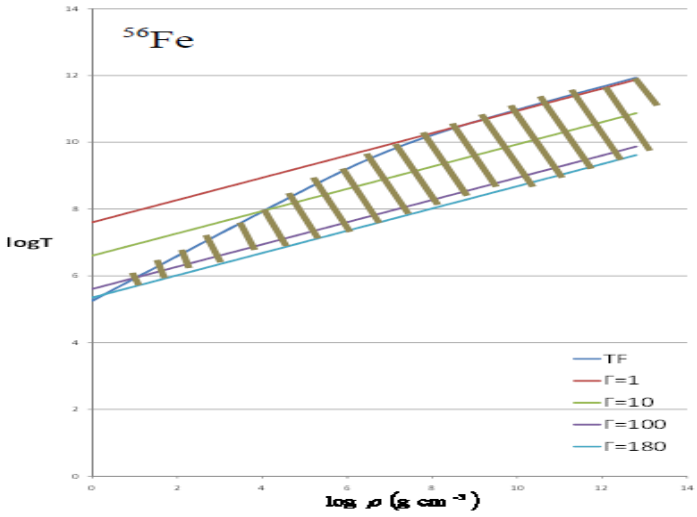

Figure 5.5: *same graphs for the ^{56}Fe (5.4).*

V.1.3. Interpolation formula:

We like to deal with partially degenerate case (ie when θ is not negligible against unite), by proposing an interpolation formulae in analogy with equation (3.87) , We replace the fitted Coulomb logarithm $\Lambda^{fit}_{\sigma,\kappa}$ equation (3.77) by an interpolation formulate, we can write the new fitted Coulomb logarithm in the form:

$$\boldsymbol{\Lambda^{Th}_{\sigma,\kappa} = \Lambda^{fit}_{\sigma,\kappa}(\epsilon_F)e^{-\theta} + \Lambda^{fit}_{\sigma,\kappa}(\epsilon_{Th})[1 - e^{-\theta}]} \qquad (\mathbf{5.28}).$$

Where $\Lambda^{Th}_{\sigma,\kappa}$ is the thermally corrected Coulomb logarithm, and ϵ_{Th}: play the role of thermally corrected energy to the non zero temperature case, then one can derive simply the corresponding parameters like $k^{Th}_{TF}, p_{Th}, v_{Th}$ which we need to compute $\Lambda^{fit}_{\sigma,\kappa}(\epsilon_{Th})$, and then $\Lambda^{Th}_{\sigma,\kappa}$.

The strongly degenerate electron approximation breakdown when the temperature become comparable to the Fermi temperature, in [Pot 10] one can compute the chemical potential at good at good accuracy –and in a simple way - using (1),(3),(6) in [Pot 10] , then we define ϵ_{Th} as:

$$\boldsymbol{\epsilon_{Th} = mc^2\tilde{\mu}} \qquad (\mathbf{5.29}).$$

B- Simulation

To study the effect of magnetic field on the MCP plasma for astrophysical conditions,by computing parall we need to define our parameters .

We consider only the effect on the strongly degenerate electrons , thus momentum levels is given by :

$$\boldsymbol{p_n(\epsilon_F) = \left[(\epsilon_F/c)^2 - (m_e c)^2 - 2m_e \hbar \omega_c n\right]^{1/2}} \qquad (\mathbf{5.28}).$$

For $n < n_{max}$, where n_{max} – is the maximum possible number of Landau levels for a given Fermi energy ϵ_F :

$$\boldsymbol{n_{max} = Int(v) = Int\left[\frac{1}{\hbar\omega_c}\frac{p_0^2(\epsilon_F)}{2m_e}\right]} \qquad (\mathbf{5.29}).$$

Note that υ is an energy parameter , and it should be clear that the Fermi energy in the presence of quantizing magnetic fields is given by (without the stress on the theory "for review see [Pot 99b]") the inversion of the equation :

$$\boldsymbol{n_e = \frac{1}{2\pi^2 a_m^2 \hbar}\sum_{n=0}^{n_{max}} g_n p_n(\epsilon_F)} \qquad \text{at fixed } n_e \qquad (\mathbf{5.30})$$

We proposed in our simulation an algorithm to deal with this non-standard numerical equation:

Initial conditions $\boldsymbol{\epsilon_F^{(0)} = m_e c^2, n_e^{(0)} = n_e(\epsilon_F^{(0)})}$

Iteration $\boldsymbol{\epsilon_F^{(i)} = \epsilon_F^{(i-1)} + i\frac{m_e c^2}{1000}}$

Repeat since $\boldsymbol{n_e^{(i)} < n_e}$

It is clear that our algorithm gives us a precision on the Fermi energy on the order of $\sim 10^{-13}$eV.

we need all that to compute relaxation times, $\tau_{\parallel}^{\sigma,\kappa}$, and $\tau_{\perp}^{\sigma,\kappa}$ from equation (5.27) and then to simulate the transport coeffitions against the mass

density of several elements at different temperatures, we compute those coefficients from the equation (3.34) , using a MATLAB codes to reach these objectives.

For multi component plasma we like to define the ion density number of the specie :

$$x_j = \frac{n_j}{n_{ion}} \qquad (5.30).$$

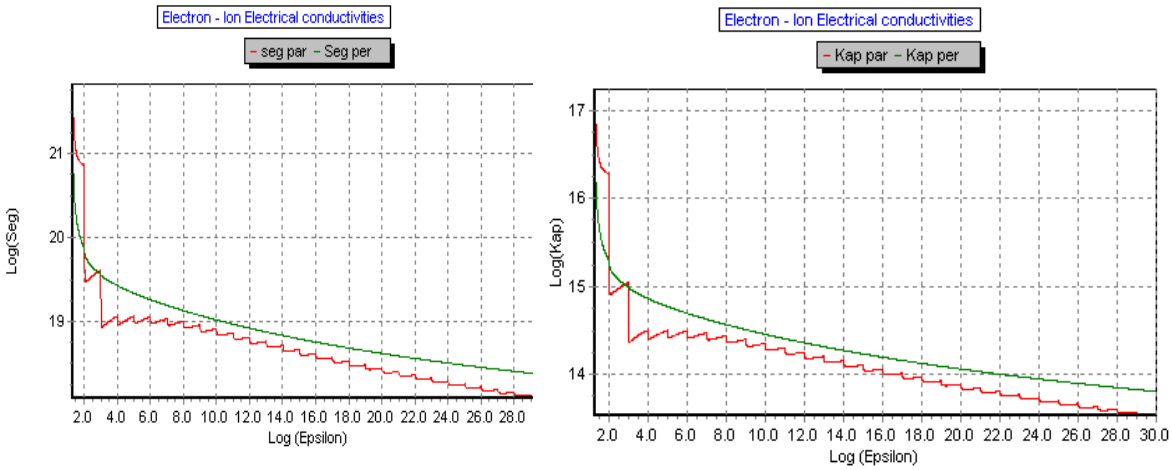

Figure 5.6 : *Electrical (Left panel) and Thermal (right panel) conductivities Vs the variable υ for* ${}_1^1H$ *at* $T = 10^8K$, *and* $B = 10^{13}G$.

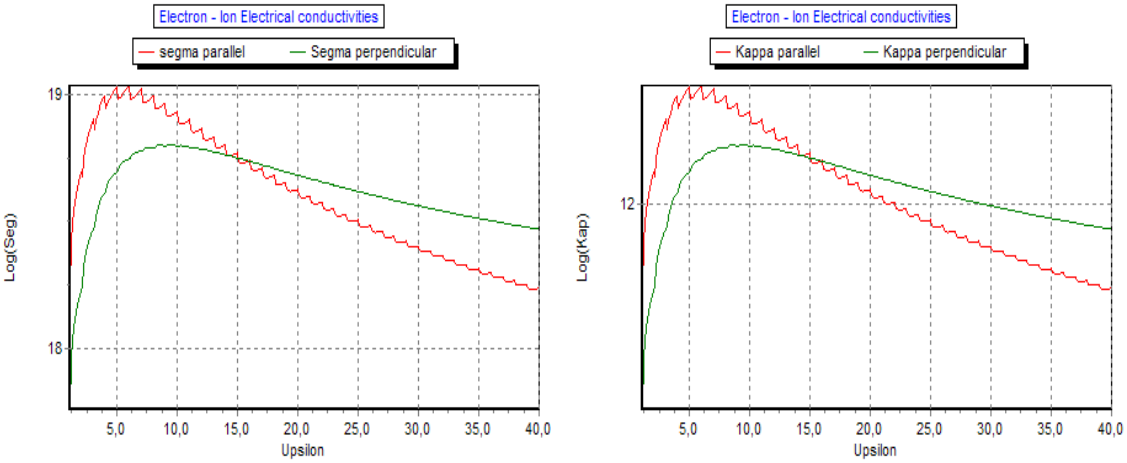

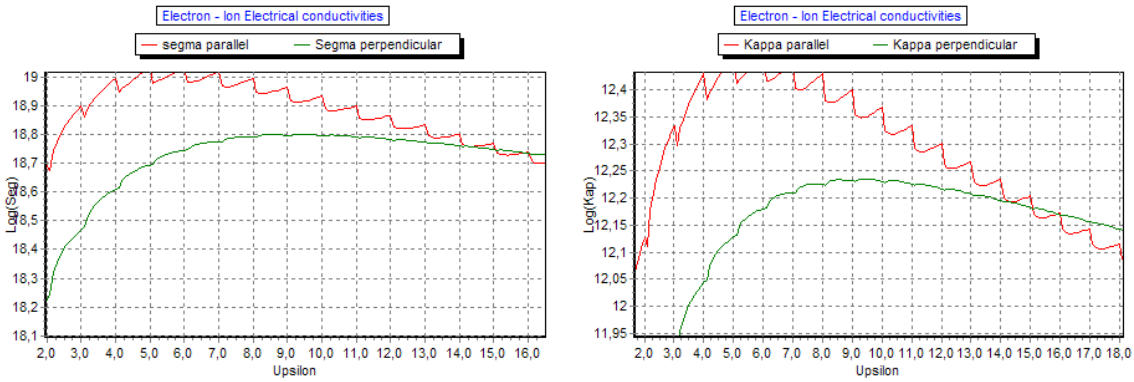

Figure 5.7 *: Electrical (Left panel) and Thermal (right panel) conductivities Vs the variable υ for the mixture* ${}_1^1H$ *with* $x_H = 4/5$, *and* ${}_2^4He$ *with* $x_{He} = \frac{1}{5}$*at* $T = 10^6 K$, *and* $B = 10^{12} G$

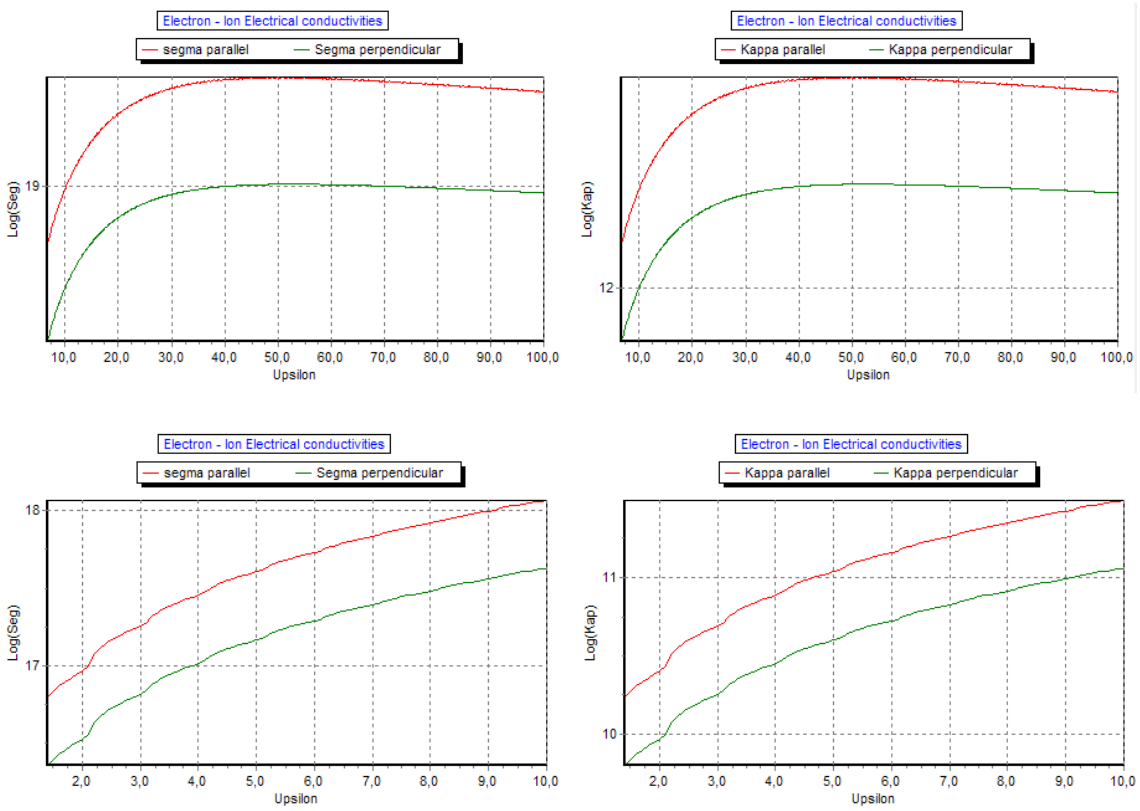

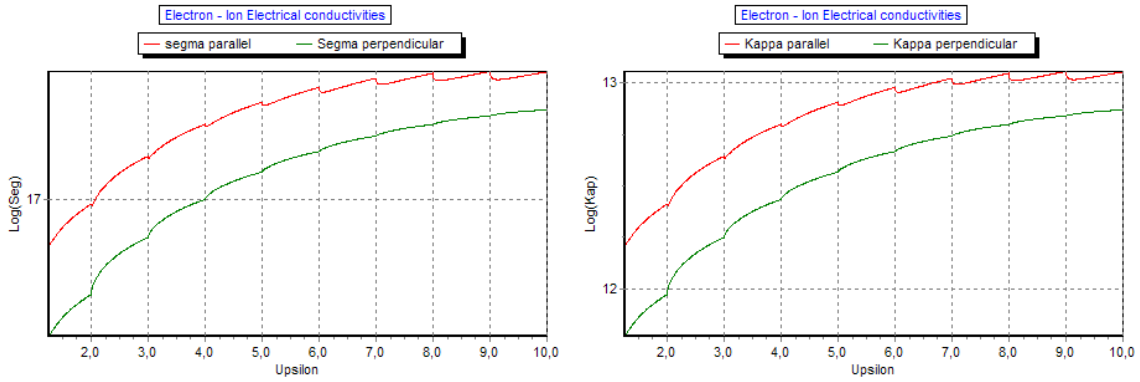

Figure 5.8 : *Electrical (Left panel) and Thermal (right panel) conductivities Vs the variable υ for the mixture* $^{52}_{25}Mn$ *with* $x_{Mn} = 1/2$, *and* $^{54}_{26}Fe$ *with* $x_{Fe} = 1/2$ *at* $T = 10^7 K$, *and* $B = 10^{13} G$

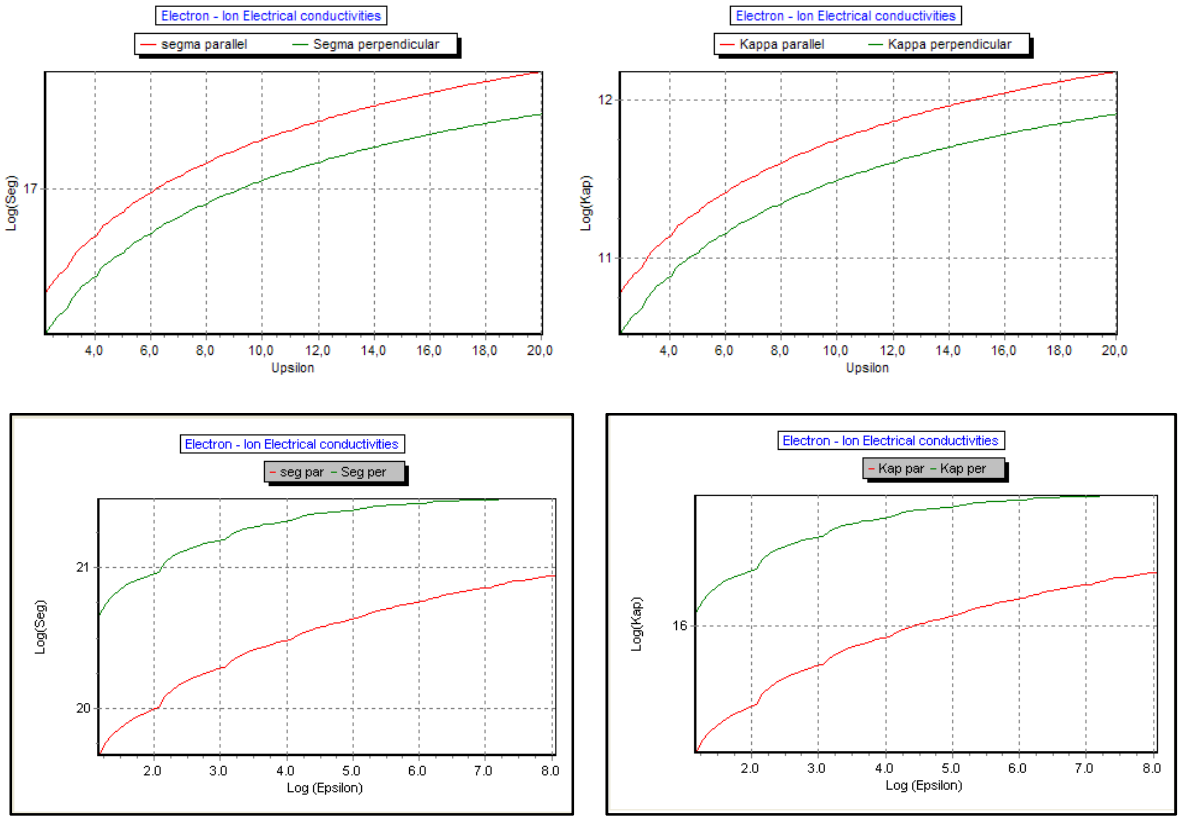

Figure 5.9 : *Electrical (Left panel) and Thermal (right panel) conductivities Vs the variable υ for the mixture* $^{3}_{2}He$ *with* $x_{He} - 1/2$, *and* $^{12}_{6}C$ *with* $x_C - 1/6$ *and* $^{16}_{8}O$ *with* $x_O - 1/6$, *and* $^{27}_{13}Al$ *with* $x_{Al} = 1/6$ *at* $T = 10^8 K$, *and* $B = 10^{13} G$

Figures. (5.6 to 5.9) shows the dependence of longitudinal and transverse conductivities on the energy parameter υ for different mixtures in a accreted neutron star envelope different values of T and B as shown in the figure.

Transverse components are non zero and are not negligible comparable to longitudinal one , which lead to a transversal transport of energy and momentum of electrons.

We see that one can get the Landau levels in the case of mixture by take a fixed ion density number for each specie in the mixture.

We don't get the second peak near each Landau threshold as the result made by A.potekhin et al [Pot 99b] (see figure 5.3) because we don't use the thermal averaging and we only take the zero temperature approximation.

We see also that the amplitude of oscillation increase with increasing magnetic field strength, decreasing with increasing mass density and number of elements.

Conclusion

In this work we present a comprehensive approach to the investigation of kinetic properties of the substance in the shells of neutron stars:

Study (1) thermodynamic functions of fully ionized plasma under conditions typical of the shells of neutron stars without magnetic field. (2) The study of the electrical and thermal conductivities using the Ioffe model for the scattering of strongly degenerate electrons by ions in a fully ionized plasma in the shells of neutron stars without magnetic field and in presence of strong magnetic field. (3) The study of the condensed matter and nuclear effects on kinetics.(4) The development basing of a software program to deal with Multi-components plasma transport coefficients including the effect of electron-electron scattering.(5)We use the Ioffe model and other physical effects to compute the shear viscosity coefficient in neutron stars curst's matter. (6) We discuss the thermal and magnetic effects lead to the break down of the strongly degenerate approximation, and we suggest an interpolation formula. .

Main results

In more detail, the main results of the thesis are as follows.

1. We calculated electronic thermal and electrical conductivity, in Coulomb liquids and Coulomb crystals in the Ocean, Outer and Inner crusts, including the effects of dipolar, Gaussian and homogenous sphere form factors, An analytical description of the transport coefficients in a strongly degenerate electrons. Created set of computer programs for the calculation of these coefficients.

2. We compute an analytical formula for the contribution of impurities basing on the Ioffe model, and we developed a simulation program to show and describe the comportment of the Multi-components plasma as we can find in accreted neutron stars.

3. We calculated also the shear viscosity coefficient , in Coulomb liquids and Coulomb crystals in the Ocean , Outer and Inner crusts, including the effects of dipolar , Gaussian and homogenous sphere form factors, An analytical description them in a strongly degenerate electrons. We created set of computer programs for the calculation of these coefficients.

4. We discuss and simulate the condition and the limiting cases of thermal and magnetic, especially the partially degenerate electrons case, and magnetic Landau levels, and we proposed an interpolation solution.

Bibliography

[Abe 59]: Abe R., 1959, "Giant cluster expansion theory and its application to high-temperature plasma," *Progr. Theor. Phys.* **22**, 213–226.

[Akh 65]: Akhiezer A.I., Berestetskii V.B., 1965, *Quantum Electrodynamics* (New York: Interscience).

[Abr 72]: Abramowitz M., Stegun I.A. (eds.), 1972, Handbook of Mathematical Functions, Dover, New York

[Bai 95] : D. A. Baiko, D. G. Yakovlev (1995). Thermal and electrical conductivities of Coulomb crystals in neutron stars and white dwarfs, *Astronomy Letters* **21**, 702.

[Bai 98]: Baiko D.A., Kaminker A.D., Potekhin A.Y., Yakovlev D.G.,'(1998) "Ion structure factors and electron transport in dense Coulomb plasmas," *Phys. Rev. Lett.*, 81, 5556-5559

[Bai 00]: Baiko D.A., Yakovlev D.G., DeWitt H.E., Slattery W.L., "Coulomb crystals in the harmonic lattice approximation," *Phys. Rev. E*, 61, 1912-1919 (2000).

[Bai 01]: Baiko D .A., Potekhin A. Y., Yakovlev D. G., "Thermodynamic functions of harmonic Coulomb crystals," *Phys. Rev. E*, 64, 057402 [4 pages] (2001).

[Bai 02]: Baiko D.A., "Effect of the electron gas polarizability on the specific heat of phonons in Coulomb crystals," *Phys. Rev. E*, 66, 056405 [10 pages] (2002).

[Bau 80]: Baus M., Hansen J.P., "Statistical mechanics of simple Coulomb systems," *Phys. Rep.*, 59, 1-94 (1980).

[Cas 07]: Cassisi, S., Potekhin, A.Y., Pietrinferni, A., Catelan., M., Salaris, M. 2007, ApJ, 661, 1094.

[Cep 80]: Ceperley D.M., Alder B.J., "Ground state of the electron gas by a stochastic method," *Phys. Rev. Lett.*, 45, 566-569 (1980).

[Cha 90a]: Chabrier G., Ashcroft N.W., "Linear mixing rule in screened binary ionic mixtures," Phys. Rev. A, 42, 2284-2291 (1990).

[Cha 90b]: Chabrier G., "An equation of state for fully ionized hydrogen," *J. Phys. (Paris) 51,* 1607-1632 (1990).

[Cha 02]: Chabrier G., Douchin F., Potekhin A.Y., "Dense astrophysical plasmas," J. Phys.: Condens. Matter 14, 9133-9139 (2002).

[Cha 09]: Chabrier G., Potekhin A.Y., 1998, "Equation of state of fully ionized electron-ion plasmas," Phys. Rev. E, 58, 4941-4949 (2009).

[Coh 69]: Cohen E.G.D., Murphy T.J., 1969, “New results in the theory of the classical electron gas,” Phys. Fluids 12, 1403–1411.

[Dal 09]: J. Daligault, S. Gupta ,2009 “Electron-ion scattering in dense multi-component plasmas: application to the outer crust of an accreting neutron star” http://arxiv.org/abs/0905.0027v2.

[Dog 56]: Doggett J.A., Spencer L.Y., "Elastic scattering of electrons and positrons by point nuclei," *Phys. Rev.*, 103, 1597-1601 (1956).

[Dou 01]: Douchin P., Haensel P., "A unified equation of state of dense matter and neutron star structure," Astron. Astrophys., 380, 151-167 (2001).

[Edw 62]: Edwards S.F., "The electronic structure of liquid metals," Proc. Roy. Soc. London A, 267, 518-540 (1962).

[Ewa 75]: Ewart G.M., Guyer R.A., Greenstein G., 1975, "Electrical conductivity and magnetic field decay in neutron stars," Astrophys. J., 202, 238-247.

[Far 93]: Farouki RT., Hamaguchi S., "Thermal energy of the crystalline one-component plasma from dynamical simulations," Phys. Rev. E, 47, 4330-4336 (1993).

[Flo 76]: Flowers E., Itoh N., "Transport properties of dense matter," Astrophys. J., 206, 218-242 (1976).

[Gal 76]: Galam S., Hansen J.P., "Statistical mechanics of dense ionized matter. VI. Electron screening corrections to the thermodynamic properties of the one-component plasma," Phys. Rev. A, 14, 816-832 (1976).

[Gne 01]: Gnedin O.Y., Yakovlev D.G., Potekhin A.Y., "Thermal relaxation in young neutron stars," Mon. Not. R. Astron. Soc., 324, 725-736 (2001).

[Hae 07]: Haensel P., Potekhin A. Y., Yakovlev D. G. Neutron Stars 1: Equation o! State and Structure. - New York: Springer, 2007.

[Ham 97]: Hamaguchi S., Farouki RT., Dubin D.H.E., "Triple point of Yukawa systems," Phys. Rev. E, 56, 4671-4682 (1997).

[Har 60]: Harris G.M., Roberts J.E., Trulio J.G., "Equilibrium properties of a partially ionized plasma," Phys. Rev., 119, 1832-1841 (1960).

[Han 77]: Hansen J.P., Torrie G.M., Vieillefosse P., "Statistical mechanics of dense ionized matter. VII. Equation of state and phase separation of ionic mixtures in a uniform background," Phys. Rev. A, 16, 2153-2168 (1977).

[Hir 54]: J. O. Hirschfelder, C. F. Curtiss, and R. B. Bird. Molecular theory of gases and liquids. Wiley, New York, 1954. xxvi + 1219 pp.,

[Hor 09]: Horowitz C.J., Caballero O.L., Berry D.K., "Thermal conductivity and phase separation of the crust of accreting neutron stars," *Phys. Rev. E,* **79,** 026103 [8 pages] (2009).

[Hub 66]: Hubbard W.B., "Studies in stellar evolution. V. Transport coefficients of degenerate stellar matter," Astrophys. J., 146, 858-870 (1966).

[Hub 69]: Hubbard W., Lampe M., "Thermal conduction by electrons in stellar matter," Astrophys. J. Suppl. Ser., 18, 297-346 (1969).

[Ich 87]: Ichimaru S., Iyetomi H., Tanaka S., "Statistical physics of dense plasmas: thermodynamics, transport coefficients and dynamic correlations," Phys. Rep., 149, 91-205 (1987).

[Ito 83]: Itoh N., Mitake S., Iyetomi H., Ichimaru S., "Electrical and thermal conductivities of dense matter in the liquid metal phase. I - High-temperature results," Astrophys. J., 273, 774-782 (1983).

[Ito 93]: Itoh N., Kohyama Y., "Electrical and thermal conductivities of dense matter **in** the crystalline lattice phase. II - Impurity scattering," *Astrophys. J.*, **404,** 268-270 (1993); erratum: *Astrophys. J.*, **420,** 943 (1994).

[Ito 08]: Itoh N., Uchida S., Sakamoto Yu, Kohyama Y., Nozawa S., "The second born corrections to the electrical and thermal conductivities of dense matter in the liquid metal phase," Astrophys. J., 677, 495-502 (2008).

[Iye 93]: Iyetomi H., Ogata S., Ichimaru S., "Quantum Monte Carlo simulation study of free energies and melting transitions in Coulomb solids," Phys. Rev. B, 47, 11703-11711 (1993).

[Jan 62]: Jancovici B., "On the relativistic degenerate electron gas," *Nuovo Cimento* 25, 428455 (1962).

[Jon 96]: Jones M.D., Ceperley D.M., "Crystallization of the one-component plasma at finite temperature," *Phys. Rev. Lett.*, 76, 4572-4575 (1996).

[Kam 99]: Kaminker A.D., Pethick C.J., Potekhin A.Y., Thorsson V., Yakovlev D.G., "Neutrino-pair bremsstrahlung by electrons in neutron star crusts," Astron. Astrophys., 343, 1009-1024 (1999).

[Kit 63]: C. Kittel, Quantum Theory of Solids (Wiley, New York,1963).

[Kit 86]: Kittel C., 1986, *Introduction to Solid State Physics* (New York: Wiley).

[Koh 65]: Kohn W., Sham L.J., 1965, “Self-consistent equations including exchange and correlation effects,”Phys. Rev. 140, A1133–A1138.

[Lam 68]: Lampe M., "Transport theory of a partially degenerate plasma," Phys. Rev. , 174, 276-280 (1968).

[LL3]: Landau, L.D., Lifshitz, E.M. 1976, Quantum Mechanics, Pergamon, Oxford.

[LL5]: Landau L.D., Lifshitz E.M., 1993, *Statistical Physics, Part 1* (Oxford: Pergamon).

[LL10]: L. P. Pitaevskii , E.M. Lifshitz ,1981, Physical Kinetics (Pergamon International Library of Science, Technology, Engineering, and Social Studies)

[Mil 06]: Militzer B., Graham RL., "Simulations of dense atomic hydrogen in the Wigner crystal phase," J. Phys. Chern. Sol. 67, 2136-2143 (2006).

[Moc 79]: Mochkovich R., Hansen J.P., "Fluid-solid coexistence curve of dense Coulombic matter," *Phys. Lett. A*, 73, 35-38 (1979).

[Nan 84]: Nandkumar R., Pethick C.J., "Transport coefficients of dense matter in the liquid metal regime," Mon. Not. R. Astron. Soc., 209, 511-524 (1984).

[Neg 73]: Negele J.W., Vautherin D., "Neutron star matter at subnuclear densities," Nucl. Phys., A 207, 298-320 (1973).

[Oya 93]: Oyamatsu K., "Nuclear shapes in the inner crust of a neutron star," Nucl. Phys., A 561, 431-452 (1993).

[Pot 97]: Potekhin A.Y., Chabrier G., Yakovlev D.G., "Internal temperatures and cooling of neutron stars with accreted envelopes," Astron. Astrophys., 323, 415-428 (1997).

[Pot 99a]: A. Y. Potekhin, D. A. Baiko, P. Haensel, D. G. Yakovlev (1999). Transport properties of degenerate electrons in neutron star envelopes and white dwarf cores, Astron. Astrophys. 346, 345.

[Pot 99b]: Potekhin A.Y., 1999, "Electron conduction **in** magnetized neutron star envelopes," *Astron. Astrophys.*, **351,** 787-797.

[Pot 00]: Potekhin A.Y., Chabrier G., "Equation of state of fully ionized electron-ion plasma. II. Extension to high densities," Phys. Rev. E, 62, 8554-8563 (2000).

[Rai 82]: Raikh M.E., Yakovlev D.G., "Thermal and electrical conductivities of crystals in neutron stars and degenerate dwarfs," Astrophys. Space Sci., 87, 193-203 (1982).

[Sha 83]: Shapiro S.L., Teukolsky S.A., 1983, *Black Holes, White Dwarfs, and Neutron Stars: The Physics of Compact Objects* (New York: Wiley).

[Sch 97]: Schmidt P., Zwicknagel G., Reinhardt P.G., Toepffer C., "Longitudinal and transversal collective modes in strongly correlated plasmas," Phys. Rev. E, 56, 73107313 (1997).

[Spi 62]: Spitzer L., Jr. 1962, Physics of Fully Ionized Gases, 2nd edition (Wiley: New York).

[Tim 99]: F. X. Timmes, D. Arnett, Astrophys. J. Suppl. Ser., 125, 277(1999).

[Tim 00]: F. X. Timmes, F. D. Swesty, Astrophys. J. Suppl. Ser., 126, 501(2000).

[Van 69]: Van Horn H.M., "Crystallization of a classical one-component Coulomb plasma," *Phys. Lett. A,* 28, 706-707 (1969).

[Wil 69]: Williams R.H., DeWitt H.E., 1969, "Quantum-mechanical plasma transport theory," Phys. Fluids, 12, 2326-2342.

[Yak 80]: D. G. Yakovlev, V. A. Urpin (1980). Thermal and electrical conductivity in white dwarfs and neutron stars, Sov. Astron. 24, 303.

[Yak 87]: D. G. Yakovlev (1987). Thermal and electrical conductivities of a degenerate electron gas with electron scattering on heavy ions in the liquid or gaseous phases, Sov. Astron. 31, 347.

[Yak 89]: Yakovlev D.G., Shalybkov D.A., "Degenerate cores of white dwarfs and envelopes of neutron stars: thermodynamics and plasma screening in thermonuclear reactions," Sov. Sci. Rev., Ser. E: Astrophys. Space Phys. 7, 311-386 (1989).

[Zim 60]: Ziman J.M., 1960, Electrons and Phonons, Oxford Univ. Press, Oxford.

ملخص

في هذا العمل ندرس بطريقة مفصلة و شاملة الخواص الديناميكية الحرارية و الحركية للعناصر في أغلفة النجوم النيترونية ، آخذين بعين الاعتبار تأثير الحقول المغناطيسية القوية و المكممة ، التأثيرات النووية و حالات المادة ، إضافة إلى إمكانية و جود أكثر من عنصر ، و كذا إنشاء برامج و خوارزميات لحساب معاملات التوصيل ، لهذه النتائج أهمية كبيرة في بناء نماذج البنية الميكانيكية و الحرارية للنجوم النيترونية و كذا طيف إشعاعها ، ما يعني الإسهام في تطوير مجال بحث يعتبر نقطة تلاق بين الفيزياء الفلكية و فيزياء البلازما – دراسة المادة عند الشروط الحدية ، تمتلك النجوم النيترونية حقولا تجاذبيه قوية ، كثافة عالية و حقولا مغناطيسية قوية .

كلمات مفتاحية: نجوم نيترونية، مادة كثيفة، ناقليه، لزوجة، حقول مغناطيسية، بلازما، نوويات.

Abstract:

In this work we deal in a detailed and comprehensive theoretical consideration of the most important thermodynamic and kinetic properties of the substance in the shells of neutron stars, taking into account the influence of strong, including quantizing, magnetic fields, nuclear and condensed matter effects , and the presence of more then one elements and created a complex computer programs to compute the transport coefficients , results which are important for modeling mechanical and thermal structure of neutron stars and their spectra thermal radiation, thus contributing to the development of important fields of research at the contemporary of astrophysics and plasma physics - the study of matter under extreme conditions, due to unique properties of neutron stars: they have strong gravity, high density and strong magnetic fields.

Key words: stars: neutron– dense matter– conduction-viscosity –magnetic fields-plasma-nuclear.

Résumé :

Dans ce travail on traite d’une manière détaillée les considérations théoriques des propriétés thermodynamiques et cinétiques les plus importantes des substances dans les enveloppes des étoiles à neutrons , prenons en considérations l’influence des champs magnétique fort quantifiant, les effets nucléaires et des états de matières , et la possibilité de présence des plusieurs éléments et la construction des programmes pour calculer les coefficients de transport , c’est résultats sont importants pour la modélisation de la structure mécanique et thermique des étoiles a neutron et leurs spectre thermique , alors la contribution a développée des domaines importants de recherche contemporain en astrophysique et la physiques des plasmas – l’étude de la matière dans les conditions extrêmes, dû aux propriétés uniques des étoiles a neutron : il ont une gravité forte , de densité élevée , et champs magnétiques intenses.

Mots clés : Etoiles : neutron-matière dense- conduction-viscosité - champs magnétiques-plasmas-nucléaire